SIGNIFICANCE OF ION INDUCED LUMINESCENCE FOR RADIATION INDUCED BYSTANDER EFFECTS

SIGNIFICANCE OF ION INDUCED LUMINESCENCE FOR RADIATION INDUCED BYSTANDER EFFECTS

By Syed Bilal Ahmad, MSc. BSc.

A Thesis Submitted to the School of Graduate Studies in Partial Fulfillment of the Requirements for the Degree PhD in Medical Physics and Applied Radiation Sciences

McMaster University DOCTOR OF PHYLOSOPY (2012), Hamilton ON

(Medical Physics and Applied Radiation Sciences)

Title: Significance of Ion Induced Luminescence for Radiation Induced Bystander Effects
AUTHOR: Syed Bilal Ahmad MSc. B.Sc. SUPERVISOR Professor Fiona E. McNeill (PhD) NUMBER OF PAGES; xv, 115

Abstract

Radiation induced bystander effects have given the cancer risk analysis a whole new paradigm. However the actual mechanism involved in producing the effects is still not clear. The basic bystander signal is assumed to be a biological signal. In this study we proposed and tried to quantify the presence of a physical signal in the form of electromagnetic radiation that can trigger a biological response in the bystander cells. In bystander effect studies where the cells are exposed to very low fluence of charged particles there could be several regions that can produce electromagnetic radiation due to the process of atomic/molecular excitations and relaxations. We focused on quantifying the number of ultraviolet photons emitted when charged particles pass through different media that have relevance to radiation biology experiments. The choice of UV photons was made due to the reason that its effects on living cells are very well documented. For this purpose we developed a system which employed the technique of single photon counting to measure the light emitted from samples irradiated under vacuum by a charged particle beam. Photon counting was done using a fast photomultiplier tube (Hamamatsu R7400p) with a peak cathode response at 420 nm wavelength.

In the early set of "proof of principle experiments" we tested polystyrene targets for ion beam induced luminescence. Polystyrene is one of the materials that are used as a cell substrate for radiation biology experiments. The luminescence yield from polystyrene was measured in terms of absolute value i.e. number of photons per second per unit solid angle. The output appeared to have a non-linear behavior with the incident Ion fluence: it rose exponentially to an asymptotic value. We irradiated the samples with beam energies varying from 1 MeV to 2.0 MeV and showed saturation at or before an incident fluence rate of 3×10^{13} $H^{+}/cm^{2}s$. The average saturation value for the photon output was found to be 40×10^{6} cps. Some measurements were performed using filters to study the emission at specific wavelengths. In the case of filtered light measurements, the photon output was found to saturate at 28×10^{3}, 10×10^{6}, and 35×10^{6} cps for wavelengths of 280±5 nm, 320±5 nm and 340±5 nm respectively. Using the IBIL signal evolution characteristics with the ion fluence we determined the ions produce a damage having a cross section of the order of 10^{-14} cm^{2} in polystyrene. The average radiant intensity was found to increase at wavelengths of 280 nm and 320 nm when the proton energy was increased. Having found an evidence of a significant production of UV in ion irradiated, biologically relevant, material we extended this study further into the measurements from other relevant materials in radiation biology.

Here charged particle irradiation was performed using positively charged protons (H^{+}) ranging in energy from 1.2 MeV to 2.2 MeV at a fluence rate of 2.7×10^{10} protons $mm^{-2}s^{-1}$. The materials chosen for this study were polypropylene, Mylar, Teflon, and Cellophane as they are all materials commonly used in radiation biology experiments as cell substrates or containers. In addition, we performed measurements of two NIST

standard materials derived from living cells: oyster tissue and citrus leaves. These materials were measured as a powder.

All the container materials were found to emit UV frequency photons at emission levels that are significant enough to warrant further investigation of the potential biological consequences. In addition, the NIST standard reference materials oyster tissue and citrus leaves also emitted UV when irradiated. This suggested that biological materials may themselves emit UV at significant levels when irradiated with charged particles.

We established this further by irradiated cells with β-particles. Cells were plated in Petri-dishes of two different sizes, having different thicknesses of polystyrene (PS) substrate. Exposure of the cell substrates (polystyrene) only resulted in the production of 1035 photons per unit activity in μCi of ^{90}Y which was equivalent to an exposure of 840 β-particles/cm^2 to the substrate. For a collimated electron beam exposure, we observed 158-167 photons per unit μCi (18 β-particles per cm^2 on the substrate) for different thicknesses of the substrate. Upon irradiating HPV-G cells plated on the PS dishes we determined that the luminescence gradually increased with the increasing exposure of β-particles; reaching up to 250 % of that of the luminescence without any cells for an activity of 180 μCi. For general irradiation conditions we found statistically significant difference in luminescence output for varying cellular densities with cells only and with the application of medium on top of the cells. The colourless medium increased the total luminescence yield while the coloured medium decreased it. When the cells were irradiated using a collimated beam of electrons it was found that the luminescence decreases with the increasing cellular density thus providing an evidence of re-absorption of photons within the surroundings.

After establishing the fact that charged particles induce light emission from the materials that have a relevance to the radiation biology experiments. We extended our study further to find out other sources of radiation that could affect the dose distribution in radiation biology experiments. In radiation biology experiments the low doses of radiation are usually delivered using a microbeam charged particle accelerator. Microbeams delivers a highly localized and small dose to the biological medium by using a set of collimators that confine the charged particle beam to a very narrow (micron level) region. Since the collimation block a significant proportion of the beam therefore there is a chance of the production of low energy x-rays and secondary electrons. We used Monte Carlo simulations to investigate the production of particle induced x-rays and secondary electrons in the collimation system and its possible effects on the final dose delivery to the biological medium. We found no evidence of the escape of x-rays or secondary electrons from the collimation system for proton energies of up to 3 MeV. The thickness of the collimators was sufficient to reabsorb all the generated low energy x-rays and secondary electrons. However if the proton energy exceeds 3 MeV then a significant proportion of 10 keV and 59 keV (K-α) x-rays can be emitted by the collimator. Further it was established that due to the phase space distribution of particles in various orientations with the beam

axis there are significant chances of hitting non-targetted cells in microbeams that employ a collimator to confine the beam. This may happen due to the beam particles travelling obliquely with the beam axis thus passing the collimator edge and hitting the non-targetted cells. Another reason could be the scatter of beam particles inside the collimator.

The evidence of the production of UV in materials relevant to the radiation biology experiments suggest that the conclusions and hypotheses derived from some radiation bystander experiments need to be re-thought, as charged particle irradiation leads to some level of UV emission in experimental materials which may be the cause of some “non-targeted” effects.

Acknowledgements

All thanks to the Almighty Allah for giving me the strength and knowledge for completing this piece of work. I am sure that the prayers and well wishes of my parents played a big role too. I came in Canada with my wife, Rabia, who supported me throughout this time and I feel that I would not have been able to accomplish my work without her help.

I show a sincere gratitude to my supervisor, Professor Dr. Fiona E. McNeill. She is a great, gentle and very calm person. I loved being her student because of her always positive and encouraging attitude. I am also very grateful for the financial support she extended towards me. I feel very lucky to have her as my supervisor.

Dr. Bill and Byun are two fantastic personalities for the department and they are there to help the students as they need it. I am very thankful to both of them for giving their honest and very encouraging opinions about my work and specially this dissertation. The technical support I got from Dr. Byun during my work was extremely worthwhile as I believe that he himself is very sound technically.

Here I would like to extend special thanks to my co-supervisors Professor Dr. Carmel Mothersill and Professor Dr. Colin Seymour. They encouraged me a lot whenever we got a chance to get together in a meeting. I thank both of them for letting me use their lab for some of the work presented in this thesis.

How can I forget Jason Falladown. Although he is no longer here in the department but the students (especially I) who got help from him in setting up the equipment and scheduling the work can never forget him. Special thanks to Scott McMaster as well. He also was always there whenever I needed any technical help.

Contents

List of Figures

List of Tables

List of All the Abbreviations and Symbols

H2AX: H2A histone family, member X

miRNA: micro-Ribonucleic acid

HZE: High Charge and Energy

LET: Linear Energy Transfer

DSBs: Double strand breaks

LINAC: Linear accelerator

FWHM: Full width and half maximum

IBIL: Ion beam induced luminescence

cps: counts per second

NIST: National Institute of Standards and Technology

NIM: Nuclear Instrumentation Modules

SRIM: Stopping and Range of Ions in Matter

HPV-G: Human papillomavirus-G

LNT: Linear No Threshold

RPMI: Roswell Park Memorial Institute

DMEM: Dulbecco's Modified Eagle Medium

FBS: Fetal Bovine Serum

EDTA: Ethylenediaminetetraacetic acid

CSDA: Continuous Slowing Down Approximation

PIXE: Particle Induced X-ray Emission

Declaration of Academic achievement

Chapter 1

Introduction

1 Introduction

1.1 Radiation induced bystander effects and the hypothesis of this dissertation

Radiation induced bystander effects refer to the effects observed in cells that are not the primary target of radiation [1]. This effect has been thoroughly investigated by many research groups after the initial report of Nagasawa and Little in 1992; when a certain biological end point (Sister Chromatid Exchange) was observed in more than 30 % of a colony of cells in which only 1 % were directly hit by α-particles [2]. Subsequent investigations confirmed the effect for a variety of biological end points such as chromosomal aberrations, cell lethality, mutation and oncogenic transformations [3]. Initially it was assumed that the effect was a result of molecular transfer through the gap-junctions (by means of intercellular communication but later it was established that cell to cell contact is not necessary and in fact the irradiated cells are capable of inducing effects in cells to which the medium from irradiated cells is transferred [4], [5], [6] and [7]. Based upon the mechanism of the induction of bystander effects, studies are divided into two major categories. In the first category of experiments, specified cells or a specified percentage of cells are targeted by radiation, using micro-beams or very low levels of ion fluence, and the effects are observed in the neighboring cells [8]. The neighboring cells could be in contact with each other (confluent) or they could be spaced well apart from each other and connected only through the medium. In the second category of experiments, cells cultured in a growth medium are irradiated (usually with x-rays or gamma rays) and then their medium is transferred to an un-irradiated colony of cells for the measurement of bystander effects [9]. This latter method is often referred to as the medium transfer bystander method. In addition to ionizing radiation, bystander effects have also been reported in response to UVA and UVB radiation [10] and [11].

Until now, most researchers have considered the bystander effect to be a result of a chemically mediated signal. This is because effects can be observed in medium transfer experiments. However, characterization of a chemical bystander signal, although having been considered important and thus the subject of much investigation, has been a difficult challenge. Several factors have been determined that are considered to be possible candidates for the chemical bystander signal. For example, in some cases the formation of γH2AX foci (as a result of phosphorylation of H2AX) in non-irradiated cells almost immediately after their treatment with the medium from irradiated cells has been linked to the presence of nitrogen species and miRNA released in the medium from the irradiated cells [12] and [13]. In other studies, the involvement of mitochondria, because of the production of reactive oxygen species, has been found to be the source of bystander signals [14]. A comprehensive review of all the possible mechanisms through which the signal can be generated and transmitted to the bystander cells is given in the reference [15].

Regardless of the form of the biological or chemically mediated signal, it is assumed to be generated in the directly hit cells from where it is secreted out into the medium or transferred to the neighboring cells via gap junctions. In other words, the possibility of the production of the so-called signal carriers in the neighboring cells via an alternative mechanism has been completely disregarded. This thesis work is intended to explore other possibilities of signal induction in neighbouring cells, beyond the currently accepted idea of a chemically mediated signal.

One of the possible effects in the neighboring or bystander cells could be because of the range of the secondary electrons or delta-rays generated along an incident primary ionizing radiation particle track. In the case of high charge and energy (HZE) particles, it has been determined that the practice of estimating the number of particle track traversals per cell or nucleus in terms of the product of LET and the cell area underestimates the total number of track traversals per cell [16]. This is because the secondary electrons can traverse a distance ranging from μm to mm. It has also been determined that secondary electrons with energies ranging from 0.1 to 4.5 keV are very efficient in producing DNA Double Strand Breaks (DSBs) mostly by direct interaction in the DNA and by producing OH free radicals [17]. In several other studies, the possible role of secondary electrons have been determined and various models are available to incorporate their contribution in producing DNA damage in the target and neighboring cells [18] and [19].

Another possibility that could initiate some biological response in the bystander cells could be the induction or disturbance of electromagnetic fields. The involvement of electromagnetic fields (such as photons) in initiating different biological processes, such as enzyme activation, and regulation of gene expression is beyond doubt. This is a subject of intensive research for the field of “mutagenic radiation” or “bio-photons”. Biological activities are not only associated with the emission of photons within a certain range but photon absorption at different frequencies can also induce different biological responses. Of the wide range of electromagnetic frequencies, the absorption of photons at visible, ultra violet, and near ultraviolet frequencies, and the subsequent effects resulting from the absorption, is potentially very important for the better understanding of the bystander effect and provides the background for this study.

The involvement of a physical signal in the production of a bystander response amongst the non-irradiated cells has been investigated in a very few studies. Mosse et.al were the first to raise a suspicion of the presence of a physical signal when they found that the bystander response was altered due to the addition of melanin, which is supposed to absorb certain frequencies of light, in both the direct exposure and medium transfer protocol experiments for radiation induced bystander effects [20]. The idea of involvement of a physical signal is further strengthened by the studies performed by two other groups. Here the cells were subjected to the direct and scattered radiation from the teletherapy units (^{60}Co and LINAC). It was observed that equally distinguishable bystander responses were

present in both the cases [21] and [22]. Investigating the source of this electromagnetic energy was the prime rationale for this dissertation.

It is a well known fact that charged particles produce dense ionizations and excitations when they pass through media. As a result of the relaxation of excited molecules, radiation can be emitted at different frequencies. We focused on measuring the emissions at ultra violet frequencies because UV has been demonstrated to produce biological responses that are similar to those observed for bystander cell studies. The hypothesis that I investigated was that UV would be emitted as a direct consequence of irradiation with charged particles. Emitted UV could then be considered as a candidate for a "physical" bystander effect signal.

1.2 Ion interaction and luminescence in organic and biological media

1.2.1 Interaction in organic materials

In radiation biology experiments, the cells are usually kept in (or attached to) containers made of various polymeric materials for irradiation. These containers are usually manufactured by using polystyrene, polypropylene or Mylar. When irradiating the cells the radiation has to pass through the container material, therefore it is important to understand the interaction of ionizing radiation, and the possible outcomes from this interaction, with these polymer materials.

Polymers are formed when a large number of repeating molecular units are linked together by covalent bonds. The basic interaction of ionizing radiation in polymers is the same as any other material. Charged particles can knock out target atoms if the energy imparted is greater than the binding energy of that atom and the knocked-out atoms can produce a collisional cascade. The binding energy of atoms in polymers is typically of the order of 15 eV, which means 30 eV is required to produce an ion pair [23]. After depositing all their energy, the incident charged particles usually come to rest by capturing electrons and become a part of the polymeric chain. The ion induced damage in polymers is not homogenous; it is more concentrated in the track core. It can be quantified using a parameter known as the damage cross section σ. This quantity can be determined using various analytical and experimental approaches. In the case of an analytical approach, the damage cross section can be related to the evolution of the signal characteristics, Y, to ion fluence ϕ [23]. This signal was light emission from the polymer in our case. Since the probability of creating damage after a certain number of impacts is proportional to the undamaged area, the signal characteristics would decrease exponentially provided all the damage processes are considered independent of each other. This fact can be expressed in terms of the following equation (eq. 1).

$$\boldsymbol{Y = Y_o \exp\left(-\sigma\phi\right)} \text{ ..... } eq\ 1$$

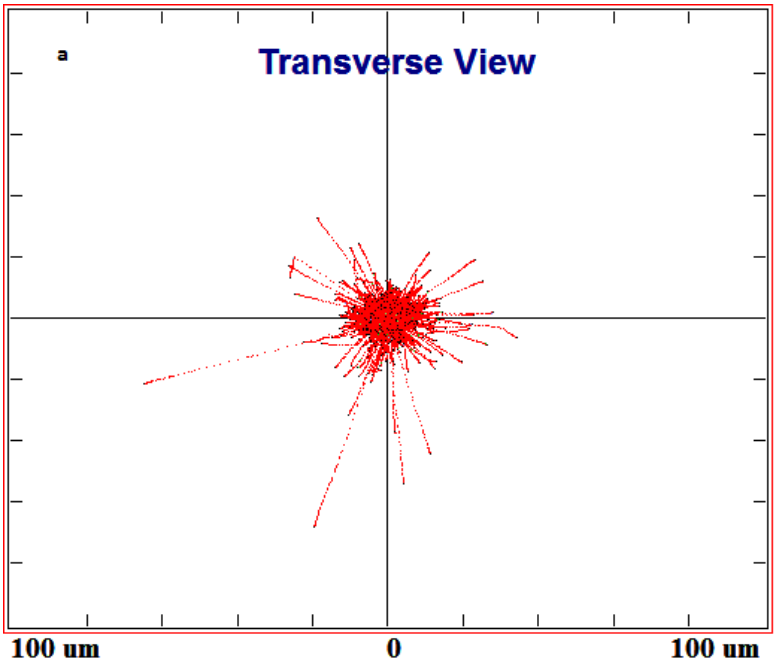
a
Transverse View
100 um
0
100 um

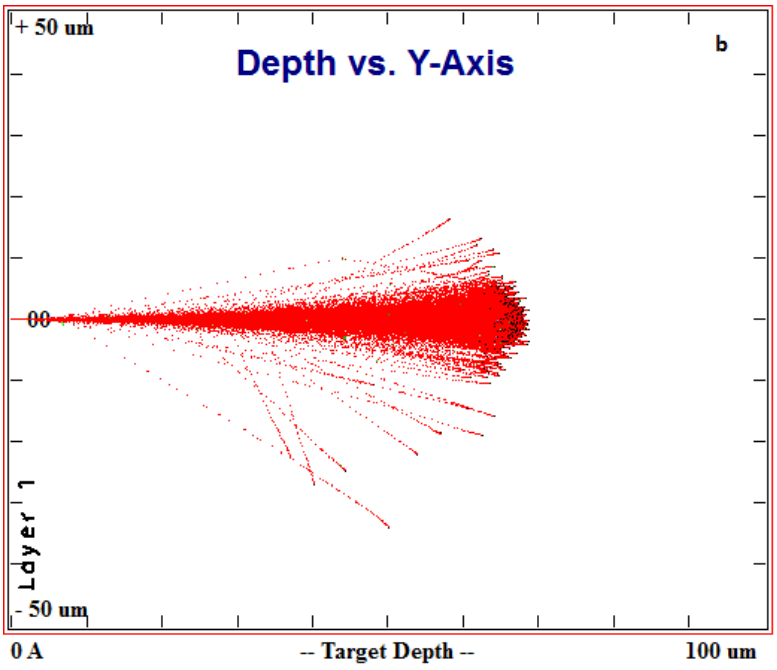
+ 50 um
Depth vs. Y-Axis
b
00
Layer 1
- 50 um
0 A
-- Target Depth --
100 um

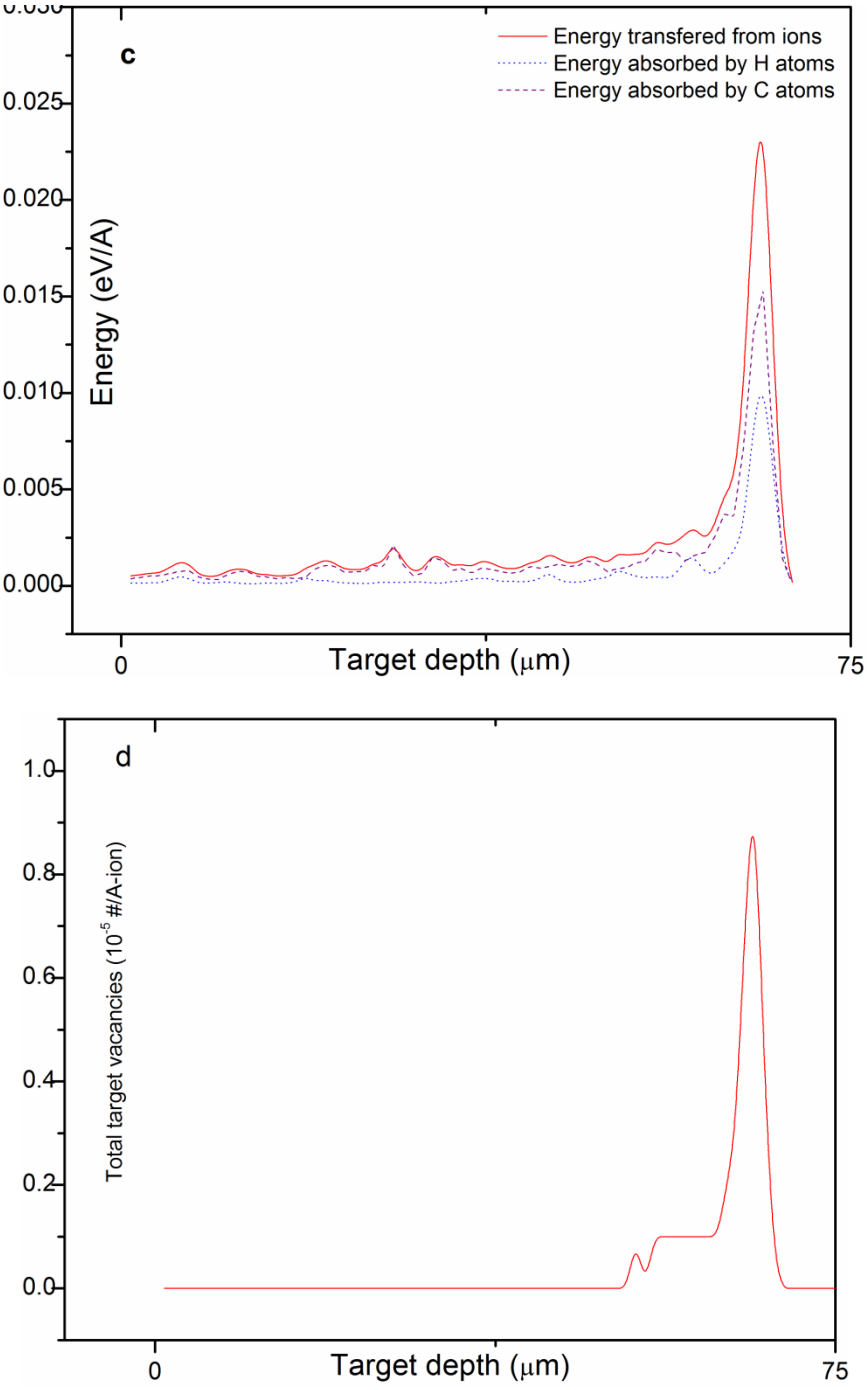

Figure 1.1(a) and (b) are the transverse and longitudinal views for the distribution of 2 MeV H^+ ions in polystyrene. (c) is the Energy transferred by the incident ions and absorbed by the Carbon and Hydrogen atoms of Polystyrene and (d) is the number of vacancies produced in the target per A per incident ion.

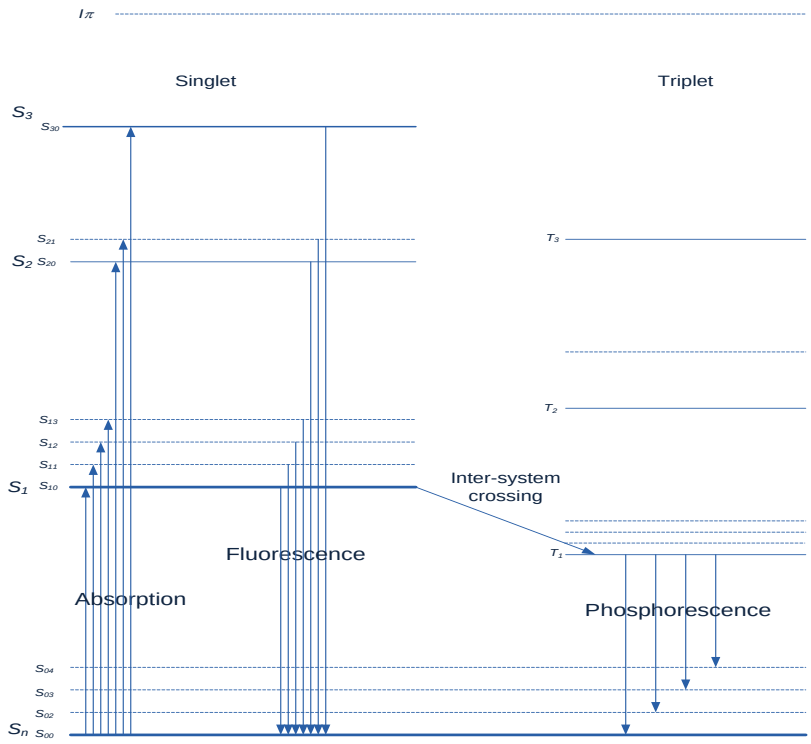

Figure 1.2 Energy level diagram for organic molecules and concept of fluorescence and phosphorescence emission

In our study, we were aiming to measure the luminescence from experimentally relevant materials. However it was observed that the luminescence degrades with increasing ion fluence which indicated that a damage process is underway in the polymer as a consequence of ion irradiation. This led to us being able to measure the damage cross section for polystyrene. This also permitted some validation of the measurement system, as there is published data for other polymers in the literature. The comparison of our data with other data provided some confidence in the developed system's ability to measure luminescence. This information is presented in the articles in Chapters 2 and 3 of this thesis.

Majority of the physics processes for ion-polymer interactions are well established and can be modeled using the Monte-Carlo technique. In radiation physics the technique of Monte-Carlo involves computational algorithms that perform random sampling of the probability distributions of radiation interactions in matter. The method is analogous to spinning a roulette wheel and seeing in which particular numbered slot the ball falls, hence the name "Monte Carlo" analysis. The probabilities of interaction are sampled, i.e. the "wheel" is spun thousands of times in a Monte Carlo code and this can be used to determine the potential tracks of particles in a medium. There are several different radiation transport

Monte-Carlo codes available. However for ion transport, such as the proton p-material interactions investigated in this thesis, the code "SRIM/TRIM", developed by J. F Ziegler et al, is commonly used [24]. This code calculates the ion-atom interactions by making use of the quantum mechanical approach to atomic collisions. Details of the code can be found in the following reference [24]. Some of the parameters measured for 2 MeV proton interactions in polystyrene, relevant in our experiments, using the code SRIM/TRIM are shown in Figure1.1.

In addition to producing damage in polymers, ions can transfer a significant proportion of their energy to the orbital electrons. The electronic energy transfers can result in excitations and ionizations of the target atoms. However the details of the electronic excitations can be quite complicated. Ions possessing kinetic energies > 1 MeV/amu, as used in this study, are primarily slowed down by ionization of the target atoms with emission of secondary electrons having high kinetic energies. The ionizations and excitations can result in radiative and non-radiative relaxations. In the case of radiative relaxation, photons at different wavelengths can be emitted with different frequencies. The competition between the radiative and non-radiative de-excitations is usually governed by the amount of energy density released by the ion along the tracks. For a high energy density release along the particle track, a quenching effect takes place that decreases the luminescence efficiency of the polymer. This effect was first described by Birks with the help of following relationship [25].

$$\frac{\Delta L}{\Delta x} = \frac{A \times S(E)}{1 + kB \times S(E)} \quad \text{..... eq 2}$$

where B represents the density of the ionized or excited molecules and k (~ 10^4) represents the radiative to the non-radiative recombinations [23]. The production of luminescence from ion irradiated polymers has been studied, verified and published in the literature according to eq. 2 for several different polymeric materials for their possible use as scintillators [26], [27], [28]and [29]. Luminescence in polymers usually results from the de-excitation of electrons in π-molecular orbitals which absorb energy from the incident ionizing radiation. A typical polymer based scintillator is expected to emit 10,000 photons per unit MeV of radiation energy absorbed in it [26]. Figure 1.2 represent an energy level diagram for π-molecular orbital and schematics of energy absorbed, fluorescence and phosphorescence emission.

As mentioned earlier, in radiation biology experiments cells are irradiated in such a manner that their container materials are exposed first. Therefore the scintillations originated from the container materials could expose the cells that were not the primary target of the radiation. These low level physical signals or electromagnetic disturbances are very similar to those that are a subject of interest for the mutagenic radiation researchers. Currently there are no models available that can incorporate the effect of these photons in radiation biology experiments. In Chapters 2 and 3 of this thesis, I describe the system I developed

to measure ion induced luminescence from experimentally relevant materials, and the results of the luminance measurements for studies of polystyrene, mylar and polypropolene. I also investigated dried oyster tissue and citrus leaves to determine whether materials derived from living organisms also produce luminescence.

1.2.2 Interactions in biological media

When the ionizing radiation interacts with the biological media, such as cells, it produces ionizations and or excitations that changes the number of negative ion groups on their surface usually by dissociation. This can bring various changes in the cells such as cell-cell interaction, the interaction between Ca^{+} ions and the cell membrane, the ion permeability of the cell membrane, and other physiological changes [30]. The process of dissociation usually occurs all the way along the track of the incident particle and produces free radicals that interact with other molecules and produce permanent damage. The life span of the free radicals is very short (typically 10^{-10}-10^{-9} s or in some cases ~10^{-4} s) unless they delocalize the unpaired electrons to reduce the spin density of the free radical centre, in which case they can become very stable [30]. In case of ions that are completely stopped inside the biological material, there could be several morphological changes because of ion-molecule interaction, in addition to the production of long-lived free radicals in large quantities. This is an important fact that could contribute to some effects seen for the medium transfer bystander effects because the long lived free radicals can be transferred with the medium to the new cell population.

The ionizations and excitations produced along the particle track can result in spontaneous emission of radiation at visible or ultraviolet frequencies. In addition to spontaneous light emission, it has also been observed that ultra-weak luminescence, over a period of several hours, is enhanced upon ionization radiation interaction. This emission is more pronounced for ions as compared to gamma rays [30]. This low level luminescence emission can enhance or suppress cellular functions such as cell division. The spontaneous emission of light at visible frequencies has been observed previously in histological and cytological samples [31]. It has also been observed for grass and human skin samples [32]. In case of human skin the emission frequency has a broad range having peaks in UV and visible regions of the electromagnetic spectrum.

The emission of UV light from biological samples as a result of charged particle interactions could be a mode of communication when it is absorbed in the surrounding cells and media. Ultraviolet radiation can cause damage to the cells either directly (UVC) or indirectly by means of free radicals and cytokines (UVB and UVA). UV B and UVA are of major research interest because of their presence in the environment (UVC is completely stopped by the ozone layer). UVB, in the wavelength ranges of 300-313 nm, can be absorbed directly by the DNA resulting in the formation of pyramiding dimers. It can also induce apoptosis by directly activating the death receptors on the cell surface [33].

UV A is responsible for the production of reactive oxygen species that produce DNA damage and subsequently cell mutation or cell death. Studies have shown that UV-A can induce a heritable mutation in mammalian cells, especially the skin cells after getting irradiated with UV-A show an increased mutation frequency [34].

1.3 Single photon counting

In general, photons can be detected by a variety of different detectors such as solid state detectors, scintillation detectors, charged coupled devices, and photomultiplier tubes. The choice of a particular detector is made based upon the energy of photons involved, the required energy resolution in case of a mixed energy photon field, the required detection efficiency etc. My application required an absolute measure of photons that can only be done using particular type of photomultiplier tube. A typical photomultiplier tube comprises a photocathode and a set of dynodes enclosed in an evacuated tube. Emission of electrons from the photocathode depends upon its work function (minimum energy required to set a bound electron free near the material's surface). Based upon cathode work functions, different PMTs have different spectral response ranges. Once the electron is set free by the incident photon it is accelerated towards the first dynode due to a potential difference applied between cathode and the dynode. Upon hitting the dynode more electrons are set free from the dynode surface and are accelerated towards the second dynode. In this manner a set of dynodes can multiply the initial number of electrons, created at the cathode of the PMT, to several orders of magnitude. The electron multiplication creates enough electrons for an external circuit to measure it in the form of a current or a voltage pulse. In case of single photon counting PMTs the signal transit time (i.e. the time between the absorption of photon at cathode to corresponding pulse at anode) is extremely fast (typically <1ns). The signal transit time is almost entirely determined by the transit time of electrons between the dynodes [35]. This fast response makes the detection of a single photon possible. Processing of the signal in order to make it meaningful for interpretation purposes has to be fast enough as well in order to keep up with the response of the photomultiplier tube.

A simple photon counting system comprises a photomultiplier tube (PMT), a discriminator and a counter. Figure 1.3 shows a schematic diagram of the system. The preamplifier output shown in Figure 1.4 is a typical output from a single photon counting photomultiplier tube R7400, by Hamamatsu, where a large number of pulses indicate the presence of photons. In usual practice, these pulses would be treated as a waveform superimposed over shot noise and the output is handled in the form of an analogue current created by a multitude of pulses. This mode of analyzing the signal is called analogue mode. In photon counting mode, these pulses are treated individually and the number of the pulses reflects the light intensity rather than the amplitude of the measured signal. The quantum efficiency (number of photoelectrons per incident photons on the cathode of the detector) of an ideal single photon detector should be 1. In case of photon interaction in the

photocathode the emitted electron is then multiplied with the help of a series of dynodes to a typical gain of 1×10^6. The photomultiplier tube used in this experiment had a rise time of 0.78 ns and the pulse width (FWHM) of ~ 5 ns. Therefore in this case, the expected output of the detector would be;

$$I_p = \frac{(1.6\times10^{-19}C\times1\times10^6)}{(5\times10^{-9}s)} = 32\mu A$$

$$V_0 = 32\mu A \times 50\Omega = 1.6mV$$

Single photon counting is used in several applications such as time resolved fluorescence spectroscopy [36], shortest life time measurements (such as positron life time measurements) [37], fluorescence anisotropy [38], auto-fluorescence measurements [39], mutagenic radiation (bio-photons) measurements [40] etc. In our case, we were interested in trying to measure the absolute number of photons emitted in situations relevant to radiation biology experiments.

For this purpose we used a fast pre-amplifier (9301), an amplifier-discriminator (9302), and a dual counter-timer (994) from ORTEC, for pulse processing. This combination is specifically designed for use with photon counting detectors. The pulses fed from the pre-amplifier are fed to the amplifier and after appropriate amplification (20 or 200 times) the pulses are compared to discriminator threshold. The discriminator threshold could be varied between 50 mV to 1 V. If the voltage of input pulses is more than the discriminator threshold, a logic pulse is generated and is counted by the counter. The photomultiplier tube used in this experiment had a photo-cathode radiant sensitivity ranging between 300 nm and 600 nm with a peak response at 420 nm photon wavelength. Count rate linearity depends upon the type of photon counting head used. Hamamatsu photomultipliers have very good count rate linearity for counts rates as high as 10^7 cps. Figure 1.5 shows the response of the PMT used in our experiments, to a light source decaying at a constant rate showing the linearity at low count rates. For count rates exceeding 10^7 cps Hamamatsu recommends use of the following correction for count rate linearity [41].

$$\dot{\mathbf{n}} = \frac{\dot{\mathbf{m}}}{\mathbf{1}-\dot{\mathbf{m}}\boldsymbol{\tau}} \text{..... eq 3}$$

It was found in the course of this thesis work, that the response of the photomultiplier tube follows a non-paralyzable behaviour (as represented in eq 3) for very high count rates. Therefore the output was corrected according to non-paralyzable model wherever necessary. '$\dot{\mathbf{n}}$', '$\dot{\mathbf{m}}$' and 'τ' in equation 3 represent the true counts, observed counts and dead time of the photomultiplier tube respectively. The development of this single photon counting system, and its application to the study of UV emission from experimentally relevant materials is described in Chapters 2 and 3. Chapter 4 describes the application of the system to the measurement of light emission from cells and cell media.

Figure 1.3 Schematic diagram of a single photon counting system

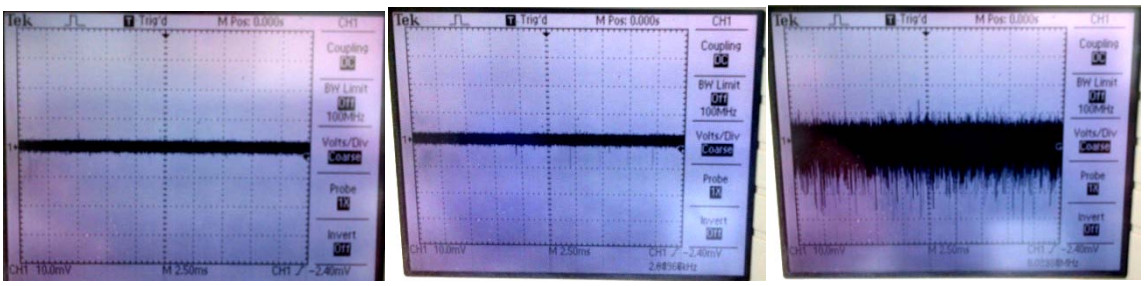

Figure 1.4 From left to right; Preamplifier output in a single photon counting unit for dark current, very low intensity light signal and very high intensity signal.

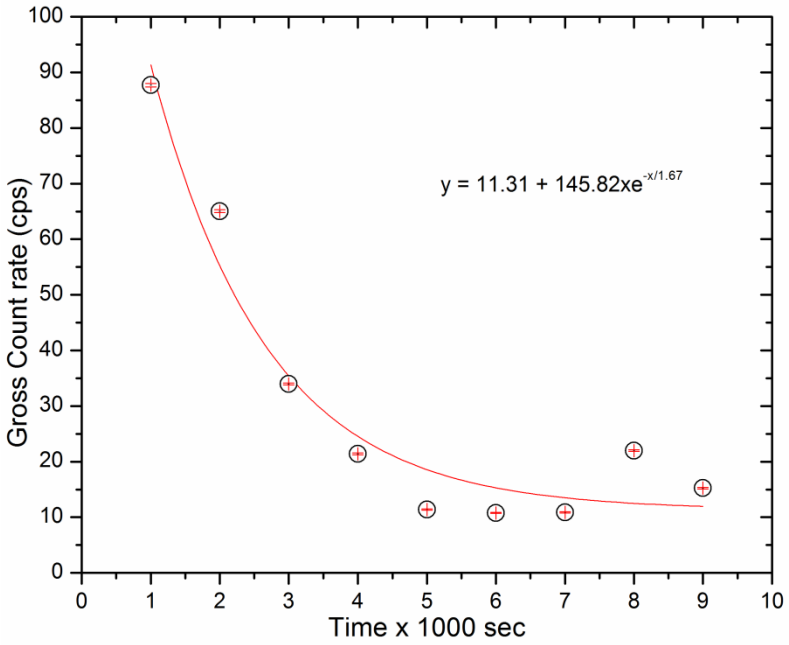

Figure 1.5 Response of R7400P photomultiplier tube used in our experiment to a decaying light source (turned off after 5000 s).

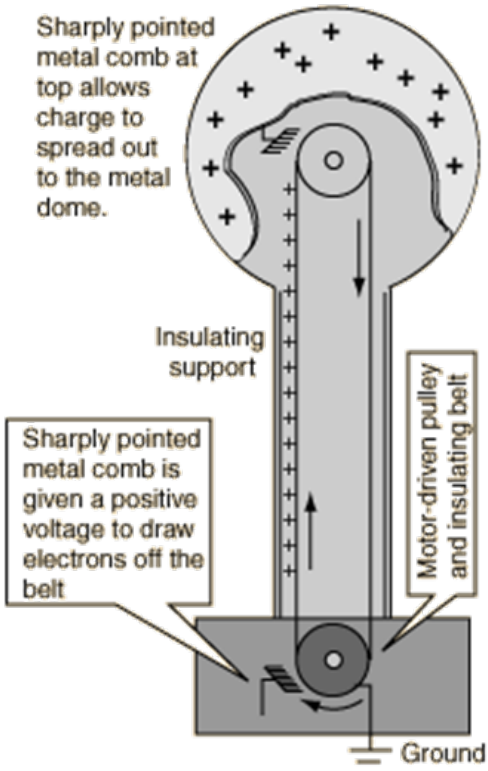

Figure 1.6 Schematic diagram of a Van de Graff generator [46]**.**

Figure 1.7 Faraday Cup

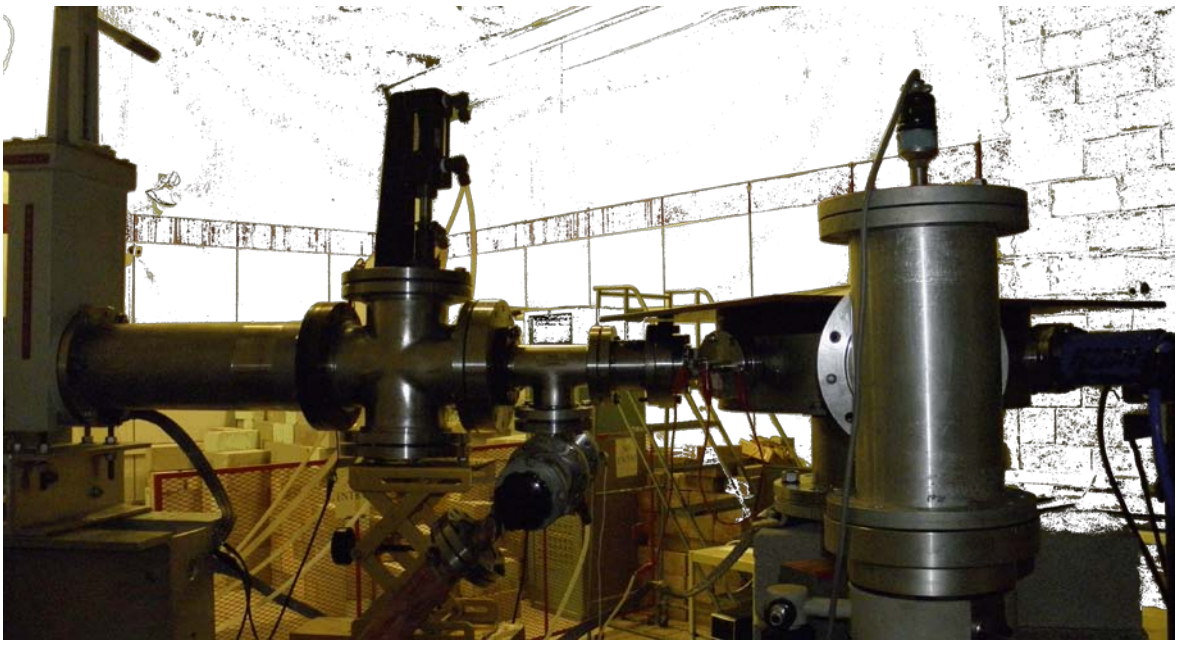

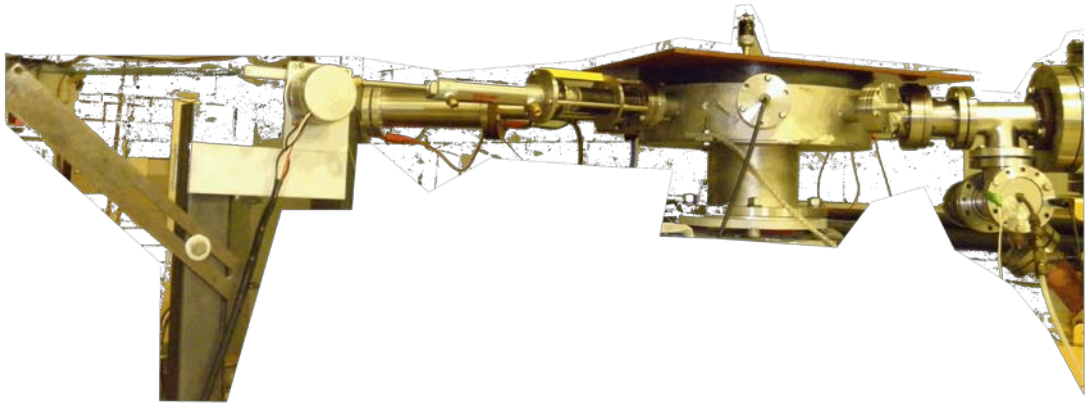

Figure 1.8 Various components in the beam line (top). (Bottom) Target chamber hooked up with the main beam line.

1.4 Production of a charged Particle Beam

Charged particle beams are usually produced in particle accelerators. The simplest example of a particle accelerator is the x-ray tube where the electrons are accelerated towards a positively charged target where they are decelerated to produce x-rays. A typical accelerator is comprised of four general components, namely the ion source, beam line, analyzing magnet, and a target. Ions are produced in the ion source and then accelerated by a voltage difference in the beam line. The accelerated ions are then passed through a magnet that selectively bends the charged particles of a required energy into a preset direction. These ions, having a specified energy, are then transported to the target. This whole operation requires a high level of vacuum, typically of the order of 10^{-6} torr.

1.4.1 KN accelerator

We implemented the ion beam luminescence measurement setup on the KN accelerator facility at McMaster University. It employs a Van de Graff type generator, for creating a high potential difference, where charge is transferred to the high voltage terminal via a moving insulated belt. Figure 1.6 shows a schematic diagram of a Van de Graff generator.

McMaster University's KN accelerator is a single ended accelerator with the ion source located inside the terminal shell. The ion source is a RF (radio frequency) discharge ion source. RF ion sources make use of a high frequency electric field to accelerate free electrons to energies that are sufficient to ionize atoms or molecules with which they collide. The RF frequency ranges between a few MHz up to a few tens of MHz [30]. Hydrogen gas is fed to the glass chamber around which the RF coils are wrapped. This creates purple coloured plasma (which is the state of a gas in which a large proportion of atoms are ionized) in the glass tube. After getting ionized the protons (positively charged) are extracted into the beam line where they are subject to high electric fields in steps. At

the final stage of acceleration; the protons can get energies as high as 3 MeV at McMaster KN accelerator facility. However the maximum protons energy used in this study was 2.2 MeV.

As the protons travel in the beam line they diverge because of the coulombs repulsion which is controlled by focusing magnets. By setting an appropriate magnetic field in the analyzing magnet the protons of a preselected energy are bent in a particular direction leading to the target chamber. Beam current is measured in a Faraday cup. A Faraday cup, shown in Figure 1.7 [42], is a metal cage that collects all the charge upon ion irradiation. By measuring the total amount of collected charge the ion beam current can be measured.

Towards the end of the beam, it can hit the target directly or it can also be brought into an irradiation chamber where all the measurements can be performed. At McMaster KN facility the proton beam normally hits a lithium target to produce neutrons that are subsequently used for neutron activation analysis studies. However, for this project, we instead extracted the beam into an irradiation chamber where it was used to bombard a moveable target. The light emitted from the target was then collected using the Hamamatsu single photon counting photomultiplier tube. Figure 1.8 a and b shows some parts of the beam line and the actual arrangement of the setup used for this project.

1.4.2 Microbeam accelerator

In radiation biology, and especially in studies of radiation induced bystander effects, very low currents are required. For this purpose, a special type of accelerator is used which is called a biological microbeam. Microbeams can deliver a counted number of ionized charged particles onto highly localized targets. In this manner, the researchers try to hit specific nucleus and non-nucleus targets inside the cells and determine the effects. Microbeams have also been used for ion implantation in biological matter, which is helpful in studying the biological effects on scientists planning on space exploration.

There are several groups around the world, mainly dealing with radiation biology studies, who are using microbeams to deliver low particle fluences to specific cells. A comprehensive review of all the microbeams used by different organizations around the world is given in chapter 2, page 27 of the book of ion beam biotechnology [30].

The basic mechanism for charge particle acceleration in the McMaster University's biological micorbeam is the same as that described earlier in this Chapter for the KN accelerator in that a charged proton beam is produced. However, the beam size and current in microbeams is reduced with the help of a set of narrow collimators. Magnetic focusing is also applied in order to reduce the beam size. McMaster University's microbeam facility uses a fine set of slits and apertures in order to reduce the beam size. The apertures and slits reduce the current reaching the cells by instead having protons hit the slits and

apertures. Relatively large proton currents are incident on the metal slits and apertures. This large current "dump" led to the question of whether x-rays could be induced in the aperture materials. The idea was to determine whether or not the low energy x-rays produced in the collimation system are capable of delivering a radiation exposure to the cells. This could potentially change the interpretation of the results established in radiation induced bystander effects. This work is described in detail in chapter 5 of this thesis.

1.5 β-particle production and HPV-G cells

In chapter 4 of this thesis, I present work where I measured the luminescence from cells and cellular materials. I used HPV-G cells for this purpose. These cells were obtained from Dr. Carmel E. Mothersill's laboratory. The HPV-G cells are epithelial cells that are derived from human foreskin primary culture and immortalized through transfections of complete Human Papillomavirus 16 genes (HPV16-Genes) [43]. This cell line has been extensively used for radiation induced bystander effect studies due to its stable response to bystander signals [9], [20], [44], and [45] and this is why it was chosen for this particular work.

The HPV-G cells were exposed to β-particles. The source of β-particles used was Y-90 which was produced in the McMaster Nuclear Reactor (MNR) facility. MNR has thermal and epithermal neutron irradiation facilities. Using a "rabbit" pneumatic system the small samples can be exposed to a flux of 3×10^{12} neutrons/cm^{2}s in the reactor core. Samples can be moved in and out of the reactor core remotely using a timed pneumatic system. Samples are encapsulated in a polyethylene tube which is pushed by air pressure through plastic tubing and is moved from the high level facility in the Nuclear Research Building into the reactor building and into the core. Y salt was exposed to the aforementioned neutron flux for a predetermined time in the reactor using the rabbit pneumatic system. The salt was then chemically dissolved in acid in order to be used and transported to another lab. Figure 1.9 shows a schematic diagram of MNR pneumatic system for radioisotope production.

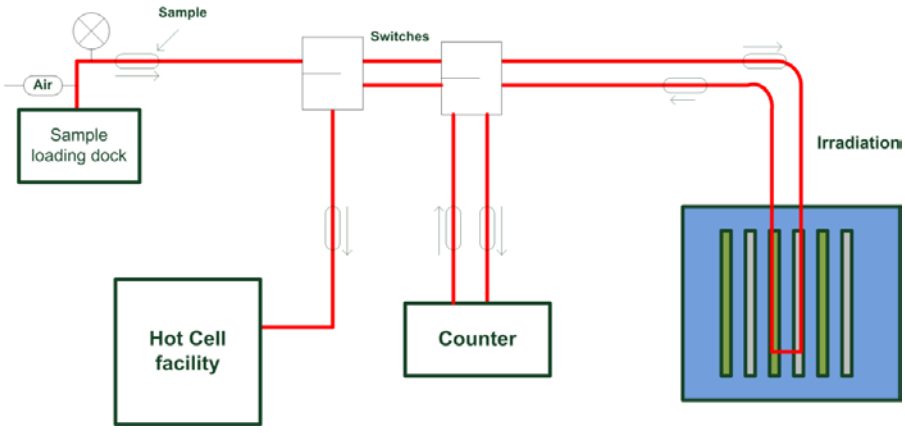

Figure 1.9 Schematic diagram of the radioisotope production process at MNR.

1.6 References

[1] C. Mothersill and C. Seymour, "Radiation-induced bystander effects: past history and future directions.," *Radiation research*, vol. 155, no. 6, pp. 759-67, Jun. 2001.

[2] H. Nagasawa and J. B. Little, "Induction of sister chromatid exchanges by extremely low doses of alpha-particles.," *Cancer research*, vol. 52, no. 22, pp. 6394-6, Nov. 1992.

[3] E. J. Hall, "The bystander effect.," *Health physics*, vol. 85, no. 1, pp. 31-5, Jul. 2003.

[4] A. Deshpande, E. H. Goodwin, S. M. Bailey, B. L. Marrone, and B. E. Lehnert, "Alpha-Particle-Induced Sister Chromatid Exchange in Normal Human Lung Fibroblasts: Evidence for an Extranuclear Target," *Radiation Research*, vol. 145, no. 3, pp. 260-267, Apr. 2010.

[5] C. M. and C. Seymour, "Medium from irradiated human epithelial cells but not human fibroblasts reduces the clonogenic survival of unirradiated cells," *International Journal of Radiation Biology*, vol. 71, no. 4, pp. 421-427, Jan. 1997.

[6] E. I. Azzam, S. M. de Toledo, T. Gooding, and J. B. Little, "Intercellular communication is involved in the bystander regulation of gene expression in human cells exposed to very low fluences of alpha particles.," *Radiation research*, vol. 150, no. 5, pp. 497-504, Nov. 1998.

[7] F. M. Lyng, C. B. Seymour, and C. Mothersill, "Initiation of apoptosis in cells exposed to medium from the progeny of irradiated cells: a possible mechanism for bystander-induced genomic instability?," *Radiation research*, vol. 157, no. 4, pp. 365-70, Apr. 2002.

[8] F. M Lyng et al., "Apoptosis is initiated in human keratinocytes exposed to signalling factors from microbeam irradiated cells.," *International Journal of Radiation Biology*, vol. 82, no. 6, pp. 393-399, 2006.

[9] L. A. Ryan, R. W. Smith, C. B. Seymour, and C. E. Mothersill, "Dilution of irradiated cell conditioned medium and the bystander effect.," *Radiation research*, vol. 169, no. 2, pp. 188-96, Feb. 2008.

[10] J. R. Whiteside and T. J. McMillan, "A bystander effect is induced in human cells treated with UVA radiation but not UVB radiation.," *Radiation research*, vol. 171, no. 2, pp. 204-11, Feb. 2009.

[11] H. Nishiura, J. Kumagai, G. Kashino, T. Okada, K. Tano, and M. Watanabe, "The Bystander Effect is a Novel Mechanism of UVA-Induced Melanogenesis.," *Photochemistry and photobiology*, vol. 88, no. 2, pp. 389-397, Mar. 2012.

[12] W. Han et al., "Constitutive nitric oxide acting as a possible intercellular signaling molecule in the initiation of radiation-induced DNA double strand breaks in non-irradiated bystander cells.," *Oncogene*, vol. 26, no. 16, pp. 2330-9, Apr. 2007.

[13] J. S. Dickey, F. J. Zemp, A. Altamirano, O. A. Sedelnikova, W. M. Bonner, and O. Kovalchuk, "H2AX phosphorylation in response to DNA double-strand break formation during bystander signalling: effect of microRNA knockdown.," *Radiation protection dosimetry*, vol. 143, no. 2–4, pp. 264-9, Feb. 2011.

[14] S. Chen et al., "Mitochondria-dependent signalling pathway are involved in the early process of radiation-induced bystander effects.," *British journal of cancer*, vol. 98, no. 11, pp. 1839-44, Jun. 2008.

[15] T. K. Hei et al., "Mechanism of radiation-induced bystander effects: a unifying model.," *The Journal of pharmacy and pharmacology*, vol. 60, no. 8, pp. 943-50, Aug. 2008.

[16] F. A. Cucinotta, H. Nikjoo, and D. T. Goodhead, "The effects of delta rays on the number of particle-track traversals per cell in laboratory and space exposures.," *Radiation research*, vol. 150, no. 1, pp. 115-9, Jul. 1998.

[17] H. NIKJoo, P. O'Neill, D. T. GOODHEAH, and M. TERRISSOL, "Computational modelling of low energy electron-induced DNA damage by early physical and chemical events," *International Journal of Radiation Biology*, vol. 71, no. 5, pp. 467-483, 1997.

[18] H. Nikjoo and D. T. Goodhead, "Track structure analysis illustrating the prominent role of low-energy electrons in radiobiological effects of low-LET radiations," *Physics in Medicine and Biology*, vol. 36, no. 2, pp. 229-238, Feb. 1991.

[19] N. Desai, E. Davis, P. O'Neill, M. Durante, F. a Cucinotta, and H. Wu, "Immunofluorescence detection of clustered gamma-H2AX foci induced by HZE-particle radiation.," *Radiation research*, vol. 164, no. 4 Pt 2, pp. 518-22, Oct. 2005.

[20] I. Mosse, P. Marozik, C. Seymour, and C. Mothersill, "The effect of melanin on the bystander effect in human keratinocytes.," *Mutation research*, vol. 597, no. 1–2, pp. 133-7, May 2006.

[21] C. Mothersill et al., "A role for bioelectric effects in the induction of bystander signals by ionizing radiation?," *Dose-response : a publication of International Hormesis Society*, vol. 5, no. 3, pp. 214-29, Jan. 2007.

[22] M. Konopacka, J. Rogoliński, and K. Slosarek, "Direct and bystander effects induced by scattered radiation generated during penetration of radiation inside a water-phantom.," *Mutation research*, vol. 721, no. 1, pp. 6-14, Mar. 2011.

[23] D. Fink, *Fundamentals Of Ion-Irradiated Polymers*, vol. 2004. Springer, 2004, pp. 155, 179, 362.

[24] "James Ziegler - SRIM & TRIM." [Online]. Available: http://www.srim.org/. [Accessed: 19-Apr-2012].

[25] J. B. Birks, "Scintillation from organic crystals: Specific flourescecne and relative response to different radiation," *Proc. Phys. Soc A*, vol. 64, pp. 874-877, 1951.

[26] Q. Chen, T. Hajagos, and Q. Pei, "Conjugated polymers for radiation detection," *Annual Reports Section "C" (Physical Chemistry)*, vol. 107, p. 298, 2011.

[27] S. Nagata, K. Takahiro, B. Tsuchiya, H. Katsui, and T. Shikama, "Ion beam induced luminescence of polyethylene terephthalate foils under MeV H and He ion bombardment," *Nuclear Instruments and Methods in Physics Research Section B: Beam Interactions with Materials and Atoms*, vol. 267, no. 8–9, pp. 1553-1556, May 2009.

[28] L. Torrisi, a. Desiderio, and G. Foti, "High energy proton induced luminescence in F-doped polyvinyltoluene," *Nuclear Instruments and Methods in Physics Research Section B: Beam Interactions with Materials and Atoms*, vol. 166–167, pp. 664-668, May 2000.

[29] A. Quaranta, A. Vomiero, S. Carturan, G. Maggioni, and G. Della Mea, "Polymer film degradation under ion irradiation studied by ion beam induced luminescence (IBIL) and optical analyses," *Nuclear Instruments and Methods in Physics Research Section B: Beam Interactions with Materials and Atoms*, vol. 191, no. 1–4, pp. 680-684, May 2002.

[30] Y. Zengliang, *Introduction to Ion Beam Biotechnology*. Hefei, China: Springer Sciences + Business Media Inc, 2006, pp. 62, 68, 146.

[31] P. Rossi, C. D. Maggio, G. P. Egeni, A. Galligioni, and G. Gennaro, "Cytological and histological structures identification with the technique IBIL in elemental microanalysis," *Nuclear Instruments and Methods in Physics Research*, vol. 181, pp. 437-442, 2001.

[32] J. Pallon et al., "Ionoluminescence technique for nuclear microprobes," *Nuclear Instruments and Methods in Physics Research B*, vol. 130, pp. 199-203, 1997.

[33] D. Kulms, B. Pöppelmann, D. Yarosh, T. a Luger, J. Krutmann, and T. Schwarz, "Nuclear and cell membrane effects contribute independently to the induction of apoptosis in human cells exposed to UVB radiation.," *Proceedings of the National Academy of Sciences of the United States of America*, vol. 96, no. 14, pp. 7974-9, Jul. 1999.

[34] R. P. Phillopson, S. E. Tobi, J. A. Morris, and J. M. and Trevor, "UV-A induces persistant genomic instability in human keratinocytes through an oxidative stress mechanism," *Free Radical Biology & Medicine*, vol. 32, no. 5, pp. 474-480, 2002.

[35] W. Becker, *Advanced Time-Correlated Single Photon Counting Techniques (Springer Series in Chemical Physics)*. Springer, 2005, pp. 213-261.

[36] M. Stefl, N. G. James, J. A. Ross, and D. M. Jameson, "Applications of phasors to in vitro time-resolved fluorescence measurements.," *Analytical biochemistry*, vol. 410, no. 1, pp. 62-9, Mar. 2011.

[37] K. Kosev et al., "Evaluation of a microchannel-plate PMT as a potential timing detector suitable for positron lifetime measurements," *Nuclear Instruments and Methods in Physics Research Section A: Accelerators, Spectrometers, Detectors and Associated Equipment*, vol. 624, no. 3, pp. 641-645, Dec. 2010.

[38] D. W. Piston, "Fluorescence anisotropy of protein complexes in living cells.," *Biophysical journal*, vol. 99, no. 6, pp. 1685-6, Sep. 2010.

[39] M. D. Keller et al., "Autofluorescence and diffuse reflectance spectroscopy and spectral imaging for breast surgical margin analysis.," *Lasers in surgery and medicine*, vol. 42, no. 1, pp. 15-23, Jan. 2010.

[40] Y. Sun, C. Wang, and J. Dai, "Biophotons as neural communication signals demonstrated by in situ biophoton autography.," *Photochemical & photobiological sciences : Official journal of the European Photochemistry Association and the European Society for Photobiology*, vol. 9, no. 3, pp. 315-22, Mar. 2010.

[41] Hamamatsu, "Technical Information APR. 2001," in *Photon Counting Using Photomultiplier Tubes*, 2001.

[42] "Faraday cup - DREEBIT GmbH." http://www.dreebit.com/en/products/faraday_cup_9/.

[43] L. Pirisi, S. Yasumoto, M. Feller, J. Doniger, and J. A. DiPaolo, "Transformation of human fibroblasts and keratinocytes with human papillomavirus type 16 DNA.," *J. Virol.*, vol. 61, no. 4, pp. 1061-1066, Apr. 1987.

[44] F. M. Lyng et al., "Apoptosis is initiated in human keratinocytes exposed to signalling factors from microbeam irradiated cells.," *International journal of radiation biology*, vol. 82, no. 6, pp. 393-9, Jun. 2006.

[45] W. Friedland, P. Kundrát, and P. Jacob, "Track structure calculations on hypothetical subcellular targets for the release of cell-killing signals in bystander experiments with medium transfer.," *Radiation protection dosimetry*, vol. 143, no. 2–4, pp. 325-9, Feb. 2011.

[46] "van de graaff generator." [Online]. Available: http://hyperphysics.phy-astr.gsu.edu/hbase/electric/vandeg.html.

Chapter 2

IBIL and Radiation Induced Bystander Effects

2 Ion Beam Induced Luminescence; Relevance to Radiation Induced Bystander Effects

S.B. Ahmad, F.E. McNeill, S.H. Byun, W.V. Prestwich, C. Seymour, C.E. Mothersill, Ion Beam Induced Luminescence; Relevance to Radiation Induced Bystander Effects, Nucl. Instr. and Meth. in Phys.Res. B (2012), Vol 288, pp 81-88

2.1 Chapter summary

This chapter has been reproduced (permission from journal attached in the Appendix) from the aforementioned publication in nuclear instruments and methods in physics research B. The aim of this paper was to try and quantify the light emitted as a result of charged particle interaction in materials which may be of relevance to radiation induced "bystander effects" studies. We have developed a system which employs the technique of single photon counting to measure the light emitted from samples irradiated under vacuum by a charged particle beam. The system uses a fast photomultiplier tube (Hamamatsu R7400p) with a peak cathode response at 420 nm wavelength. It has been tested in a proof-of-principle experiment using polystyrene targets. Light output, as a result of irradiation, was measured. The luminescence yield appears to have a non-linear behavior with the incident Ion fluence: it rises exponentially to an asymptotic value. The target was irradiated with beam energies varying from 1 MeV to 2.0 MeV and showed saturation at or before an incident fluence rate of 3×10^{13} $H^{+}/cm^{2}s$. The average saturation value for the photon output was found to be 40×10^{6} cps. Some measurements were performed using filters to study the emission as specific wavelengths. In the case of filtered light measurements, the photon output was found to saturate at 28×10^{3}, 10×10^{6}, and 35×10^{6} cps for wavelengths of 280±5 nm, 320±5 nm and 340±5 nm respectively. The light output reaches a maximum value because of damage induced in the polymer. Our measurements indicate a "damage cross section" of the order of 10^{-14} cm^{2}. The average radiant intensity was found to increase at wavelengths of 280 nm and 320 nm when the proton energy was increased. This was not found to occur at 340 nm wavelengths. In conclusion, the light emission at specific wavelengths was found to depend upon the incident proton fluence and the proton energy. The wavelengths of the emitted light measured in this study are in ranges that have significance for the understanding of radiation induced bystander effects.

All the work represented in this article was performed by me (First author) and the manuscript was revised by all the co-authors. The funding for this work came from McMaster University and Natural Sciences and Engineering Research Council of Canada under the supervision of Dr. Fiona E. McNeill (Associate Vice President Research and International Affairs, McMaster University).

2.2 Introduction

The assessment of radiation risk at low doses has been controversial in the scientific community for several years, with both "harmful" and "beneficial" effects of low dose radiation having been observed. In order to better understand the effects of the lowest radiation dose, that is, a single charged particle in a single living cell, many biological micro-beams have been developed. Many of the micro-beams around the world use protons or ^{3}He particles for irradiation. The focus of these studies is to quantify and better understand low dose radiation effects. The radiation induced "bystander effect" has been widely studied under conditions of low dose exposures, but is still not well understood. There are principally two forms of bystander experiment used in the radiation biology community. One form of the bystander effect is observed through medium transfer experiments. Cells are irradiated and the medium from those cells is removed and added (or "transferred") to a separate group of non-irradiated reporter cells. Changes are observed in the reporter cell line, despite their not having been a direct radiation target. A second experimental form of the bystander effect is where micro-beams are used to irradiate certain cells on a plate, and effects in non-irradiated cells nearby are studied. Both sets of experiments are labeled as "bystander" but they are, of course, different in character and experimental design.

Both types of bystander or non-targeted effects have been quantified in terms of several different biological end points and a detailed account of these biological end points is given by Dieter et al and Mothersill et al [1, 2, and 3]. Of interest to our research group has been the fact that these end points have not only been observed for charged particle radiation, but also for x-rays, gamma rays [1, 4] and ultraviolet light [5]. The medium diffusible signal has been analyzed for its depth of penetration and it has been reported [4] that the distance between irradiated cells and bystander cells is not a critical parameter, and each cell has equal probability of receiving the signal within a given radius around the targeted cell. Since the actual chemistry of the signal is yet to be determined in medium transfer "bystander effect" studies and bystander models, it is assumed that the signal is able to multiply itself i.e. when one cell encounters a bystander molecule it respond to that and produce another signal molecule. However micro-beam studies have shown that the damage distribution is not random but shows a tendency for clustering amongst the damaged non-irradiated cells [7].

Our hypothesis is that several separate events or types of signal are taking place and this is confusing the understanding of the "bystander effect". It is not a single effect but, in fact, several. There is obviously the biology and chemistry of the process, as effects are observed using medium transfer experiments. Some signal molecule is in the medium that is transferred. However, the extensive use of charged particle beams for such studies suggests, to us, a further need for the investigation of the physics of the interactions. We wished to study the secondary radiation produced as result of the dense excitation and

ionization along the track of the charged particle. The range of δ-rays, i.e. energetic secondary electrons, have been quantified and the physics of this type of secondary radiation is well documented, but the role of emitted UV and visible light has not been explored extensively in the context of radiation biology effects.

Molecular (or atomic) excitations can lead to the production of a significant amount of light in the UV and visible wavelength ranges. If molecular de-excitation is occurring and creating photons in the UV range then the possibility arises of absorption of these UV photons in cells, not originally targeted by the ion beam and the subsequent triggering of a biological response. Studies with UV exposed cells have shown that UV (especially UVB) is involved in the production of oxides of nitrogen that are considered to be one of the candidates for inducing non-targeted effects in bystander cells [6, 7, 8, 16].

The goal of the present study was to develop a system to measure and quantify the visible and UV light that may be emitted from a primary beam of charged particles incident on an organic and ultimately biological sample in order to discover whether some "bystander effects" observed in micro-beams may actually be arising from a physical, that is UV signal, rather than from a biological or chemical signal. This article describes the development of the system, and provides details of the ability to measure light emitted from polystyrene targets irradiated with protons.

2.3 Materials and Methods

2.3.1 Irradiation Configuration

Targets made of organic material, polystyrene, were irradiated with protons with energies ranging from 1 MeV to 2.0 MeV. The protons were produced by a 3 MV KN Van de Graaff accelerator. The proton fluence rate was kept in the order of ~ 10^{13} protons/cm^2s by means of a copper aperture that was isolated from the rest of the system using ceramic pellets in order to provide information regarding total current incident on the aperture. The first generation configuration is shown in Figure 2.1 (enlarged picture). This method of current measurement was found to ultimately not to be accurate as a method of quantifying the target current, but was used to properly steer the proton beam through the aperture.

In the initial set of experiments using this first generation system, the target was fixed on an aluminum mount at an angle of 45^o to the beam line direction. Figure 2.1 shows the general measurement setup. The whole system was kept under vacuum in a light tight chamber. In this setup, the simultaneous measurement of target light output and proton fluence (or target current) was not possible. In order to determine the proton current, a removable conducting plate, isolated from the rest of the chamber, had to be fixed at the opposite end to the aperture. This method could only provide an estimate of current falling on the target because once the current was measured; this plate had to be

removed by venting the chamber. The chamber then had to be re-pumped down to vacuum for the light output measurement.

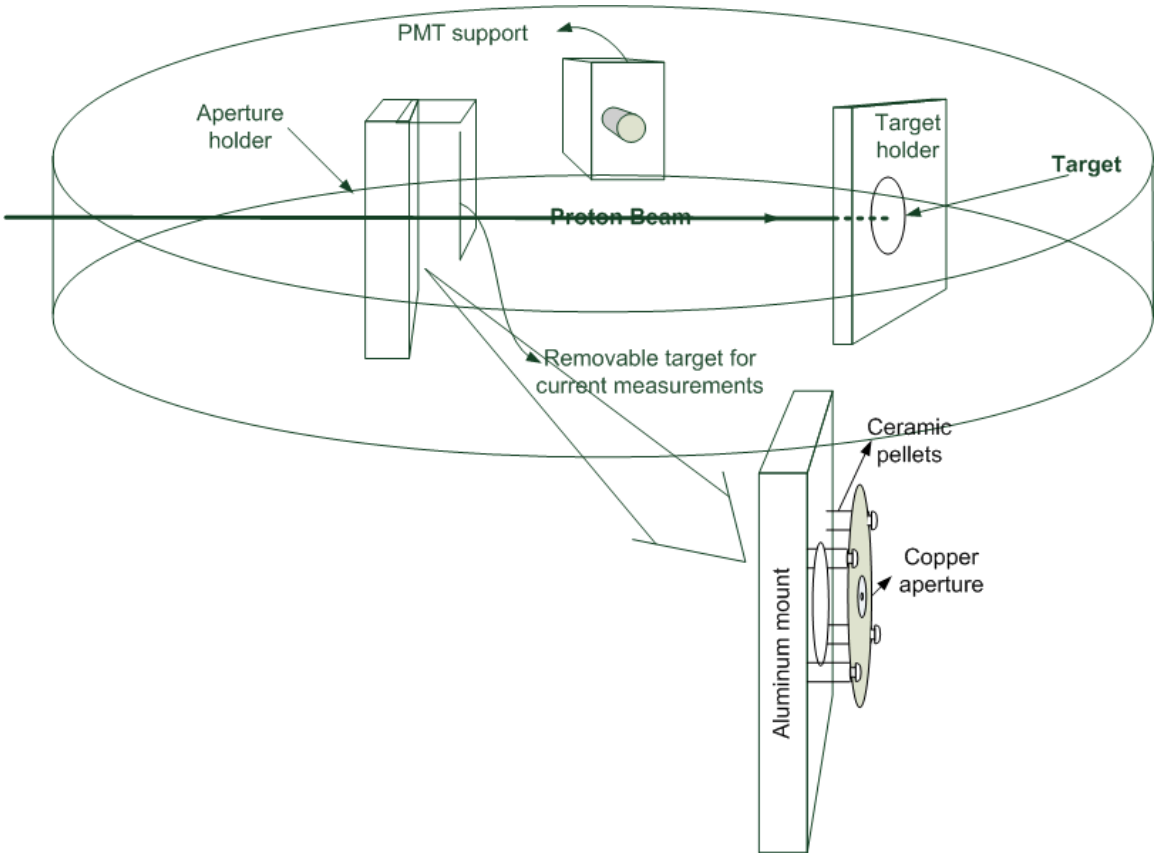

Figure 2.1 Experimental setup for IBIL (ion beam induced luminescence) measurement. The enlarged figure shows a copper aperture mounted on an aluminum mount aligned with beam center.

Measurements performed with this setup indicated the need for correct fluence rate measurement. We therefore developed a second generation system that employed the technique of moving the target in and out of the beam path so that the beam could be captured in a Faraday cup like arrangement. This did not require venting the chamber. The target could be moved from outside of the chamber. The target was placed out of the beam, the current measured, and then the target moved back into the beam. The total length of this arrangement was kept to 22 cm. The beam hits a flat aluminum flange which is isolated from the rest of the chamber using a pendex type fitting. This makes a hollow tube arrangement, so that any secondary electrons emitted from the flat aluminum flange as a result of the incident proton beam can be reabsorbed: a concept similar to the one that is used in a Faraday cup. This current measurement setup was calibrated against the Faraday

cup that is in the beam line just before the chamber. We found a 100 % agreement between the beam line Faraday Cup measurements and measurements made in our arrangement, for currents up to 5 μA. A full schematic diagram of the experimental setup is shown in Figure 2.2.

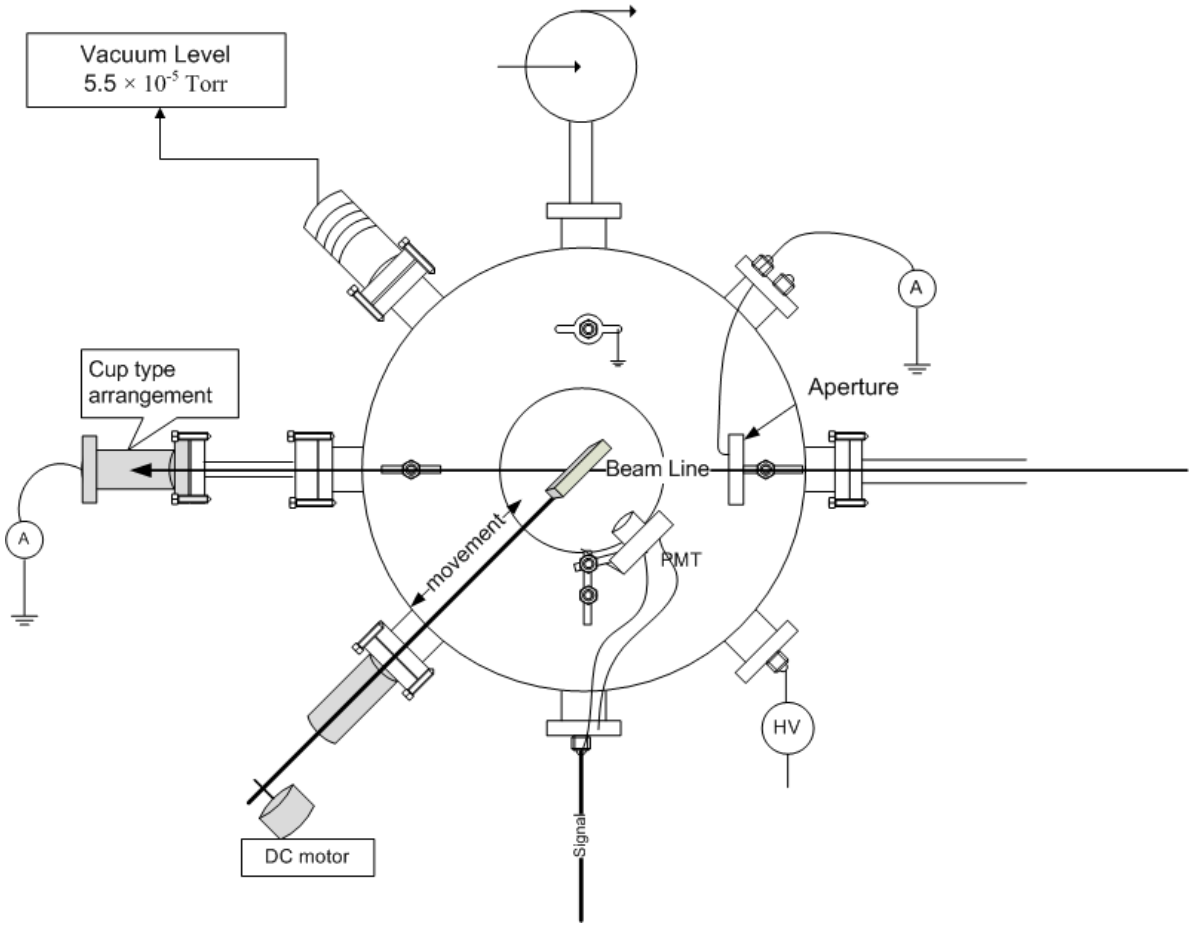

Figure 2.2 Schematic diagram of the complete experimental setup

The chamber shown in Figure 2.2 has a diameter of 34 cm and has several ports with various purposes as shown in the figure. Movement of the target was controlled remotely through one of the ports that was fitted with a bellows actuator, capable of providing a linear motion of 2 inches. The position of the target was monitored using a scale, fixed close to the DC motor outside of the chamber that could be seen using a camera from the KN accelerator operating station. The face of the light detector, i.e. photomultiplier tube (PMT), was kept parallel to the face of the target. The beam enters the target at an angle of 45^{o} making the detector perpendicular to the beam line. Using this system of moving the target, a series of experiments was performed at various proton fluences and energies.

2.3.2 Target material

This proof-of-principle and system development study required a sample that can be placed inside a vacuum, yet still has radiation interaction properties similar to a biological sample. We also chose a material that would be relatively transparent to most of the visible and UV spectrum, to prevent self-absorption, so that the photons could be measured outside of the sample. We therefore used thin polystyrene sheets as the target material during the development of the system and initial proof of principle experiments. The goal will ultimately be to measure a series of biological and organic materials relevant to radiation biology experiments.

Polystyrene has the advantage of a long history of use in the field of radiation meteorology. It has an effective atomic number of 5.96 and is therefore a suitable tissue equivalent material for radiation dosimetry. The target samples were prepared from pure polystyrene pellets in the form of 5×2 cm^2 slabs. The thickness of each slab was set to 500 μm so that the proton beam was completely absorbed in the polymer.

2.3.3 Photon Counting

We focused on measuring the luminescence in terms of absolute value using the technique of single photon counting. Using this second-generation system, mentioned earlier, photon counting was performed using a Hamamatsu Photomultiplier tube (R7400P), having peak photo-cathode's radiant sensitivity at a wavelength of 420 nm, operated at -800 V. The high voltage was supplied through an ORTEC standard NIM module 459. Pulse processing was performed using an ORTEC pulse single photon counting unit. This unit comprises a fast preamplifier, model 9301, amplifier/discriminator, model 9302, and a counter/timer module, model 994, capable of counting at a frequency of 100 MHz for negative input pulses and 20 MHz for positive input pulses. We set the counter to negative input pulse mode.

In order to quantify the presence of different wavelengths in the spectrum of emitted photons, band-pass Interference filters were used. These filters have very small (FWHM, 10 nm) transmittance across the substrate and are extremely angle sensitive. Because they offer a very narrow band for transmission, their transmission is reduced. In order to keep the emitted IBIL light perpendicular to the surface of the filters, the light was collimated with the help of UV fused silica double convex lens. It has a linear transmittance of 90 % for wavelengths ranging from 210-1000 nm. The combination of lens, filter and PMT was mounted in a hollow tube of varying radii to accommodate all of these together. During the experiment the lens was kept at a distance of 1.8 cm (focus of the lens) from the point of interaction of the ion beam with the polystyrene target.

The angular spectral radiance was calculated using the following relationship;

$$L_\lambda(\vec{\Omega}) = (h\frac{c}{\lambda})\frac{\dot{C}}{\varepsilon}\frac{1}{A_C}\frac{1}{\Delta\lambda}\frac{1}{\Delta\Omega}\frac{1}{\cos\theta} \quad \text{..... eq 1}$$

h; Plank's Constant

$\dot{C}$; is the photon count rate

ϵ; is the detector efficiency for the range of wavelengths in question

$\Delta\Omega$; is the PMT solid angle

$\Delta\lambda$; is the filter band width

A_c; PMT collimator area

θ; angle between viewing direction and small area surface

Each presented result of measurement of the polystyrene target is an average of 5-10 separate measurements. The target was irradiated for a period of 5 or 10 seconds and the counts were recorded. After the first measurement, the target was moved to a new position for a second measurement and so on. The final result was an average of the series of measurements. The average was calculated from 5-10 different readings at the same nominal fluence rate. The variance of the average value should therefore incorporate variance due to fluctuations in light output that arise from fluctuations in the beam current on the target. Since the beam current was not measured simultaneously with the IBIL measurements, we had estimated the level of beam fluctuation prior to the IBIL measurements and observed it to be less than 3 %.

All the data represented in this paper were background corrected. Here the "background counts" do not refer to the PMT dark current (which was less than 20 counts per second) but by this we mean the count rate observed when the proton beam was on, but no sample was present in the beam. This background is generated as a result of beam interactions with the residual gases in the chamber, and possibly from the interaction of beam with the aluminum flange, or Faraday cup (Figure 2.2).

2.4 Results and Discussion

Initial experiments were performed using the first generation system (shown in Figure 2.1) to measure an optimum time for irradiating the polymer. After a certain amount of time, losses due to damage in the polymeric structure can become significant. Here the losses refer to IBIL losses. However ion induces damage can also alter, significantly, the

optical properties of the polymer [9]. Measurements performed over long time scales could, in principle, show reduced absolute luminescence. There is limited data available on this issue, but other authors have shown degredation of the polymer with a resulting luminescence loss [15]. These authors have published various "degradation parameters". For example A. Quaranta et al studied a relationship between the evolution of optical and chemical properties of Polymethylmethacylate (PMMA) and the IBIL spectrum using H^+, He^+ and N^+ ions [10]. Another study was performed for IBIL measurements in thin film Polyvinyltoluene (PVT) in order to evaluate the degradation of intrinsic fluorescence bands of the polymer upon ion beam irradiation [11]. These studies provide the evidence of the emission of light from ion irradiated polymers, but also evidence of losses with time.

The luminescence yield decreases with the time of irradiation, as shown in Figure 2.3a, and the rate of reduction is a function of the primary incident particle fluence rate. For incident proton fluence rates kept to the order of 10^{13} particles/cm^2.s, the decrease was found to be exponential, but with a shoulder that indicates that the actual exponential loss starts only after a certain time (approximately 60 s). An exponential fit in the later part of the graph shows a decrease at a rate of $7\pm0.4\times10^{-3}$ cps and $13\pm2\times10^{-3}$ cps for 1×10^{13} and 5×10^{13} particles cm^{-2}s^{-1} respectively. In the case where the incident fluence rate was increased to $\sim10^{15}$ particles cm^{-2}s^{-1} the loss in luminescence was much more prominent and followed a bi-exponential behaviour with the first exponential decaying at a rate of 30×10^{-3} cps and the second exponential decaying at 9×10^{-3} cps. The rise time of the photomultiplier tube (0.78 ns) suggests that data can be acquired with a rate limited only by the counter's counting frequency which is stated to be 100×10^6 cps. However, as is evident from Figure 2.3a, the photomultiplier tube seems to saturate much earlier at a count rate of $\sim20\times10^6$-30×10^6 cps.

The measurement set-up was different for the irradiations performed at $\sim10^{15}$ particles/cm^2.s, where the PMT was placed at a much longer distance (7.45 cm) from the source, compared to the 1.8 cm for the $\sim10^{13}$ particles/cm^2.s irradiations. The reason for setting a closer distance in the latter case was that a collimating system with a lens focal length of 1.8 cm was used.

A solid angle correction applied to the data (shown in Figure 2.3b) indicates that the light output for a proton fluence rate of the order of 10^{13} particles/cm^{2}s could be much more than that observed. Figure 2.3a shows that if PMT saturation were not a limiting parameter in the experiment then the light output could become proportional to the incident fluence as observed in Figure 2.3b in the case of 1×10^{13} particles/cm^{2}s. The backward projected exponential gives a value of counting frequency of 32×10^6 cps and in the case of 5×10^{13} particles/cm^{2}s it gives a value of 39×10^6 cps.

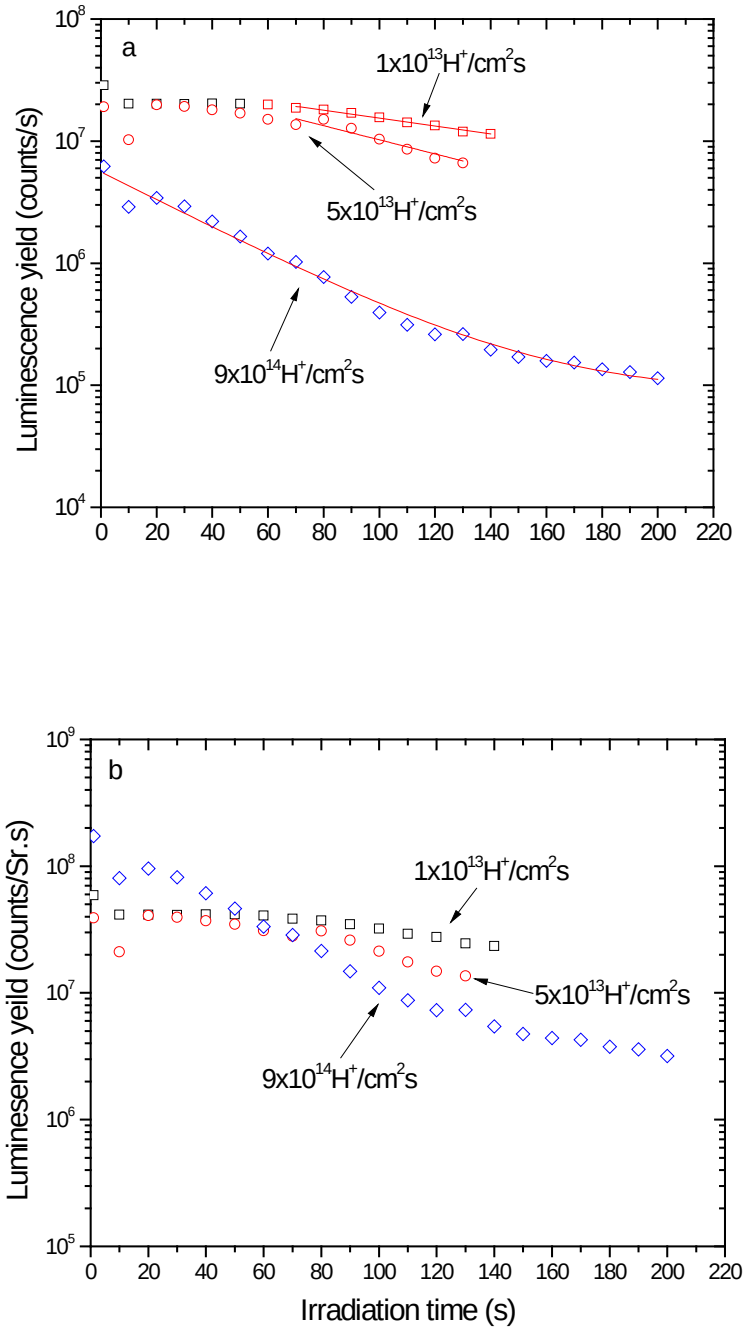

Figure 2.3 Decaying light with the incident proton irradiation. Data in 'a' has not been corrected for solid angle in order to observe Photomultiplier saturation. 'b' shows the data after solid angle correction.

Previous studies with other polymers have shown that luminescence yield increases with the increase in incident particle fluence, if the fluence is kept below 10^{12} particles/cm^2 [12, 14]. In these studies, the response has been normalized to the proton fluence, however since we used a single photon counting detector, we present the luminescence yield in absolute terms. However other studies [13], performed for a different polymer, show a bi-exponential decrease in emission intensity with time if the incident particle fluence is more than 10^{14} particles/cm^2. The objective of this study was to quantify the actual light output from the interaction of charged particle in biological media so that its potential significance to bystander effects can be understood.

The results of the photon output variation with the variation in incident proton (H^+) fluence rate are plotted in Figure 2.4 for two different energies of 1.0 MeV and 1.2 MeV. Each data point represents an irradiation of 5-10 sec. Results were normalized to time in order to calculate a count rate. As mentioned previously in this article, the count rate was not observed to reduce significantly over a 10 second irradiation. We therefore collected the data over a 10 second interval for each data point, in order to obtain better statistics. This data has been corrected for the solid angle and the lens transmission only in Figure 2.4a, and solid angle, lens transmission and photomultiplier dead time in Figure 2.4b. Figure 2.4a suggests that for lower values of incident fluence, the luminescence yield can become proportional to the incident fluence (consistent with [13]) and saturates at a fluence of approximately 3×10^{13} particles/cm^2. This saturation could be attributed to the photomultiplier tube saturation; however, the literature shows that an increase in incident ion fluence reduces the luminescence yield. This is because of loss of the primary electrons that were supposed to contribute to the luminescence for low LET radiation. The same phenomenon occurs because of quenching for high LET radiation [14]. In order to eliminate the effect of PMT saturation, arising from dead time effects, we corrected the data for the PMT dead time. It can be seen that with the dead time correction applied, the saturation trend in Figure 2.4b remains the same as in Figure 2.4a. The saturation can therefore be attributed to effects in the polymer itself, and is not a count rate effect.

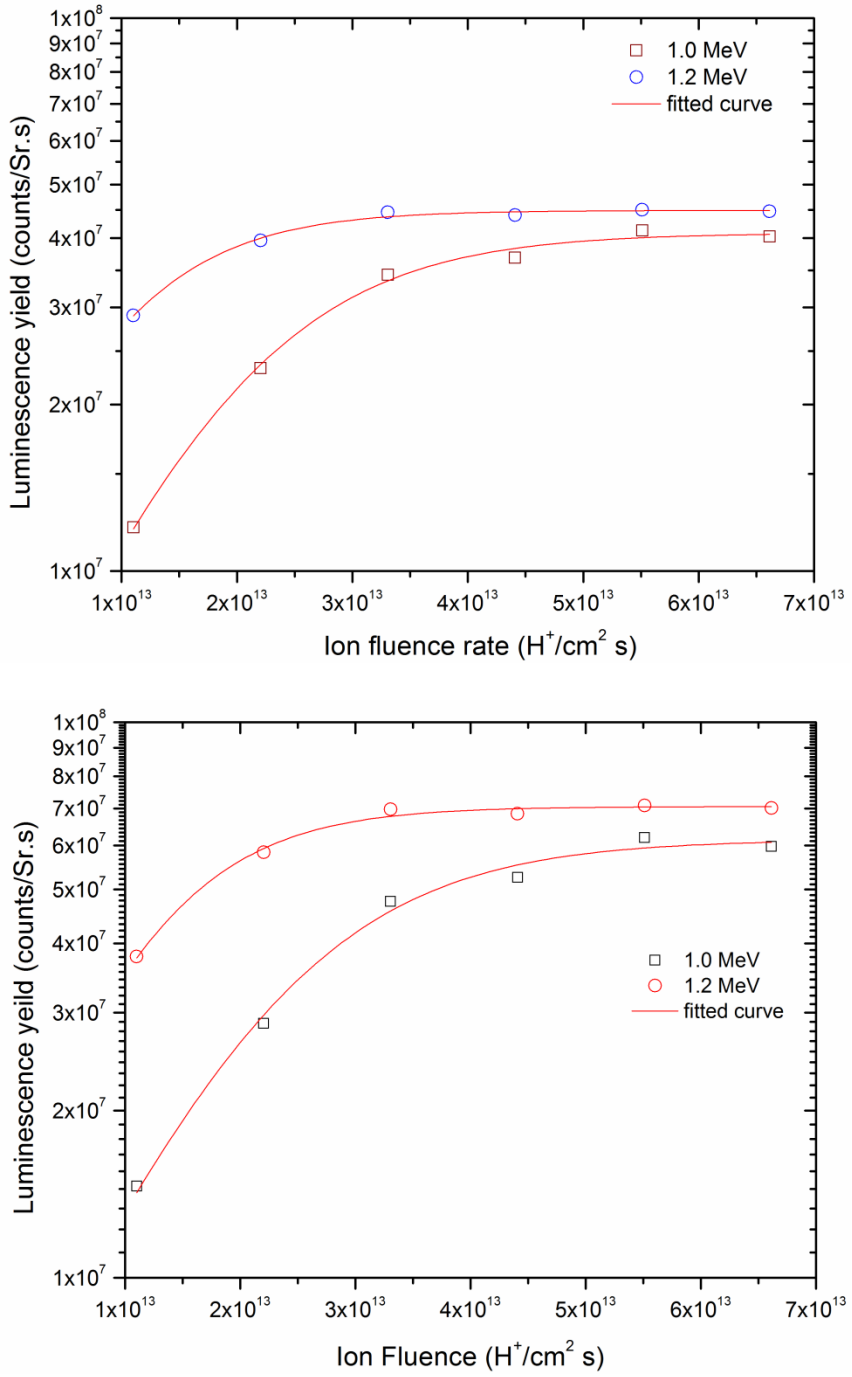

Figure 2.4 Variation of light output with incident ion fluence, (a) without PMT dead time correction (b) with PMT dead time correction

Table 2.1 describes this information more fully. In order to analyze the polymer saturation effects mathematically, the data was fitted using a least square fit described in equation 2 and Table 2.1 provides the results of the fits with and without dead time corrections. The data in the Table 2.1 demonstrate that the measured count saturation is occurring predominantly because of the damage to the polymeric structure rather than because of the PMT saturation, which we infer from the fact that the damage constant σ has similar values for both before and after the dead time correction. Luminescence yield as a function of energy lost per unit length shows a similar trend for a variety of other polymers and the data can be fitted according to a relationship developed by J. B. Birks [17]. Combining the data presented in Figure 2.3 and 2.4 suggests that the luminescence yield rises to reach a maximum asymptotic value for low incident ion fluences which then starts to fall exponentially if the fluence is increased further. As mentioned above, the light yield from polymers has been demonstrated previously to increase exponentially with the Ion fluence, but only when the fluence is kept very low. It has also been shown to decrease exponentially for higher Ion fluences.

Table 2.1 show values of various parameters used for a least square fit to the data in Figure 2.4 according to equation 2.

$$I(\varphi) = \frac{\mathrm{I_{max}}}{1+\mathrm{e}^{-\sigma(\varphi-\varphi_o)}} \ldots\ldots\ldots\ldots\ldots\ldots\ldots\ldots \text{Eq 2}$$

Here φ is the incident ion fluence and σ is the damage cross section. I_{max} and ϕ_o represent the saturation value for the light output and a fitting parameter for the data respectively. I_{max} is higher than the photomultiplier saturation (20×10^6-30×10^6 cps) in these cases because the data is corrected for solid angle and the lens transmission. The damage cross section indicates the size of the ion core track. Similar damage cross sections have been measured for a different polymer [13]. The calculations for damage cross section assume that the effect of quenching is negligible. We base this assumption upon the fact that the average LET within the polymer is low, and quenching effects are small compared with the effects of permanent damage in the polymer.

Table 2.1 Least square fitted parameters calculated for data in Figure 2.4

	Energy per proton	I_{max} (cps/Sr)	σ (cm^2)	φ_o ($cm^{-2}.s^{-1}$)
a (without dead correction)	**1 MeV**	$4.12\pm0.02\times10^7$	$11\pm1\times10^{-14}$	$1.92\pm0.09\times10^{13}$
	1.2 MeV	$4.53\pm0.04\times10^7$	$13\pm1\times10^{-14}$	$0.67\pm0.07\times10^{13}$
b (after dead time correction)	**1 MeV**	$6.15\pm0.23\times10^7$	$10\pm2\times10^{-14}$	$2.27\pm0.15\times10^{13}$
	1.2 MeV	$6.15\pm0.09\times10^7$	$14\pm2\times10^{-14}$	$1.00\pm0.07\times10^{13}$

Figure 2.5 shows data generated for light output variation against proton fluence rate measured at different times for beam energy (per proton) of 1.6 MeV in order to check the reproducibility of the measurements. A paired sample t-test shows that the mean of the two distributions is not significantly different from each other at a significance level of p = 0.05. The average deviation of all the data points is measured to be less than 12 %.

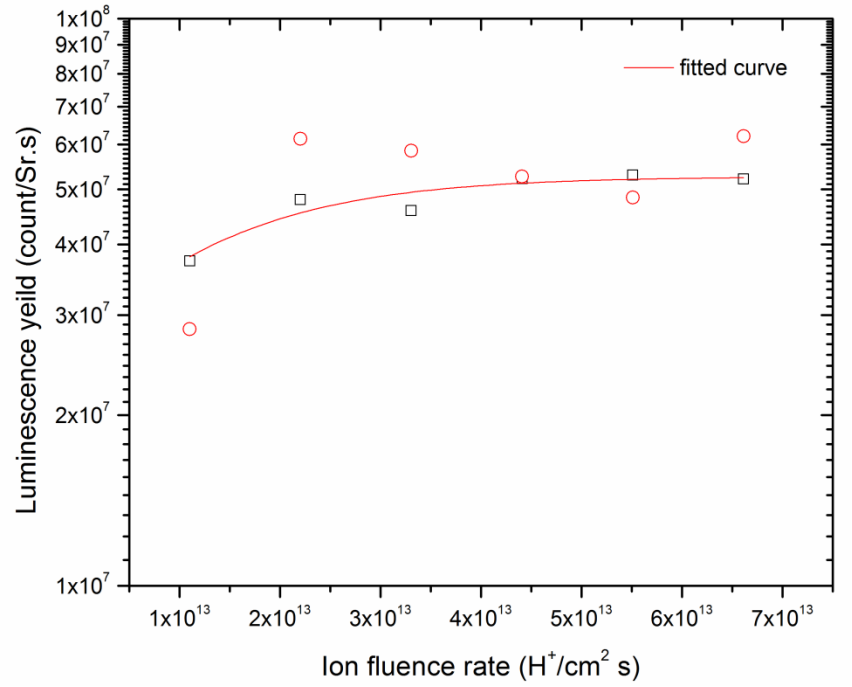

Figure 2.5 Reproducibility of the data measured at different times for a beam of energy 1.6 MeV. Solid line shows a fitted curve with a σ value of $8\pm4\times10^{-14}$ cm^2

Similar results were obtained (not shown here) for other incident particle energies up-to 2 MeV. However the light output saturates much more quickly for higher energies indicating that the damage increases with the beam energy. Thus both the increase in energy of the incident beam and fluence affect the luminescence yield.

The focus of this study was to investigate the presence of UV frequency light in the emitted light spectrum in order to establish a potential relationship between the emission of ion beam induced light and radiation induced bystander effects. Therefore we reduced the overall intensity of the light by filtering out every other frequency except for frequencies in the UVA and UVB range. UVA and UVB light have been shown to produce the same biological endpoints as found in some bystander experiments [8]. We filtered the light using three highly sensitive interference filters for wavelengths of 280 nm, 320 nm and 340 nm. These filters have a very narrow pass band (10 nm) around the centre frequencies. This high sensitivity reduces the efficiency of the filters down to 25 % and the collimating

lens reduces the light passing through by 90 %. This reduction in light proved useful in terms of keeping the PMT under its saturation value so that the effects can be observed for increasing Ion fluence.

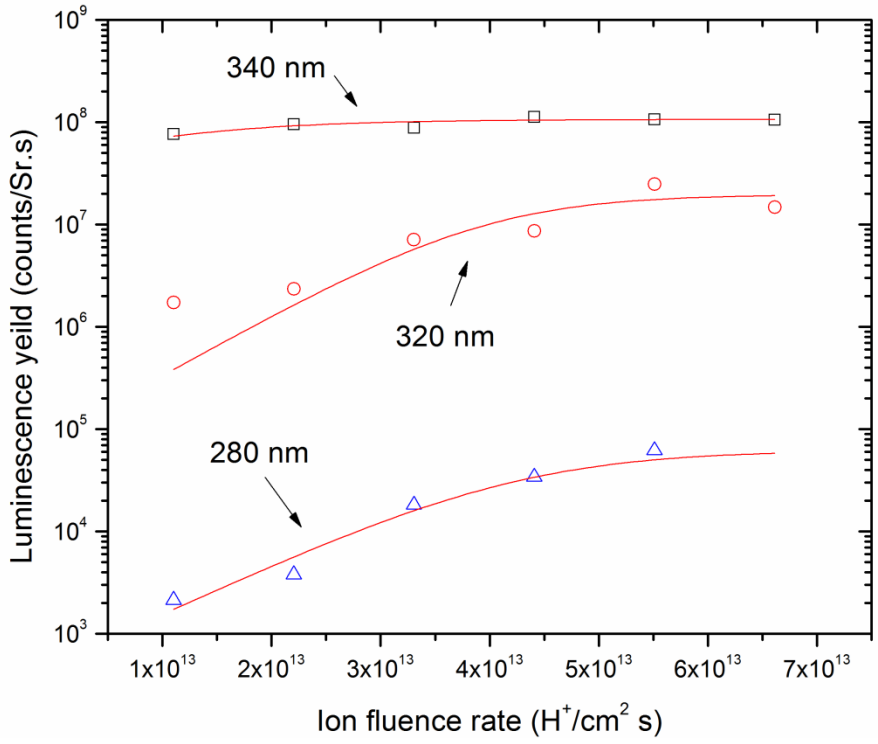

Figure 2.6 Variation of luminescence yield against the 1 MeV Proton fluence. Solid lines represents fit according to Eq. 2.

Figure 2.6 shows the light output against proton fluence rate at three different photon wavelengths. The energy of protons in this case was 1 MeV. In this graph the fitted curve shows a similar damage cross section to that shown earlier (values are quoted in Table 2.2), however the measured count rate was much lower (a max of 7.6×10^3 cps in the case of 280 nm, 3×10^6 cps in the case of 320 nm photons, and 27×10^6 cps in the case of 340 nm photon, before making any corrections for lens, solid angle etc) than the one at which the PMT was found to saturate. This indicates that increasing the proton fluence can only increase the luminescence yield up-to a certain limit, beyond which the damage in the organic structure causes a loss of proportionality between the light output and the incident fluence.

Table 2.2 Proton damage cross section for polystyrene calculated for photon output at different wavelengths using least squares fit. Values shown for the I_{max} in brackets represent saturation value without the filter correction.

	I_{max} (cps/Sr)	σ (cm^2)	φ_o (cm^{-2}.s^{-1})
280 nm	$6.22\times10^4(2.64\times10^4)^*$	$11\pm2\times10^{-14}$	$4.2\pm2.7\times10^{13}$
320 nm	$2.0\times10^7(1.08\times10^7)^*$	$14\pm14\times10^{-14}$	$4.0\pm0.9\times10^{13}$
340 nm	$1.07\times10^8(3.77\times10^7)^*$	$9.7\pm3\times10^{-14}$	$3.1\pm0.9\times10^{13}$

For all the other energies used in the experiment, the data shows a similar trend. However in the case of 340 nm photons the light output becomes significantly higher at proton energy of 1.2 MeV than the count rate that the photomultiplier tube can handle.

The data presented in Figures 2.4 to 2.6 confirm the production of photons in polystyrene at UV A and B frequencies. It also confirms the phenomenon of radiation induced damage. However this data cannot be extrapolated directly down to lower proton fluences, as there could be a different damage pattern at lower ion fluences.

Figure 2.7 shows a comparison of radiance output at frequencies of 280 nm, 320 nm and 340 nm for three different energies of the incident proton beam.

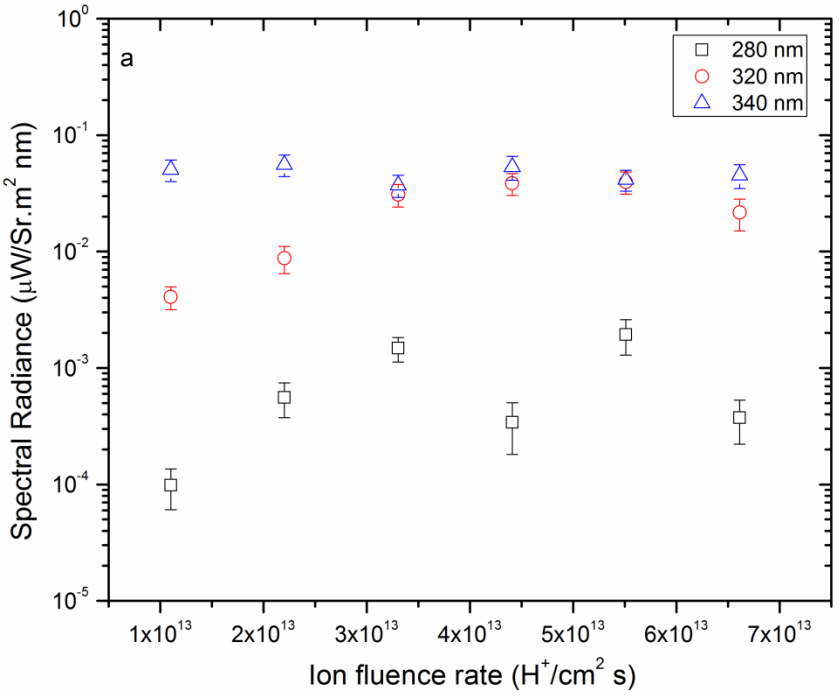

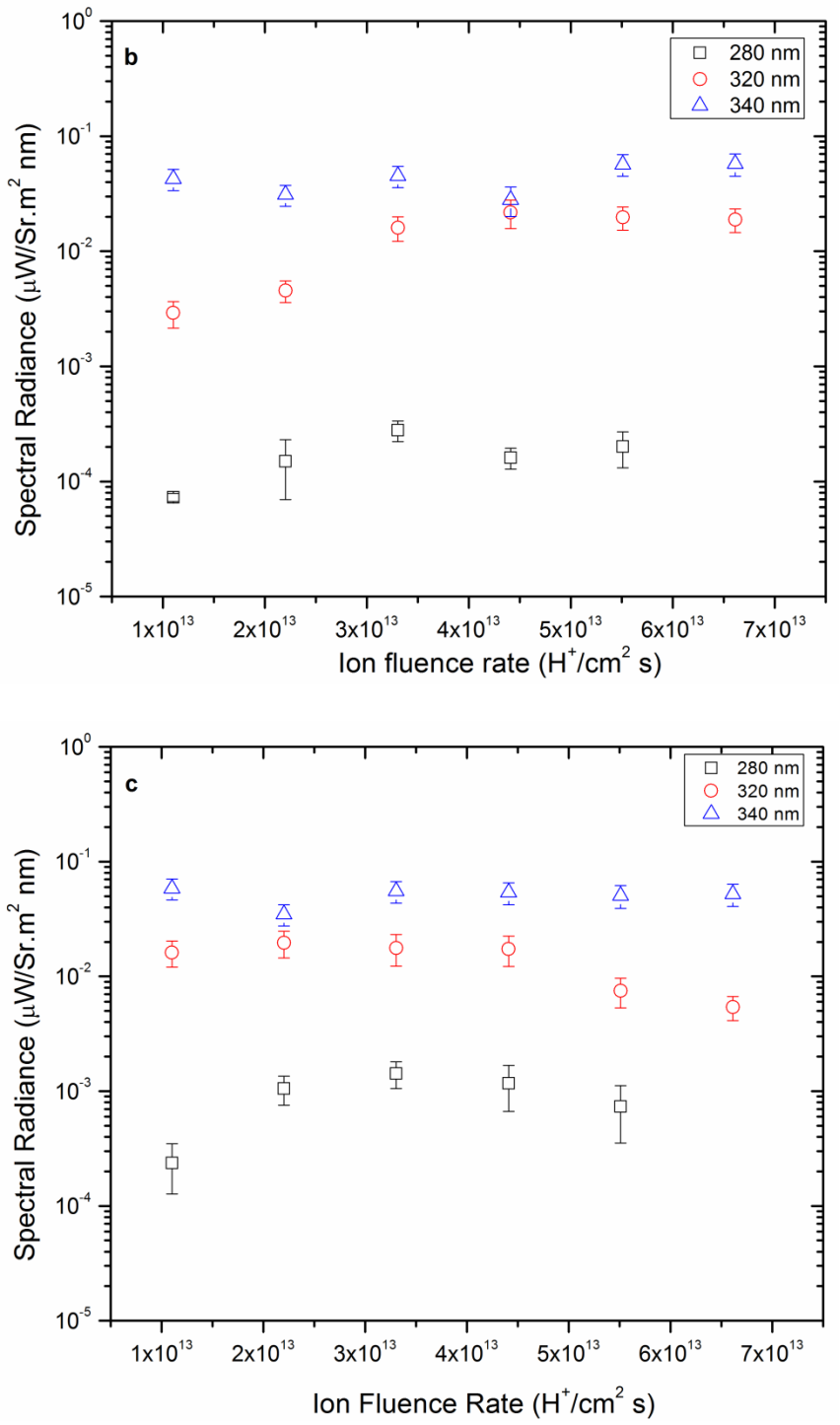

Figure 2.7 Comparison for the radiance output at 280 nm, 320 nm and 340 nm for beam energies of (a) 1.4 MeV (b) 1.6 MeV and (c) 1.8 MeV

The narrow wavelength range data represented in all of the above figures do not show a noticeable variation in light output with the variation in energy of the incident protons. (The three figures represent different incident energies.) However we also plotted the radiance at different wavelengths against the beam energy in order to further investigate if there is any variation of light output against the beam energy. Since the light output seems to saturate for incident ion fluences of more that ~10^{13} particles/cm^2.s, we averaged the light output data for all different ion fluences above ~10^{13} particles/cm^2.s and calculated the radiance which is plotted in Figure 2.8. This graph shows that increasing the energy of the incident proton beam does not contribute significantly towards increasing the overall luminescence yield but the yield at a specific light frequency may increase. We noticed an increase in the radiance output at frequencies of 280 nm and 320 nm as the beam proton energy was increased. However the radiance output at 340 nm does not change with the beam energy. This may indicate that the overall spectrum may shift with incident beam energy. It is difficult, however, to draw conclusions about the full spectrum with only three narrow spectral filters.

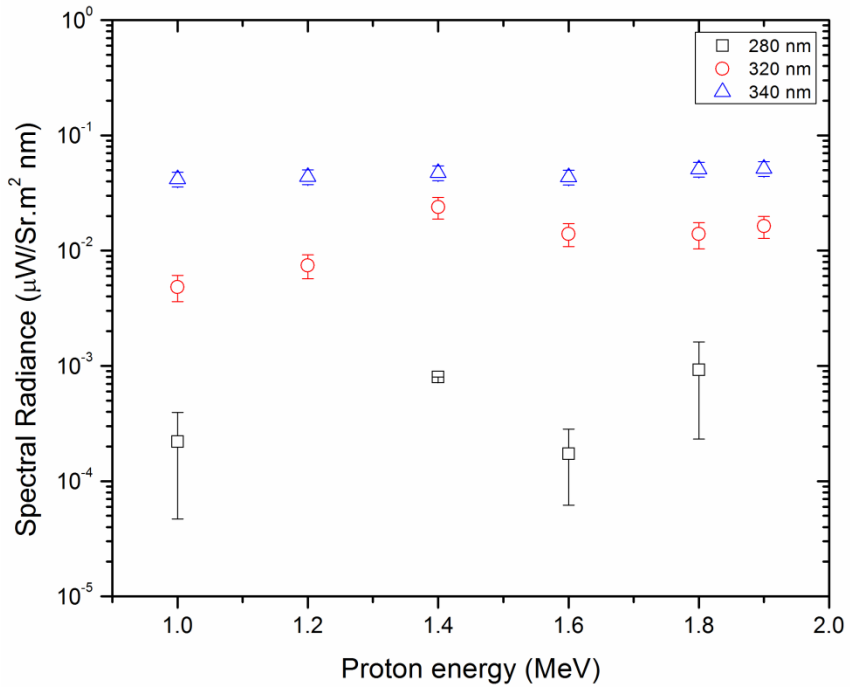

Figure 2.8 Radiance measured at different photon wavelengths against the energy of incident beam

As mentioned earlier, it is difficult to extrapolate data on light output from high proton fluences on polystyrene in a quantifiable way down to the low proton fluences used on biological materials in charged particle micro-beam experiments. However, we have in this manuscript demonstrated the development of a system that can measure the light output from proton irradiated materials, and have importantly shown, in a proof-of-

principle experiment, that UV frequency light is being emitted from materials irradiated with charged particle beams. We believe the role of these UV photons in the production of the "bystander response" seen using charged particle micro-beams needs further investigation. We suggest that future experiments should include measurement of light yield per unit path length against the linear energy transfer of the incident particles in biological media as this data generally does not exist for biological media. This data has been determined for some organic materials where the intention was to use them as scintillators. In addition, most of the available literature for IBIL measurements on polymers shows the light output in terms of arbitrary units, and is measured for very high incident ion fluences. Since the light yield rises asymptotically according to the Birks relationship, the output at low incident ion fluences or low energy lost per unit path length could be a significant proportion of the asymptotic or saturation value. Further experiments need to be performed on materials directly relevant to radiation biology experiments i.e. the biological materials themselves, but also the flasks and vessels used for experiment, at the proton fluences used in radiation biology experiments, in order to quantify the exact effect these visible and UV photons may have on the endpoints used in the experiments. This could lead to some useful information regarding the potential nature of some "bystander" interactions.

2.5 Conclusions

Charged particles are capable of producing dense ionizations in biological media that can either be neutralized thermally or with the emission of electromagnetic radiation. The emission and re-absorption of UV range electromagnetic quanta could have a biological significance and may explain some aspects of radiation induced bystander effects. We have built a system to measure the light output produced by charged particle beams and in a proof-of-principle experiment using polystyrene have demonstrated the emission of photons in the UV range induced by interaction with a proton beam. The emission intensity was found to saturate for a fluence of 3×10^{13} $H^{+}/cm^{2}s$. This saturation was attributed to damage in the polymer as dead time effects were accounted for. Variation in energy of the incident beam increased the light output count rate for low fluence but does not appear to change for higher fluence values. The light emission frequency spectrum appears to have a relationship with the incident proton energy, i.e. the colour of light emitted changes as the particle energy changes.

2.6 References

[1]. Frankernberg D., Greif K-D., and Giesen U., Radiation response of primary human skin fibroblasts and their bystander cells after exposure to counted particles at low and high LET, Int J. Radiat. Biol., Vol 82, No. 1, January 2006, pp. 59-67

[2]. Mothersill C. and Syemour C., Radiation-induced bystander effects: Past History and Future directions, Radiation Research, 155, 2001, 759-767

[3]. Mothersill C., and Seymour C., Medium from irradiated human epithelial cells but not human fibroblasts reduces the clonogenic survival of unirradiated cells, Int. J. Radiat. Biol. 1997, No 4, 421-427

[4]. Schettino G., Folkard M., et al, Low dose studies of bystander cell killing with targeted soft x-rays, Radiat. Res. 160, 2003, 505-511

[5]. Whiteside JR., McMillan TJ., A bystander effects is induced in human cells treated with UVA but not UVB radiation, Radiat. Res., 2009, 171(2), 204-11

[6]. Roméro-Graillet C., Aberdam E., et al, Nitric oxide produce ultraviolet-irradiated keratinocytes produced melanogensis, J. Clin. Invest., Volume 99, Number 4, February 1997, 635–642

[7]. Folkard M., Prise K., et al., New Insights into the cellular response to radiation using micro-beams, Nuclear Instruments and Methods in Physics Research B 231, 2005, 189-194

[8]. Banerjee G., Gupta N., et al, UV induced bystander signalling leading to apoptosis, Cancer Letters, 223, 2005, 275-284

[9]. Kudo H.., Sudo S., et al, Ion-beam irradiation effects on polyimide-UV–vis and infrared spectroscopic study, Radiation Physics and Chemistry, Volume 78, Issue 12, Dec 2009, 1067-1070

[10]. Quaranta A., Vomiero A., et al., Polymer film degradation under ion irradiation studies by ion beam induced luminescence (IBIL) and optical analyses, Nuclear Instruments and Methods in Physics Research B, 191, 2002, 680-684

[11]. Quaranta A., Recent developments of ion beam induced luminescence: radiation hardness study of thin film plastic scintillators, Nuclear Instruments and Methods in Physics Research B, 240, 2005, 117-123

[12]. Udalagama C. N. B., Bettiol A. A., et al, Proton beam micromachining dose normalization for SU-8 using ionoluminescence detection, Nuclear Instruments and Methods in Physics Research B 210, 2003, 256-259

[13]. Nagata S., Takahiro K., et al, Ion beam induced luminescence of polystyrene terephthalate foils under MeV H and He ion bombardment, Nuclear Instruments and Methods in Physics Research B, 2009, 267, 1553-1556

[14]. Torrisi L, Desiderio A, Foti G, High energy proton induced luminescence on F-doped polyvinyltoluene, Nuclear Instruments and Methods in Physics research B, 166-167, 2000, 664-668

[15]. Fink D (Ed)., Fundamentals of ion irradiated polymers, Springer-Verlag Berling Heidelberg, 2004, pp 361-364

[16]. Xie K., Huang S., Dong Z., and Juang S.H., Destruction of bystander cells by tumor cells transfected with inducible nitric oxide (NO) synthase gene, Journal of National Cancer Institute, vol 89, No. 06, 1997, 421-427

[17]. J. B. Birks, Scintillations from Organic Crystals: Specific Fluorescence and Relative Response to Different Radiations, Proc. Phys. Soc. A., 1951, 64, 874-877

Chapter 3

UV Quantification for Radiation Biology Related Materials

3 Quantification of ultraviolet photon emission from interaction of charged particles in materials of interest in radiation biology research

S.B. Ahmad, F.E. McNeill, S.H. Byun, W.V. Prestwich, C. Seymour and C.E. Mothersill

Submitted in Nuclear Instruments and Methods in Physics Research B, June 21, 2012

3.1 Chapter Summary

Biological cells are known to respond to electromagnetic radiation of a range of frequencies including in the UV range. There is a type of radiation biology experiment where cells are irradiated using charged particles with the intention that only a specified number of cells are hit by the primary ion track. However, in aiming to hit only individual cells, several other materials such as the cell container and the growth media are also irradiated. If UV radiation is emitted from these materials, it could potentially interact with the cells and confuse the interpretation of these experiments. We have hypothesized that some "bystander effects" that are thought to be chemically mediated, may be, in fact, a physical effect, where UV is emitted as a consequence of the primary particle beam interaction, and this interacts with non-targeted cells. In order to test this hypothesis, we have performed measurements of the level of UV emission from materials of interest in radiation biology experiments.

The measurements were performed using a single photon counting system in a scattering chamber under vacuum. Charged particle irradiation was performed using positively charged protons (H^+) ranging in energy from 1.2 MeV to 2.2 MeV accelerated in the 3 MV Van de Graff accelerator facility at McMaster University. The materials chosen for this study were polypropylene, Mylar, Teflon, and Cellophane as they are all materials commonly used in radiation biology experiments as cell substrates or containers. In addition, we performed measurements of two NIST standard materials derived from living cells: oyster tissue and citrus leaves. These materials were measured as a powder.

We measured UV emission from every material we studied. However, we determined in our initial sets of experiments that the proton current used in our experiments produced so much light (including in the UV range) that the PMT could be saturated. This limited the ability to quantify the UV emission because of saturation effects. We therefore reduced the current to 10 nA for a set of subsequent measurements: this was equivalent to a proton fluence rate of 2.7×10^{10} protons $mm^{-2}s^{-1}$.

The effect of beam energy was studied using this low proton current of 10 nA. All the container materials were found to emit UV frequency photons at emission levels that are significant enough to warrant further investigation of the potential biological consequences. In addition, the NIST standard reference materials oyster tissue and citrus

leaves also emitted UV when irradiated. This suggests that biological materials may themselves emit UV at significant levels when irradiated with charged particles. This also warrants further investigation.

All the work represented in this article was performed by me (First author) and the manuscript was revised by all the co-authors.

3.2 Introduction

Ultraviolet (UV) radiation is known to cause damage to cells. The most extensively studied wavelength ranges of UV in radiation biology lie between 280 nm and 400 nm (which are described as UV A and B). UV C (which lies between 100nm and 280 nm) can cause direct damage to DNA, but since it is stopped by the ozone layer; it is generally not a subject of great interest to the radiation biology community. UV B and UVA, on the other hand, are of major research interest. UVB, in the wavelength ranges of 300-313 nm, can be absorbed directly by DNA, resulting in the formation of pyramiding dimers. It can also induce apoptosis by directly activating the death receptors on the cell surface [1]. UV A is responsible for the production of reactive oxygen species that produce DNA damage and subsequently cell mutation or cell death. Studies have shown that UV-A can induce a heritable mutation in mammalian cells: skin cells after irradiation with UV-A show an increased mutation frequency [2].

In radiation biology experiments, cells can be irradiated using a biological microbeam. We suggest that the potential involvement of UV radiation (as a consequence of charged particle irradiation) should be considered by researchers studying the effects of ionizing radiation on living systems. The secondary emission of UV may play a role in experimentally observed direct and indirect effects and genomic instability. That is, researchers studying the effects of x-rays, γ-rays and charged particles on living systems need to consider the consequences of production and re-absorption of UV wavelengths which may be produced as secondary radiation emission by these primary ionizing radiations. In particular, many bystander effect studies which involve irradiation of cells with charged particles using micro-beams may need to consider secondary UV emission. Charged particles may be capable of producing UV photons through interaction with container materials or the organic/biological medium of tissue. If UV photons are generated, they may then interact with cells that are not targeted by the original charged particle.

Cells are usually irradiated after plating them onto materials to which they can adhere. In many cases, the materials used are polystyrene (which is used to make Petri-dishes), Mylar or polypropylene. In this manuscript, we present evidence that these materials can be a source of UV when charged particles pass through them.

The production of light (in the range from visible through to UV) from charged particle traversal through different media has not been given much attention in terms of the potential biological impact. However, the luminescence that arises from charged particle irradiation from organic media has been of interest to the physics and engineering community. These researchers are interested in light production as a mode of imaging, or as a technique with which to determine the elemental and molecular composition of materials. Light, in the form of both visible and UV photons, is a clearly documented

phenomenon that arises as a consequence of charged particle irradiation. For example, in an experiment performed by P. Rossi et al, cytological and histological tissues (breast fibroadenoma, thyriod adenoma and liver) were examined using a technique called Ion Beam Luminescence (IBIL) [3]. The IBIL maps plotted for various samples indicated regions of strong and weak luminescent signals. In the case of breast fibroadenoma samples, a strong lumiscent signal was seen from connective tissues, while breast tissues provided a low light signal. In these studies, the beam current was kept low (1 pA) so that the samples recived a low radiation dose. Luminescence was, however, measurable.

The luminesence from many organic compounds has been attributed to the molecules having loosely bound π electron configurations [4]. J. Pallon et al performed a study to measure the luminescence spectrum from grass and human skin samples. They observed light emission, and reported a decrease in the intensity as the time of the irradiation was increased. The decrease being attributed to irreversible damage to the molecular bonds with increased radiation dose [4]. According to this article, the strongest luminescence signal from human skin was seen in a layer that contains a high content of keratinocytes. Human keratinocytes have also been a subject of extensive study for the induction of skin cancer because of UV absorption. UV irradiation of keratinocytes activates various molecular pathways that result in either appoptosis or cell mutation [5] and [6].

This observed phenomenon of the ggeneration of light (including photons in the UV range) from biological samples as a result of interaction with ionizing radiation raises a series of questions. If both visible light and UV are emitted, is there is a preferential absorption of this generated light at certain frequencies in the surrounding tissue? Can this absorbed visible or UV light lead to subsequent biological effects?

In this context, this article describes a first stage study to *quantify* the emission of UV produced when biologically relevant materials are exposed to charged particle radiation. From this, it should be possible for further research to calculate the potential biological impact of this secondary UV emission on cells. Our hypothesis is that many “bystander effects” that are currently interpreted as being mediated by a chemical signal, are in fact a consequence of secondary emission of UV that arise from charged particle ionization. This UV then interacts with cells that are not necessarily those that are directly targeted by the charged particles, with subsequent biological effects. In this paper, we describe the measurements of the UV emitted from container materials that are commonly used in charged particle experiments.

3.3 Materials and Methods

3.3.1 Target materials and irradiation configuration

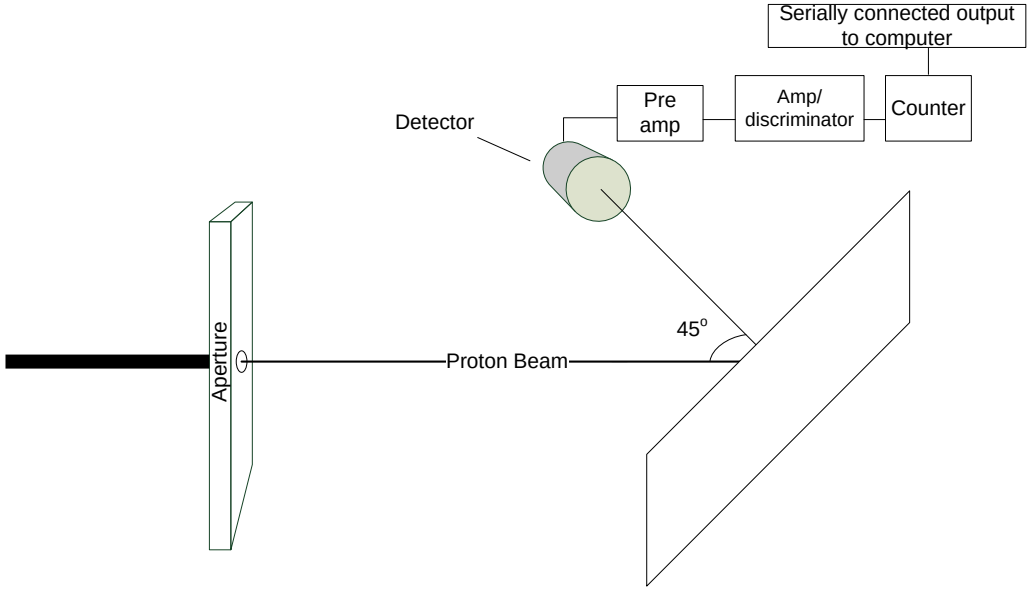

Figure 3.1 Sample irradiation configuration in vacuum chamber.

A previously described [7] system has been built that permits the simultaneous irradiation of materials by a charged particle beam and measurement of light emission. Materials can be placed in a target holder in a light tight chamber mounted on the end of a beam line. The sample holder was attached to a motorized actuator so the sample position inside the chamber could be continuously monitored using a camera and an external scale attached to the actuator. We employed a technique of moving the target continuously at a slow rate of ~2 mm/s to reduce localized heating of the sample and prevent target damage. Figure 3.1 shows the setup employed for the measurement. This setup was kept inside a light-tight scattering chamber with several feed-throughs for monitoring various signals or supplying the power to the detector.

Table 3.1 Material used for proton induced light emission measurements

Material		**Thickness (µm)**
Polypropylene		6 ± 1 , 124 ± 3
Teflon		24 ± 2, 134 ± 1
Cellophane	Transparent tape	42 ± 3
	Opaque tape	58 ± 4
	Wrap	9 ± 1
Mylar		104 ± 1
Oyster Tissue		9 ± 4
Citrus leaves		99 ± 12

The materials used for this study were polypropylene, Mylar, Teflon, cellophane, and two NIST standard reference materials: oyster tissue and citrus leaves. The first four materials are commonly used for containers or as wrapping and sealing materials in radiation biology research. The NIST materials are derived from animals and plants and were used as a test to see if UV emission could be observed in materials derived from living tissue. Ideally, we would like to test living tissue, but this is not possible under vacuum, so we used these NIST reference standards as surrogate materials.

We used two different thicknesses for polypropylene and Teflon to assess the effects of a wider range of energy deposition in the target on light output. The thickness and types of materials studied are tabulated in Table 3.1.

Oyster tissue and citrus leaves are both in the form of a powder; they needed to be contained in some way in order to be measured. Pelleting would have required a lot of material, which was not available, so we used an alternative method where a thin layer of powdered materials was deposited on a suitable backing material. The substrate material chosen for this purpose was cellophane. This, of course, meant that the measurements of these materials were of a mixed material: cellophane and NIST reference material. This is a complex measurement to unfold as the reference materials not only act as a source of light themselves, but as a potential absorber of light emitted by the cellophane. However, the purpose of the experiment was to determine whether, in principle, UV was emitted by these biologically derived materials.

In order to measure the photon emission at specific frequencies we used two optical band pass filters (Edmond optics), having pass bands of ± 10 nm (FWHM) around centre frequencies of 320 nm and 280 nm. These filters received collimated light from a lens having a focal length of 1.8 cm. The lens was capable of 90 % transmission of light over a wide range of photon frequencies.

The ion beam evacuated line was operated at a pressure level of 10^{-6} torr, and the beam was collimated by using an aperture of 0.86 mm in diameter. The beam current on the target was determined using a Faraday cup type arrangement. The current would be adjusted to an appropriate level: the target would then be brought in to intercept the beam using the actuator system. Light output was measured using a single photon counting photomultiplier by Hamamatsu. The signals were processed through the NIM standard ORTEC modules (previously described in [7]) for single photon counting.

In the previously published work, we demonstrated the feasibility of the system and tried to demonstrate the absolute amount of light emitted per proton for polystyrene. We observed that due to the high proton fluence rates, this relationship could not be established unless the proton fluence was reduced to very low values because of saturation in the PMT.

An initial suggestion was that the problem of reducing the current on the sample could be tackled by rastering the proton beam by which we mean moving the position of the beam back and forth over the target for predetermined times and repetition frequencies (called a duty cycle). This method can deliver a wide range of averaged beam currents to the target and average current as low as 10^{-5} nA can be achieved using this technique. However, it was quickly understood that it is the instantaneous current that is important when trying to reduce dead time losses in a single photon counting system: the average current over a certain time period is not significant. It is the instantaneous current that determines the response of a single photon counting unit. As long as the instantaneous current is the same, reducing the average current by rastering would not help in reducing the dead time losses of the photomultiplier tube. However, we used the raster scan with different instantaneous currents and a wide variety of pulse repetition frequencies on a Mylar target and determined the effective detector response per unit pulse. This method was used to determine the expected photon count rate from a variety of energies in Mylar.

We initially tried to perform the raster scan experiment with the use of a synchronization pulse where the counter was enabled only when the raster scan was on target. During the experiment, however, it was observed that the count rate was severely reduced, far beyond prediction, with synchronization. There are several potential reasons for this. Firstly, there is a finite time gap between the start of the synchronization pulse and the actual current appearing on target. Secondly, in our measurement setup, we had an aperture, approximately 8 times smaller than the aperture of the analyzing slits, distanced ~ 1 m away. In between the analyzing slit and the aperture inside the scattering chamber, there was no mechanism by which to steer the beam. This means that a small deflection of the beam can significantly reduce the current falling on the target while the raster scan and the sync pulse are still on (a schematic diagram is shown in Figure 3.2). We therefore enabled the counter for extended periods using the software preset time only (which was set to 3-5 sec), and then averaged the counts over the raster time in order to determine the count rate.

3.3.2 Light output per unit path length

The light output per unit path length (dL/dx) can be determined using various different empirical formulae amongst which the Birk's relationship given in eq 1 is the generally accepted fundamental equation [9].

$$\frac{dL}{dx} = \frac{F.S(E)}{1+kB.S(E)} \dots\dots\dots\dots\dots\dots eq\ 1$$

where S(E) is the stopping power and kB is the non-linear coefficient which accounts for the processes which do not result in a de-excitation with the emission of a photon after the material is ionized by energetic charged particles. F is the absolute scintillation efficiency.

However we used the formulation laid down by G. T. Wright and given in equation 2 below for numerical simplicity [10].

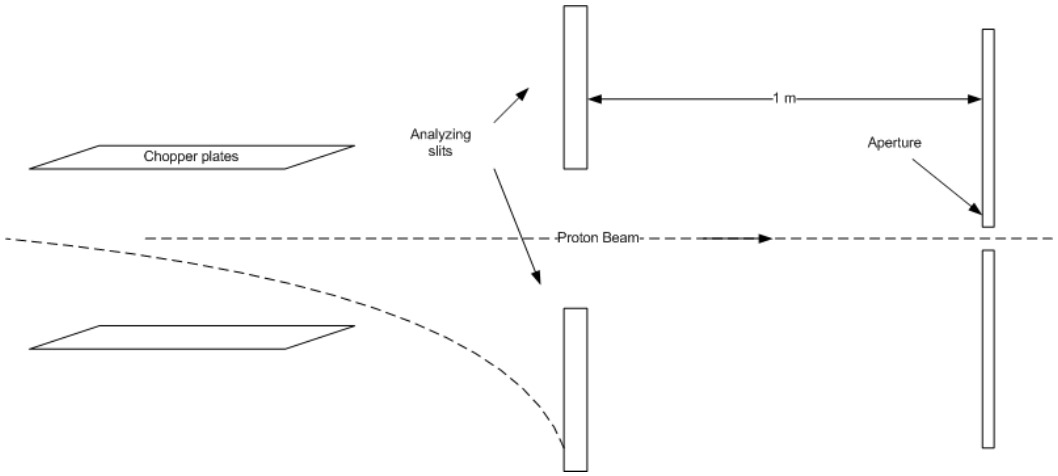

Figure 3.2 Schematic diagram of the KN accelerator raster scan. Details can be found in [8]

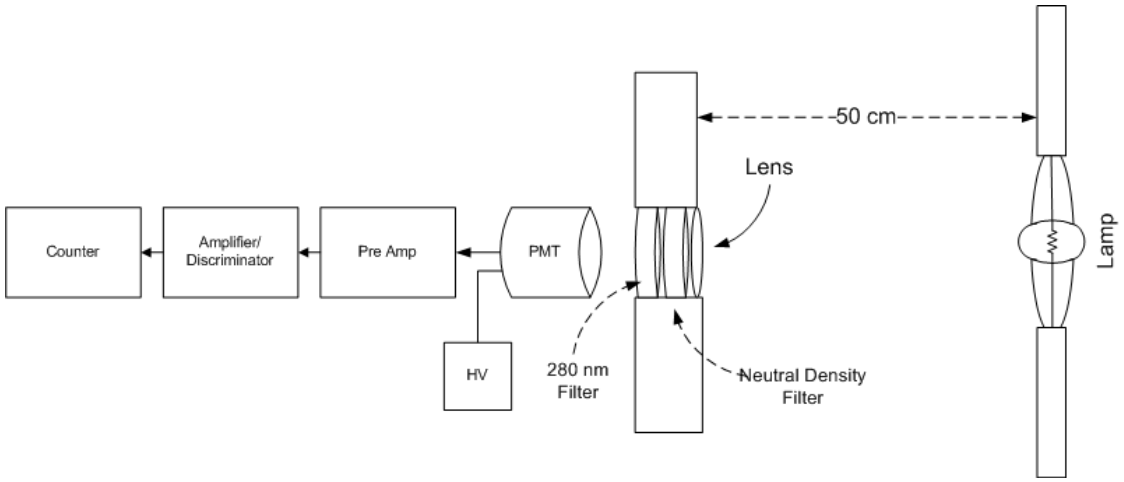

Figure 3.3 Schematic diagram for the measurement of PMT dead time

$$\frac{dL}{dx} = Aln(1 + \alpha S(E)) \dots\dots\dots\dots\dots\dots eq\ 2$$

or the total light yield can be represented as

$$L(E) = A\int_0^R \ln(1 + \alpha S(E))\, dx \dots\dots\dots\dots\dots eq\ 3$$

where A is the absolute scintillation efficiency and α is the non-linear coefficient. We fitted the SRIM calculated values of stopping powers versus the depth in the medium (x) for various initial energies of the protons with the following function;

$S(E) = S(E_o)\mathrm{e}^{\mathrm{b}/(\mathrm{x}+\mathrm{c})} \ldots\ldots\ldots\ldots\ldots eq\ 4$

Substituting equation 3 in 2 gives the following relationship for the total light yield

$L(E) = A\int_0^R \ln\left(1 + \alpha S(E_o)e^{b/(x+c)}\right) \mathrm{dx} \ldots\ldots\ldots\ldots\ldots eq\ 5$

3.3.3 PMT dead time measurement

In order to try and quantify the performance of the PMT, and use this to quantify beam line measurement data, the dead time of the system needed to be calculated. For the measurement of the photomultiplier tube dead time, we used a calibrated 200 watt, quartz halogen, tungsten filament lamp from ORIEL instruments. This lamp is calibrated for radiance output, in a plane parallel to the plane of lamp, 50 cm away from the source. Power to the lamp was supplied using a radiometric power supply model 68830 by ORIEL. The geometry is shown in Figure 3.3.

The neutral density filter represented in Figure 3.3 was used to reduce the beam intensity. In this configuration, the PMT was exposed to a count rate of approximately 158×10^6 counts/sec and the observed count rate on the photomultiplier tube was 48×10^6 counts/sec. Using a non-paralyzable model, given in equation 6, for dead time behavior [11] the dead time was measured to be 15 ns.

$1/m^{\cdot} = \tau + 1/n^{\cdot} \ldots\ldots\ldots\ldots eq\ 6$

The reasoning behind the use of the paralyzable dead time behavior model was based on the results shown in Figure 3.4. Here we exposed the photomultiplier tube to count rates beyond the single photon counting regions. As the actual incident photon count rate increases, the observed count rate also increases, showing that the photomultiplier tube is not paralyzed. This model is also recommended by the manufacturer of the photomultiplier tube.

3.4 Results and Discussion

The objective of this study was to determine the absolute photon emission rate at UV frequencies from a variety of materials relevant to radiation biology experiments. The aim was to determine whether there is a potential physical component to some previously labeled radiation induced bystander effects i.e. whether observed effects arise from interaction with UV rather than from a chemical signal.

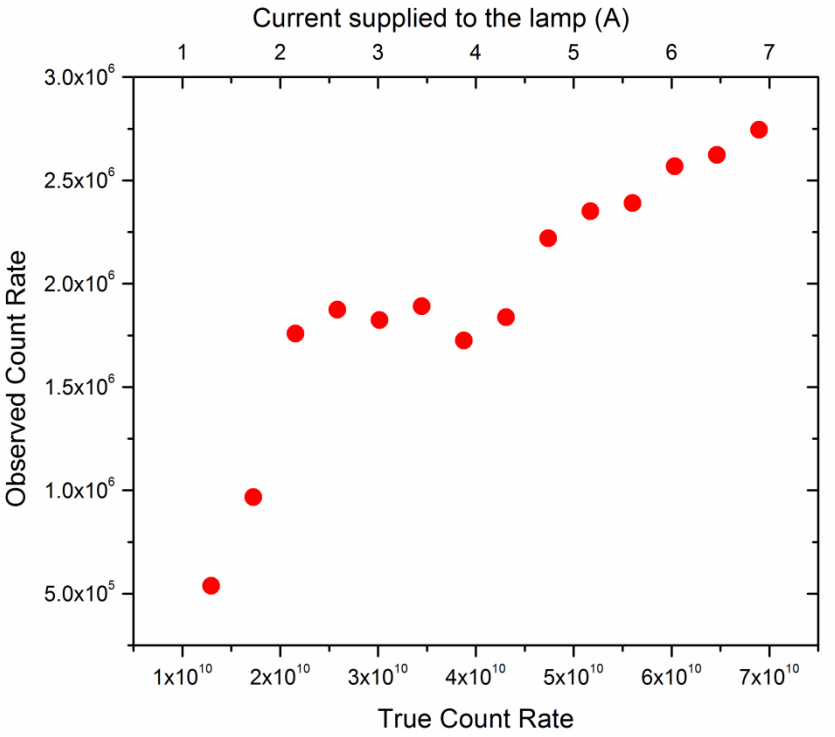

Figure 3.4 Behaviour of the PMT to very high input photon fluence rate

Ion induced luminescence in organic materials, especially polymers, has been observed in several studies such as [12]. The literature shows that ion beam luminescence depends both upon the charged particle fluence and beam energy [13] and [14]. The materials that have been investigated thus far usually show luminescence peaks in the wavelength range from 400 nm to 600 nm. Generally the light yield increases with ion fluence and energy up to a maximum and then starts to drop exponentially. In our previous study [7], we showed these trends for Polystyrene, which is generally the material from which Petri-dishes are manufactured. Here we extended our study to the luminescence measurements from several other materials that have relevance to the radiation biology research. Our previous experience showed that due to high light yield absolute measurements become difficult with higher proton fluence. Proton fluence can be reduced by collimation, which is in fact what is utilized in microbeam accelerators, however this method is, technically, very challenging. Special set of arrangements are required in order to reduce the beam size down to micro-meters in diameter. We used a raster scan with the idea of pulsing the beam to reduce the effective current delivered to a target.

3.4.1 Raster scan measurements

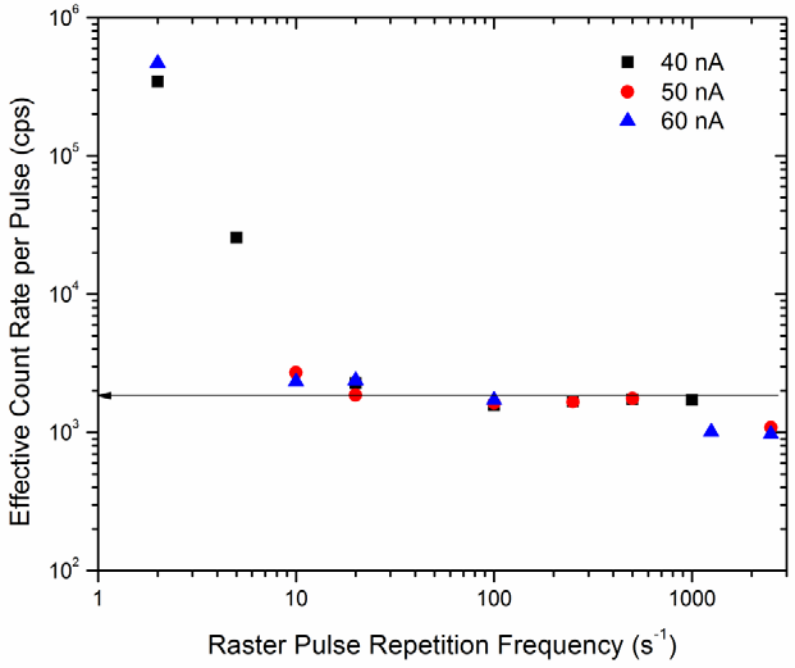

Figure 3.5 Light output per unit raster pulse for a wide range of pulse repetition frequencies. The instantaneous current was changed between 40 nA and 60 nA.

A variety of duty cycles were used to deliver average currents varying in the range of 10^{-5} nA to 10 nA to a Mylar target. Mylar was chosen for this purpose since it is a commonly used material in radiation biology studies. In bystander effect studies, cells are usually grown in mono-layers with Mylar as a substrate and then exposed to very low fluences of charged particles [15]. As mentioned earlier, when dealing with single photon counting, the effective current delivered using a raster scan is not useful because dead time effects in the system depend on instantaneous currents not averaged currents. However, we measured an effective light yield per unit pulse for a wide range of pulse repetition frequencies. Figure 3.4 shows the photon count rate observed from Mylar at a wavelength of 320 nm for different instantaneous currents (40 nA, 50 nA, and 60 nA) and a wide range of raster scan pulse repetition frequencies. It can be observed that by increasing the frequency, the count rate per unit pulse (of width 20 μs) decreases and becomes almost constant after the repetition frequency of 10 s^{-1} is reached. This indicates the effects of dead time and demonstrates the PMT's capacity for handling an input count rate. The average value to which the count rate per unit pulse settles is $1.75 \pm 0.06 \times 10^3$ cps. Each pulse had a width of 20 μs; therefore, for a continuously delivered current the expected recorded count rate from Mylar would be approximately 1×10^9 cps. This count rate would be subject to a correction for the lens and filter transmission and the solid angle of the detector subtended

on the sample. After making these corrections, the count rate would be expected to be approximately 1×10^{10} cps. This gives an idea regarding the expected recorded count rate for continuous delivery of the beam current. However, for all the subsequent measurements, we kept the beam current to a low value of 10 nA which permitted stable operation of the accelerator while minimizing dead time effects and keeping the photomultiplier in a single photon counting region. This current corresponds to a fixed proton fluence rate of 2.7×10^{10} protons/mm^{2}s.

3.4.2 Luminescence measurements for varying beam energies

3.4.2.1 Mylar

Mylar was irradiated, with a fixed proton fluence rate (2.7×10^{10} protons/mm^{2}s) with a variety of incident proton beam energies. It can be seen in Figure 3.5 that increasing the proton energy does not increase the luminescence yield at a wavelength of 320 nm in Mylar, however it does increase at a rate of $0.229 \pm 0.04 \times 10^6$ counts Sr^{-1}s^{-1} MeV^{-1} when the light is filtered through a 280 nm filter. Here the material was thick enough to completely stop the particles for the range of energies we used. Regardless of the pattern of luminescence increase with the beam energy, the data presented in Figure 3.5 provides evidence of a significant enough production of light that it should be investigated further for the potential biological consequences. It may be noted that the luminescence yield represented in Figure 3.5 has been obtained using filters with a very narrow pass band. A significant amount of luminescence may also be present over a range of other frequencies which are known to have biological consequence as well.

3.4.2.2 Polypropylene

Polypropylene is generally used in micro-beam studies to hold the cells in place for irradiation. It is considered to be non-flouresent to ion beam irradiation [16]. Usually the thickness of the polypropylene film used is 6 μm or less. We did not observe polypropylene to be non-fluorescing. We observed the emission of UV as a consequence of irradiation of polypropylene. Figure 3.6 shows the light output at two different photon wavelengths from polypropylene for a constant proton fluence rate of 2.7×10^{10} protons.mm^{-2}s^{-1}. The availability of a very thin polyproplyene sample made it possible to observe the light output for a series of varying LET measurements from 0.178 to 0.217 MeV.cm^2.mg^{-1}. The inset of Figure 3.6 shows the light output per unit path length as a function of LET. The data presented in Figure 3.6 show that polyproplyene emits an average of 1.09×10^7 photons/Sr.s.μm at 320 nm for an average LET of 0.922 MeV.cm^{2}mg^{-1}. The corresponding dose rates, calculated using Geant4, for the thin (6 μm) polypropylene target lie between 7.49 and 11.5 nGy per proton.

For a thicker (124 μm) polypropylene target, the dose rates were slightly reduced, ranging between 4.03 to 6.11 nGy per proton. Since the protons were completely stopped

in the material, they imparted a wider range of LETs in the medium. Here the total light output can be determined theoretically using equation 4. We used a non-linear coefficient value of 0.00129 $g.MeV^{-1}.cm^{-2}$ [17] from the literature and integrated the equation 5 for the range (calculated from SRIM/TRIM, [18]) of protons in polyproplyene in order to determine the total light yeild. The values of stopping powers were also calculated using SRIM/TRIM [18].

Figure 3.7 shows the normalized total light yield (calculated for a proton fluence of 2.7×10^{10} protons/mm^2.s) as a funciton of the energy deposited in thick polypropylene according to eq 5. Here the normalization for total light yield was peformed for the absolute scintillation efficiency of polypropylene. The comparison shows that the theoretical and observed light output vary in a similar pattern, although the theoretically calculated values seem to be less than the observed light output. These are, however, normalized for the absolute scintillation efficiency. This shows that there ought to be, at least, more than 10 UV photons per unit distance (μm) that should emitted per proton irradiation from Polypropylene. It should be noted that when calculating the theoretical light output, the non-linear coefficient only takes into account the processes which compete for de-excitation by emitting light and de-excitation by producing heat. It does not take into account the absoption, scattering or attenuation of light when it travels in the medium. The theoretical value could therefore be expected to be higher than the measured in general, as is observed here.

3.4.2.3 Teflon Measurements

Figure 3.8 shows the light yield from a Teflon target as a function of the incident proton beam energy at 320 and 280 nm photon wavelengths. The inset in Figure 3.8 shows the variation of light output per unit path length from a thin Teflon target for different LETs. Here the combination of the beam energy and the target thickness (24 μm) did not allow a uniform LET in the Teflon, therefore the error in the LET is large compared to that determined for polypropylene (inset Figure 3.6). It was observed that for an average LET of 0.152 $MeV.cm^2.g^{-1}$ the light emitted from a thin Teflon target at 320 nm wavelength is 1.95×10^6 photons/Sr.s.μm for an incident proton fluence of 2.7×10^{10} protons.$mm^{-2}s^{-1}$. The photon output determined here is almost an order of magnitude less than that observed for polypropylene. This sample was delivered the radiation in a dose rate ranging from 9.10 to 12.2 cGy per proton. Figure 3.8 also shows the light yield from a thick (134 μm) teflon target (where the particle completely stops in the material). In this case the material was subjected to a dose rate of 0.219 to 0.449 nGy per proton.

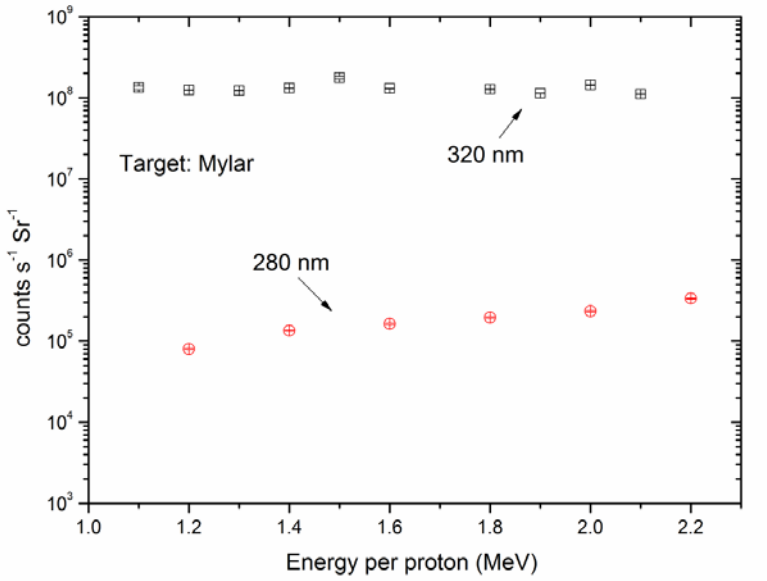

Figure 3.6 Luminescence yield from Mylar at 320 nm and 280 nm photon wavelengths for beam energy varying from 1.1 to 2.2 MeV.

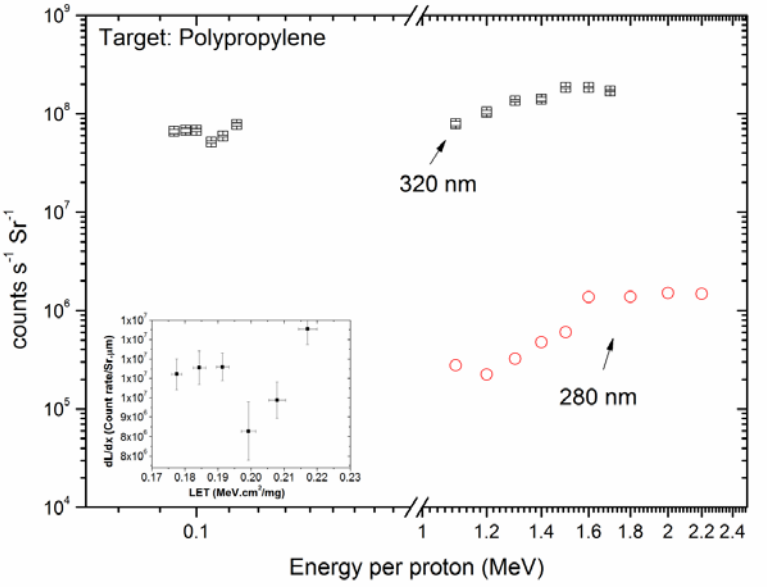

Figure 3.7 Luminescence yield from polypropylene for different levels of energy deposited per proton in the material. The inset shows the Light output per unit path length in polypropylene against the LET of the proton radiation.

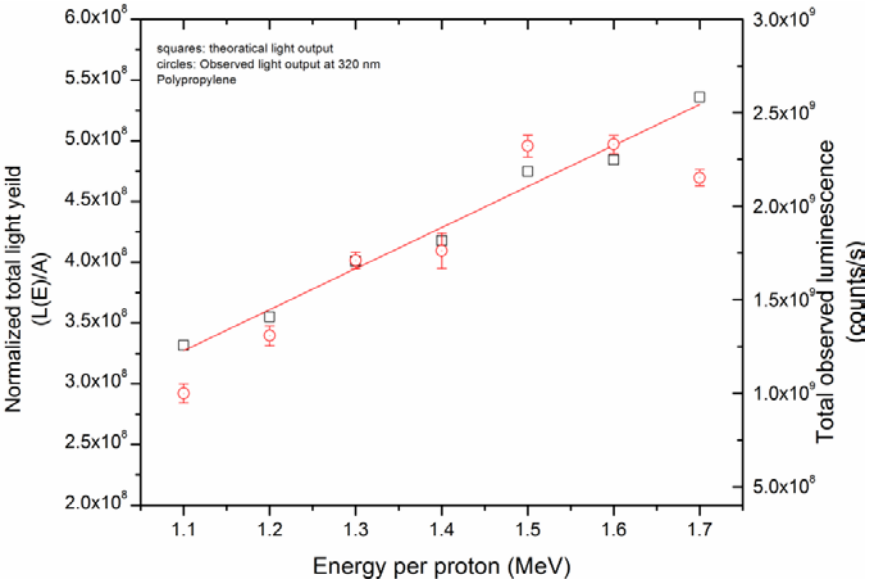

Figure 3.8 Graph for theoretically calculated luminescence normalized for the luminescence emission from polypropylene normalized to the absolute scintillation efficiency against the proton beam energy. For comparison the total observed light yield (in all the directions) is also shown.

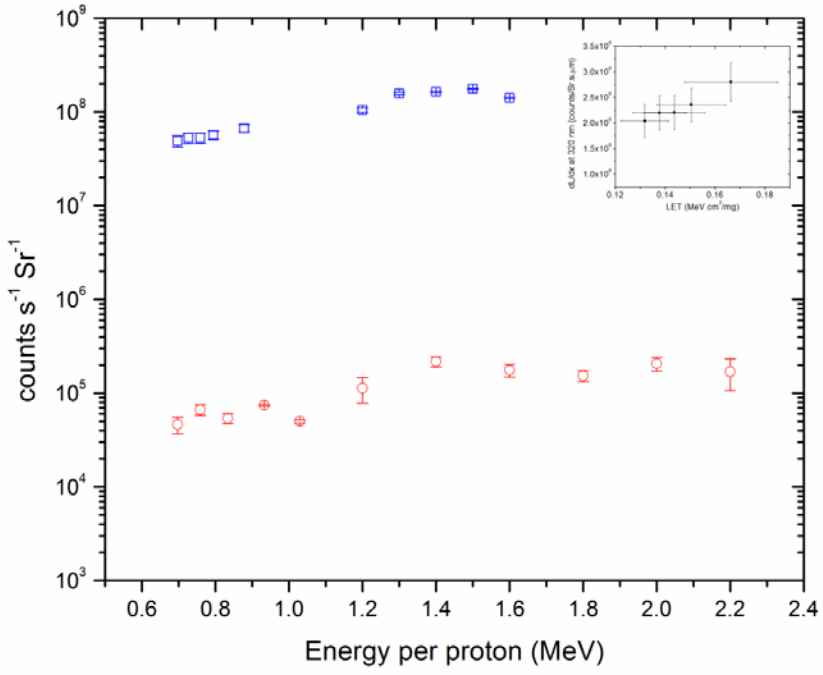

Figure 3.9 Luminescence yield against the total energy deposited per proton in Teflon. Inset show the light output per unit path length plotted against the LET of proton radiation.

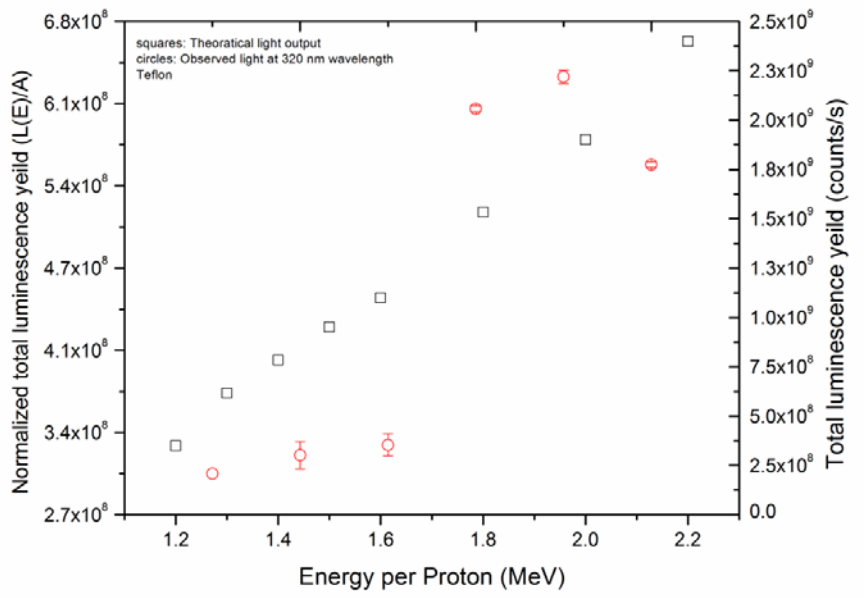

Figure 3.10 Normalized, theoretical light output against the total energy deposited per proton in Teflon. For comparison the light output at 320 nm for a fluence rate of 2.7 × 1010 protons/mm2s is also shown.

Dose deposited at lower rates in Teflon resulted in higher count rate compared to polypropylene case which indicates that the at higher dose rates the damage in the polymer increases thus reducing the light yeild.

We also calculated the theoretical light output for Teflon shown in Figure 3.9. Here the same non-linear co-efficient was used i.e. 0.00129 g MeV^{-1} cm^{-2}, and the output has been normalized for the absolute scintillation efficiency. Again, it can be observed that the variation of observed light yield at 320 nm follows a similar pattern as the theoretical light yield. Figure 3.9 also suggests that the absolute scintillation efficiency must be at least 10 photons per proton for Teflon.

The theoretical values determined for Teflon are similar to those calculated for polypropylene; this is mainly because we used the same non-linear coefficient for both cases. This emphasizes the fact that a more thorough investigation of these materials for their light emission characteristics in terms of the LET of the radiation is required.

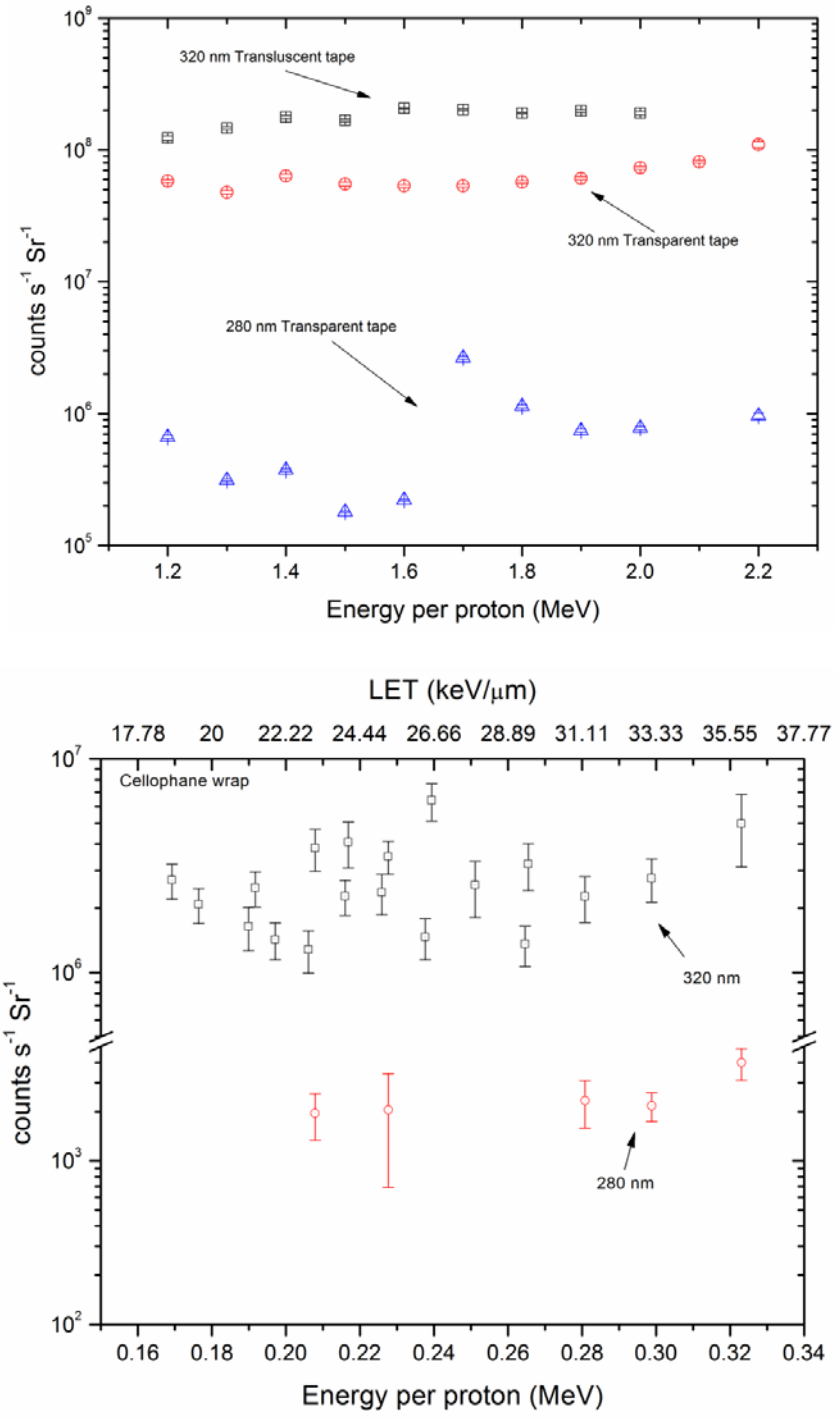

Figure 3.11 Luminescence output from Cellophane in different commercially available forms. (a) shows the luminescence yield at 320 nm for transparent and semi-transparent adhesive tapes and at 280 nm for transparent tape. (b) shows the output from thin wrap at 320

3.4.2.4 Cellophane Measurements

We also measured the light output from different brands of commercially available cellophane materials. For this purpose we used transparent and semi-transparent adhesive tapes and thin cellophane material usually used as food wrapper. The transparency here refers to the transparency of visible light. Figure 3.10a gives a comparison for the light output measured for the adhesive tapes at 320 nm and 280 nm. The output at 320 nm for the semi-transparent tape is higher than that of the transparent tape. The rate of increase for the semi-transparent tape is measured to be $8 \pm 2 \times 10^7$ counts.Sr^{-1}.s^{-1}.MeV^{-1} and $4 \pm 1 \times 10^7$ counts.Sr^{-1}.s^{-1}.MeV^{-1} in the case of the transparent tape. The dose rates, calculated from Geant4, were varied from 8.76 to 13.4 nGy per proton for transparent tape and 5.82 to 9.73 nGy.s^{-1} per proton for the semi-transparent tape. The luminescence yield at 280 nm measured from the transparent adhesive tape was measured in two different phases. The measurements for beam energies between 1.7 to 2.2 MeV were taken for different lengths of time compared to the measurement for beam energies varying from 1.1 to 1.6 MeV. The behavior of the data, where there seems to be a transition in luminescence between 1.6 and 1.7 MeV could perhaps be the result of a self annealing process where the polymer anneals itself after radiation damage.

Figure 3.10b shows the light output from very thin sheets of cellophane wraps. Here the material was subjected to dose rates varying between 9.1 to 20.9 nGy per proton. Since the sample was very thin, the linear energy transfer was quite uniform in the material. Figure 3.10b also shows the TRIM [18] calculated LETs. It is evident from Figure 3.10b that there is not a significant variation in the observed light output for the range of LETs deposited in this sample. The average luminescence observed from cellophane for an average LET of 25.5 keV/μm, was 2.76×10^6 counts Sr^{-1}.s^{-1} for the proton fluence of 2.7×10^{10} protons/mm^2s.

Table 3.2 provides a summary of the average observed light yield for all the materials mentioned above per unit dose deposited in that material.

Table 3.2 Summary of the photon output at 320 nm and 280 nm for cell container materials in terms of per unit dose deposited in that material

Material	Thickness (μm)	Dose range ($nGy.s^{-1}$ per proton)	Average light yield (Photons.Sr^{-1}.s^{-1}.cGy^{-1})	
			320 nm	280 nm
Mylar	104	4.61	4.58×103	7
Polypropylene	6	4.03 – 6.11	4.91×10^3	14
	124	7.49 - 11.5	1.10×10^3	---
Teflon	24	9.10 – 12.2	719	1
	134	0.219 – 0.449	9.36×10^4	93
Cellophane	42	8.76 – 13.4	0.977×10^3	---
	58	5.83 – 9.73	3.69×10^3	11
	9	9.10 – 20.9	0.375×10^3	2.74×10^{-2}

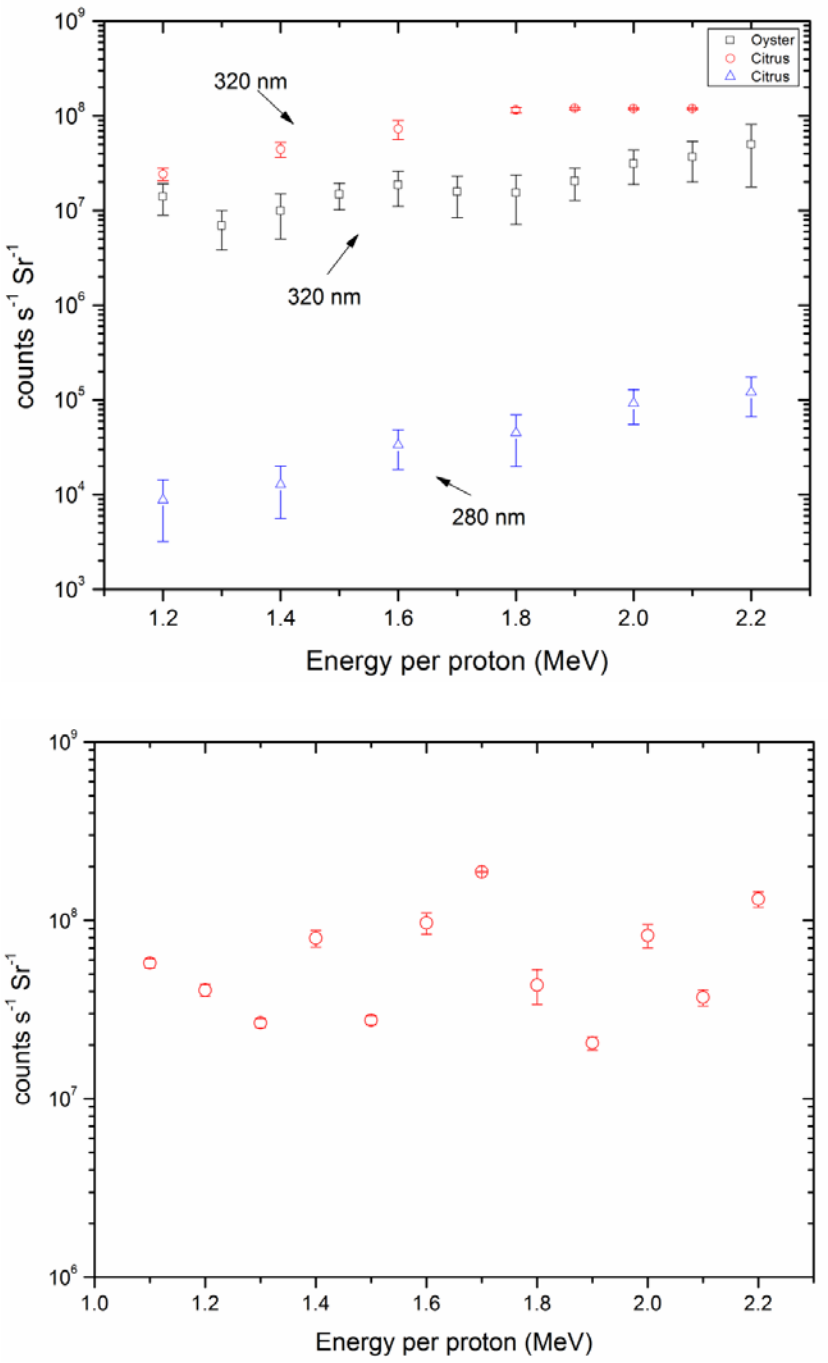

Figure 3.12 Luminescence yield measured for NIST reference Oyster tissue and Citrus tissue. (a) Both materials were deposited in the form of thin layer on cellophane tape. (b) Thick Oyster tissue without any backing material.

3.4.2.5 Oyster Tissue and Citrus Leaves Measurements

It is obvious that generation of light is an inherent property when particulate radiation travels through a medium. The measurements listed above represent those measurements that would be expected when the radiation passes through the cell container material prior to the interaction in the cells themselves. When the primary beam passes through the cells the physics of the radiation interaction does not, of course, change. Therefore biological media should themselves perhaps be expected to give off secondary radiation similar to that observed for the container materials. Figure 3.11a shows the light output measured for the NIST standard materials, oyster tissue and citrus leaves. The results shown in Figure 3.11a are for the case when these materials were deposited in thin layers on a transparent adhesive tape. Here not all the energy carried by the proton beam is deposited in the thin layer of powdered material, but some of the energy is deposited in the substrate material (i.e. the adhesive tape). Although the actual light yield from the deposited materials is difficult to unfold but the luminescence increases at a rate of $2.22 \pm 0.27 \times 10^8$ and $1.16 \pm 0.17 \times 10^5$ cps per MeV energy deposited in citrus leaves at a photon wavelength of 320 nm and 280 nm respectively. Similarly it increases at a rate of $3.37 \pm 0.64 \times 10^7$ cps per MeV energy deposited in oyster tissue at photon wavelength of 320 nm. Figure 3.11b shows the light output measured, for oyster tissue, without any backing (substrate) material present, so all the energy is deposited in the thick layer of oyster tissue. There is no clear pattern for the increase in luminescence against an increase in ion energy. The average observed count rate was found to be 2.13×10^7 cps per Sr. We studied these materials to see if UV could be observed from plant and animal derived material i.e. from materials in living systems studied in radiation biology. UV light is indeed observed as a consequence of their irradiation with protons.

3.5 Conclusion

We have measured significant UV light output arising from irradiation with charged particles of several materials commonly used in radiation biology experiments. We also measured two materials derived from plants and animals and determined significant UV emission from those materials.. We conclude that the results of many charged particle radiation biology experiments, especially those using biological microbeams, which have observed a “radiation bystander effect”, may need to be re-considered with this evidence in mind. Observed effects, which have been attributed to a chemical signal, could, in fact, be a consequence of the UV induced by the charged particle tracks in the experimental containers or within the cells or cellular media.

3.6 References

[1] D. Kulms, B. Pöppelmann, D. Yarosh, T. a Luger, J. Krutmann, and T. Schwarz, "Nuclear and cell membrane effects contribute independently to the induction of apoptosis in human cells exposed to UVB radiation.," *Proceedings of the National Academy of Sciences of the United States of America*, vol. 96, no. 14, pp. 7974–9, Jul. 1999.

[2] R. P. Phillopson, S. E. Tobi, J. A. Morris, and J. M. and Trevor, "UV-A induces persistant genomic instability in human keratinocytes through an oxidative stress mechanism," *Free Radical Biology & Medicine*, vol. 32, no. 5, pp. 474–480, 2002.

[3] P. Rossi, C. D. Maggio, G. P. Egeni, A. Galligioni, and G. Gennaro, "Cytological and histological structures identification with the technique IBIL in elemental microanalysis," *Nuclear Instruments and Methods in Physics Research*, vol. 181, pp. 437–442, 2001.

[4] J. Pallon, C. Yang, R. J. Utui, M. Elfman, K. G. Malmqvist, P. Kristiansson, and K. A. Sjijland, "Ionoluminescence technique for nuclear microprobes," *Nuclear Instruments and Methods in Physics Research B*, vol. 130, pp. 199–203, 1997.

[5] O. Reelfs, I. M. Eggleston, and C. Pourzand, "Skin protection against UVA-induced iron damage by multioxidants and iron chelating drugs/prodrugs," *Current Drug Metabolism*, pp. 242–249, 2010.

[6] E. Maverakis, Y. Miyamura, M. P. Bowen, G. Correa, Y. Ono, and H. Goodarzi, "Light, including ultraviolet.," *Journal of autoimmunity*, vol. 34, no. 3, pp. J247–57, May 2010.

[7] S. B. Ahmad, F. E. McNeill, S. H. Byun, W. V. Prestwich, C. Seymour, and C. E. Mothersill, "Ion Beam Induced Luminescence; Relevance to Radiation Induced Bystander Effects," *Nuclear Instruments and Methods in Physics Research B*, 2012.

[8] W. Matysiak, K. Chin, S. Mcmaster, W. V. Prestwich, and S. H. Byun, "Relative Enhancement of a 3 He Ion Chamber Response to Fast Neutrons by TOF Rejection of Slow Neutrons With a Pulsed Neutron Source," vol. 56, no. 1, pp. 266–271, 2009.

[9] J. B. Birks, "Scintillation from organic crystals: Specific flourescecne and relative response to different radiation," *Proc. Phys. Soc A*, vol. 64, pp. 874–877, 1951.

[10] G. T. Wright, "Absolute Scintillation Efficiency of Anthracene Crystals," *Proceedings of the Physical Society. Section B*, vol. 68, no. 11, pp. 929–937, Nov. 1955.

[11] G. F. Knoll, *Radiation Detection and Measurement*. John Wiley & Sons, 2010, p. 122.

[12] S. Nagata, H. Katsui, K. Takahiro, B. Tsuchiya, and T. Shikama, "Radiation-induced luminescence of PET and PEN films under MeV ion and pulsed UV laser irradiation," *Nuclear Instruments and Methods in Physics Research Section B: Beam Interactions with Materials and Atoms*, vol. 268, no. 19, pp. 3099–3102, Oct. 2010.

[13] M. Fujiwara, T. Tanabe, H. Miyamaru, and K. Miyazaki, "Ion-induced luminescence of silica glasses," *Nuclear Instruments and Methods in Physics Research B*, vol. 116, pp. 536–541, 1996.

[14] P. J. Chandler, F. Jaque, and P. D. Townsend, "Ion beam induced luminescence in fused silica," *Radiation Effects*, pp. 43–53, 2006.

[15] W. F. Morgan, "Non-targeted and delayed effects of exposure to ionizing radiation: I. Radiation-induced genomic instability and bystander effects in vitro.," *Radiation research*, vol. 159, no. 5, pp. 567–80, May 2003.

[16] G. Randers-Pehrson, C. R. Geard, G. Johnson, C. D. Elliston, and D. J. Brenner, "The Columbia University single-ion microbeam.," *Radiation research*, vol. 156, no. 2, pp. 210–4, Aug. 2001.

[17] G. V. O'Rielly, N. R. Kolb, and R. E. Pywell, "The response of plastic scintillator to protons and deuterons," *Nuclear Instruments and Methods in Physics Research Section A: Accelerators, Spectrometers, Detectors and Associated Equipment*, vol. 368, no. 3, pp. 745–749, Jan. 1996.

[18] "James Ziegler - SRIM & TRIM." [Online]. Available: http://www.srim.org/. [Accessed: 19-Apr-2012].

Chapter 4

UV emission from HPV-G cells

4 Ultra-violet light emission from HPV-G cells irradiated with Low LET radiation from Y-90; consequences for radiation induced bystander effects

S.B. Ahmad, F.E. McNeill, S.H. Byun, W.V. Prestwich, C. Seymour, C.E. Mothersill, A. Armstrong, C. Fernandez

Article submitted in Dose Response, September 11, 2012

4.1 Chapter Summary

In this study, we aimed to establish the emission of UV photons when HPV-G cells and associated materials (such as the cell substrate and cell growth media) are exposed to low LET radiation. The potential role of UV photons in the secondary triggering of biological processes led us to hypothesize that the emission and absorption of photons at this wavelength explain some radiation induced "bystander effects" that have previously been thought to be chemically mediated. Cells were plated in Petri-dishes of two different sizes, having different thicknesses of polystyrene (PS) substrate, and were exposed to β-radiation from ^{90}Y produced by the McMaster Nuclear Reactor. UV measurements were performed using a single photon counting system employing an interference-type filter for selection of a narrow wavelength range, 340±5 nm, of photons.

Exposure of the cell substrates (which were made of polystyrene) determined that UV photons were being emitted as a consequence of β particle irradiation of the petri-dishes. For a tightly collimated β-particle beam exposure, we observed 167 photons in the detector per unit μCi in the shielded source for a 1.76 mm thick substrate and 158 photons/μCi for a 0.878 mm thick substrate. A unit μCi source activity was equivalent to an exposure to the substrate of 18 β-particles/cm^2.

The presence of cells and medium in a petri-dish was found to significantly increase (up to a maximum of 250 %) the measured number of photons in a narrow measured band of wavelengths of 340±5 nm (i.e. UVA) as compared to the signal from an empty control petri-dish. When coloured growth medium was added to the cells, it reduced the count rate, while the addition of transparent medium in equal volume increased the count rate, as compared to cells alone. We attribute this to the fact that emission, scattering and absorption of light by cells and media are all variables in the experiment. Under collimated irradiation conditions, it was observed that increasing cell density in medium of fixed volume resulted in a decrease in the observed light output. This followed a roughly exponential decline. We suggest that this may be due to increased scattering at the cell boundary and absorption of the UV in the cells.

We conclude that we have measured UVA emitted by cells, cell medium and cell substrates as a consequence of their irradiation by low LET β particle radiation. We suggest that these secondary UV photons could lead to effects in non-targetted cells. Some effects that had previously been attributed to a chemically mediated "bystander effect" may in fact be due to secondary UV emission. Some radiation bystander effect studies may require re-interpretation as this phenomenon of UV emission is further investigated.

The work presented in this chapter was carried out by me in the high level labs of McMaster University. The work facility and timely availability of radioisotope Y-90 was kindly arranged by Andrea Armstrong. Cells were cultured and plated in the petri dished by Cristian Fernandez in Dr. Carmel Mothersill's Lab. Manuscript was written by me and revised by all the co-authors.

4.2 Introduction

Deviation from the linear-no-threshold (LNT) theory for very low doses of radiation has been a subject of debate amongst the scientific community for some time. Various effects have been observed that include increased sensitivity of cells, both towards protection against further radiation insult, and also toward more cell death [1], [2] and [3]. Amongst these low radiation dose study observations, the effects on the non-targeted cells have been studied quite extensively, and are usually described as "radiation induced bystander effects" [4]. This phenomenon not only challenges the LNT model for low doses of radiation, but also indicates the fact that damage to the cell nucleus is not a basic criterion for producing overall damage to the cell [5]. Cellular irradiation in bystander effect studies is often performed using micro-beams that can deliver a quantified (and small) number of particles to specified cells. An alternative method to microbeams used in bystander effect studies is where a very low fluence of charged particles is employed, so that only a small proportion of the overall population of cells is traversed by primary charged particle tracks. Irrespective of the method of irradiation cells are plated on a variety of different substrate materials such as polypropylene, mylar or polystyrene that could fluoresce upon irradiation.

It is a well-known fact that charged particles, while passing through media create dense ionizations and excitations. In organic materials the neutralization or de-excitation of the ionized/excited molecules can occur in a variety of different ways that include subsequent emission of radiation at different frequencies, from x-ray through to UV and optical frequencies and also production of heat in the medium. Electrons are also known to produce bremsstrahlung radiation when their trajectory is altered around a nuclear field (or they are decelerated in the medium). In addition, in the case of electrons passing through a dielectric medium, with velocities greater than the phase velocity of light in that medium, Cerenkov light can be observed as a result of de-excitation of the molecules. If the refractive index of tissue is considered to be 1.4 then the minimum energy required of β particles to generate Cerenkov light is 0.219 MeV [6]. In this experiment, we used β-particles from Y-90 where the end point energy is 2.28 MeV and the average β energy was 0.93 MeV. This energy of β-particles would certainly create Cerenkov photons. However the energy lost through the Cerenkov process is much less than that lost by ionizations (40 keV/m in case of Cerenkov energy loss and 200 MeV/m in case of ionization energy loss [7]). The purpose of our experiment was to measure the level of UV photons detectable outside of irradiated cells and medium. The mechanism of generation of the UV (whether it be from ionizations or through the Cerenkov interaction) is not really relevant to our purpose. We wished to determine the production of photons at particular wavelengths which could subsequently lead to the production of a biological response upon absorption by cells.

In simple polymeric structures, or other simple molecular structures, it is possible that the emission and absorption bands do not overlap if the de-excitation occurs in the form of electromagnetic radiation. However, when the molecular structures become more and more

complex, such as in the case of cells and their media, there is a strong chance that emission and absorption bands overlap for a wide range of electromagnetic frequencies. This means, for example, that if UV emission occurs in the cell culture as a consequence of irradiation, then the UV photon can be re-absorbed elsewhere in the cell culture and perhaps lead to effects at a distance from the original site of irradiation. It becomes important not to ignore the potential consequences of re-absorption of this UV radiation in the surrounding medium in the conceptualization of "bystander" experiments.

In previous studies, we have demonstrated considerable production of light (including UV frequencies) from a variety of experimentally relevant cellular substrate materials as a consequence of charged particle irradiation [8]. Emission frequencies were found to lie within the visible and ultra-violet ranges. Several other studies have also shown the production of light in the UV and visible ranges when experimentally relevant materials (and polymers) are irradiated with charged particles [9],[10] and [11]. However, we wished specifically to study whether cells and cell media would also emit light, especially in the UV range, as a consequence of irradiation. This fluorescent emission of light at UV frequencies can occur both for high and low LET radiation. This is, of course, the basis of liquid scintillation counting: light is emitted in certain organic materials (liquid scintillators) when either energetic electrons or other charged particles are mixed with them. [12], and [13]. Our previous studies made use of proton beams (high LET radiation) to irradiate experimentally relevant materials. The irradiation was performed under vacuum which is not feasible for cells and cell media. We therefore performed this study to quantify the UV emission as a consequence of irradiation of cells and cell media by low LET β-particles.

4.3 Materials and Methods

4.3.1 HPV-G cell culture

We used the HPV-G cell line due to its extensive use in radiation induced bystander effect studies [14], [15], and [16]. Cell cultures were performed in a bio-safety cabinet level II. We used a cell growth medium (RPMI 1640 by Gibco) having a composition of DMEM/F12 medium containing 60 ml FBS, 5 ml penicillin-streptomycin, 5 ml L-glutamine, 15 mM Hepes buffer, and 1 mg/ml hydrocortisone. Cell cultures were kept in T75 flasks until they were 90-95 % confluent. Using 0.25% w/v trypsin/1 mM EDTA solution (1:1) the cells were removed from the flasks and were placed in an incubator for 8 to 10 minutes for a complete detachment. In order to neutralize trypsin, 10ml of growth medium was used. The detached cells were re-suspended in medium, and an aliquot was counted using a Z2 Coulter Particle Count and Size Analyzer. Appropriate numbers of cells were then plated in either 35 × 10 mm or 100 × 15 mm sterilized dishes. Cells were then harvested with either 3 ml or 10 ml RPMI 1640 medium for small and large dishes respectively. After 6 hours of incubation at 37^{o} C, the cells were checked, under a microscope, to see if they were attached to the dishes. The medium from the attached cells was then removed carefully. In order to obtain permission to study cells and media in a

non-biosafety-controlled physics laboratory, McMaster University biosafety requirements meant that the cells were required to be killed prior to transfer. Cells were killed by adding a 70 % ethanol solution to the cells. After 5-10 minutes, the ethanol solution was carefully pipetted out, and the cells were transported to the physics laboratory for irradiation and light counting.

4.3.2 Source preparation (Y-90)

We used ^{90}Y as a source of energetic electrons for our experiments. ^{90}Y is considered to be an almost pure beta particle emitter with a 100% beta yield with an average energy of 0.9337 MeV. The end point energy of the emitted β-particles is 2.28 MeV. This emission is accompanied by two other β-particle energies and 3 different gamma rays; however their yield is so very low as to usually be considered negligible. The ^{90}Y source was prepared using standard irradiation procedures at the McMaster Nuclear Reactor (MNR). A flame-sealed quartz tube containing yttrium salt was irradiated in the reactor core then transferred to a fume hood in our controlled High Level laboratories. The activity present in the sample was quantified in a dose calibrator. After scoring and snapping open the quartz tube, behind Plexiglas shielding in a fume hood, the yttrium salt was dissolved in appropriate media. The resulting solution was dispensed into a glass vial which was placed in a shielded container. Due to the highly energetic nature of the β-particles emitted from ^{90}Y, the source handling was performed in the fume hood behind a 1.3 cm thick Lucite shield.

4.3.3 Irradiation and photon counting

Figure 4.1 shows the schematic diagram for the general irradiation configuration. The whole set-up shown in Figure 4.1 was kept inside a light tight aluminum chamber which was placed in a fume hood. The source (^{90}Y) was received in a liquid form. It was placed in a 35 mm diameter (or in some cases a 100 mm diameter) Petri-dish. There was a 10-15 mm air gap between the source and the bottom of the Petri-dish containing the cells. Cells were attached to the bottom of one of two types of polystyrene Petri-dish which had a substrate thickness of either 0.878±0.006 mm or 1.760±0.005 mm.
We used a single photon counting system for the detection of UV light. This system employs a 16 mm diameter single photon counting photomultiplier tube (R7400P) by Hamamatsu. The PMT was operated at -800 V using a standard NIM based power supply from ORTEC. The output of the PMT was processed by an ORTEC model 9301 preamplifier, whose output was fed to an ORTEC model 9302 amplifier/discriminator and subsequently to the counter (ORTEC model 994). The maximum count rate that can be handled for negative input pulses in the counter was 100×10^6 counts/s and 25×10^6 counts/s for positive input pulses. The counter can be hooked up to a computer through a serial port. We performed all the experiments in conditions where the PMT dark current was very low i.e. of the order of 4-10 cps.

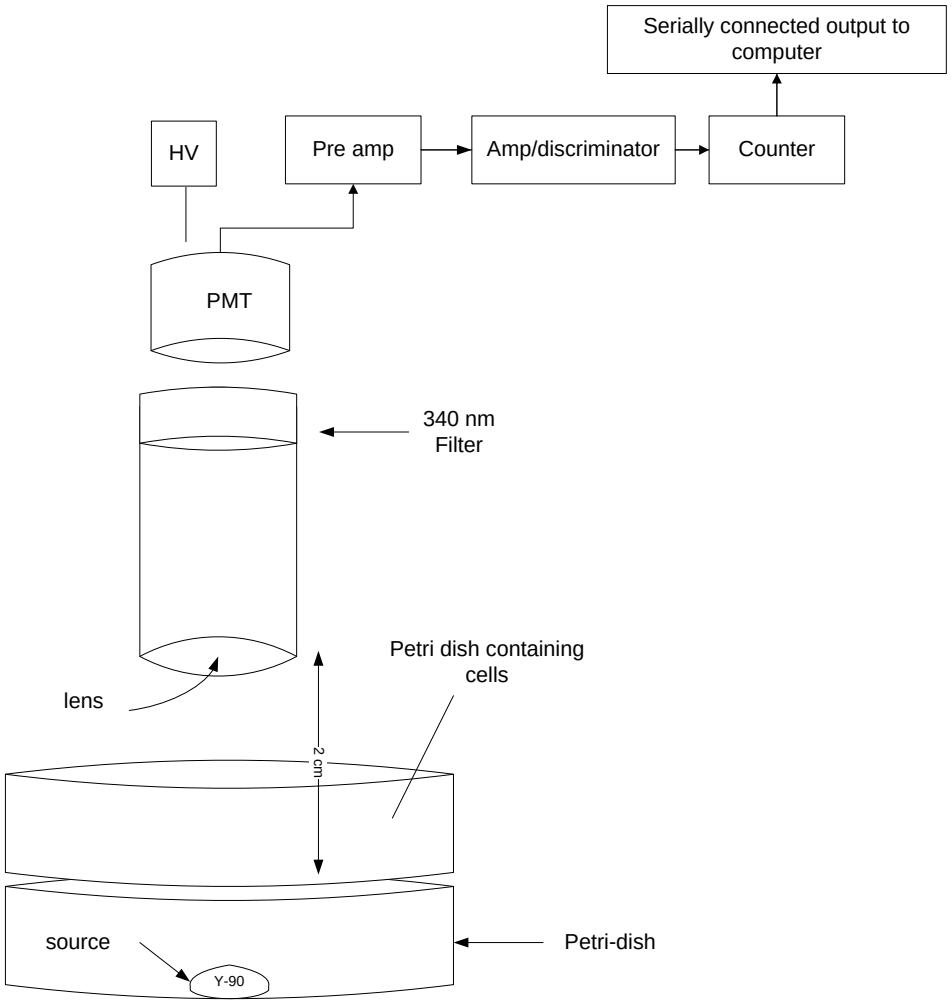

Figure 4.1 Schematic diagram of the setup for cell irradiation using 90Y source in the liquid form and measurement of light output using single photon counting instrumentation.

The photons were collected using a band pass interference-type filter from Edmond optics. The filter has a FWHM of 10 nm around a centre wavelength of 340 nm and thus should only permitting photons in the UVA range to pass through the filter. The lens requires a collimated beam of photons in order to obtain the manufacturer claimed efficiency of 25 %. For this purpose we used a UV-Vis fused silica lens having a focal plane at a distance of 1.8 ± 0.2 cm. The cellular material was kept approximately 2 cm away from the lens in order to collimate the photons. Since the beta particles generated by the source are energetic enough to reach the lens, this configuration results in a measurement where the total luminescence observed by the PMT comes in part from the lens of the collimating system.

The irradiation of the HPV-G cell samples was performed in two different orientations.

4.3.3.1 Poor geometry conditions

The general irradiation configuration shown in Figure 4.1 can be considered as a "poor" geometry condition because the whole Petri-dish is being irradiated, and a significant number of measured photons are scattered photons that did not originate from the focal point of the lens, but do reach the lens.

4.3.3.2 Good geometry conditions

In order to reduce the significant contribution of scattered photons reaching the lens, we used an aluminum collimator which helped to establish a relationship between the cell density and light output for a fixed irradiance. The aperture (2 mm diameter) in the collimation shield allowed the electron interaction at a small fixed spot in the cell-containing dishes, but reduced the contribution of scattered photons in the collection system.
In both the poor and good geometry conditions we determined the electron flux reaching the Petri-dish containing the cells and the lens of the collimating system using the Geant4 Monte-Carlo toolkit. The source was considered to have a semi-ellipsoidal shape and a Gaussian energy distribution with a mean of 1.12 MeV and a Gaussian width, σ, of 0.4 MeV. This modeling of the source energy as a Gaussian is an approximation: the β particles will be emitted from the ^{90}Y in a Fermi distribution and this energy distribution will be modified because the ^{90}Y is dissolved in solution. We suggest, however, that the use of a Gaussian model around the mean source energy as a first approximation of the β particle energy distribution at the surface of the solution permits a preliminary estimate of the flux reaching the lens.

4.3.4 Sources of error

One of the sources of random error in our experiments was the use of differently prepared specific activities for ^{90}Y in different experiments. This error would be introduced due to the fact that for the same nominal activity the source volume may be different in different experiments and this could change the irradiation characteristics of the samples. The volume varied from 200 µl to 1 ml for activities ranging from 500 µCi to 1 mCi. A uniform irradiation would be expected when the source is intact with high specific activity in the form of a point source. In addition we also had a systematic error due to the limited transmission of photons from the lens and filter. The lens transmits 90 % of the light over a wide range of electromagnetic spectrum; however the filter has a transmission efficiency of 25 % when it is illuminated with a collimated beam of light.

4.4 Results

We irradiated blank dishes, that is, Petri-dishes without any cells, for a range of ^{90}Y activities in both the good and poor geometry conditions. The luminescence observed was used to set a control or base-line luminescence. The end point energy of ^{90}Y β-particles allows some particles to travel up to 1.2 cm (using the Continuous Slowing Down Approximation, CDSA, range) in polystyrene (PS) before losing all their energy. This means that some energy will be deposited in the polystyrene cellular substrate (which was 0.878-1.76 mm thick), but some particles will pass through and interact with the fused silica lens which is a part of the collimation system for the single photon counting system (please refer to Figure 4.1). Therefore the light observed on the photomultiplier tube is a combination of scintillations originating from the polystyrene and the scintillation from the interaction of electrons with the lens. It is important to determine the relative contribution of each, and to think of this as an overall complex system of interaction, because in the case of Petri-dishes filled with cells and cellular media, the beta-particle flux on the lens would be expected to be reduced because of the interactions by beta particles in the cell medium, which will reduce the count rate resulting from the lens itself as compared to the control measurements.

Figure 4.2a shows the observed luminescence from the empty 35 mm diameter dishes for a range of ^{90}Y activities. Here the count rate was observed to be varying according to the following relationship

$$C.R = b \times \ln(A_o + c) - a \dots\dots\dots\dots\dots\dots eq\ 1$$

where *a, b* and *c* (> 0) are the fitting parameters *C.R* is the count rate and A_o is the activity. The fact that the lens in the collimating system is made of fused silica implies that there could be a significant proportion of scintillations coming from the lens itself. Fused silica has been studied for the emission of light using Sr-Y sources. It emits light at wide range of frequencies with varying intensities [17]. In order to identify the relative contributions to luminescence from the lens we irradiated it both in the presence and absence of the cellular substrate (polystyrene). Figure 4.2b shows the scintillations observed for both cases. For the poor geometry conditions there was a 4.35 % (on average) increase in the observed count rate because of the presence of the cell substrate in between the lens and the source. This indicates that under the poor geometry conditions, the photon count rate measured by the PMT is dominated by the scintillations occurring in the lens, most possibly because of scattered radiation (both beta particles and photons) reaching the lens.

The high energy of the beta particles and the known scintillation of the lens glass under irradiation, led us to believe that for the poor geometry, the flux of β-particles on the lens would primarily determine the light output observed in the control experiment. In order to estimate this, the β-particle flux was calculated using the Geant4 Monte-Carlo toolkit. Figure 4.3 a&b shows the results of the simulations. The results in Figure 4.3a shows a predicted reduction in β-particle flux in the lens when the dishes are filled with cells and cellular media, and an estimate of the number of β-particles per unit area incident on the

cells can be obtained using Figure 4.3b. For the sake of simplicity, we used water as a substitute for cell medium for the simulations. The height of cell medium was kept to approximately 3 mm above the cellular layer. The reduction in light output when water is added to the dish in the simulation results is attributed to absorption of the beta-particles in the water, reducing the number of beta particles incident on the lens.

The results of the simulation and the fact that the observed light output from the polystyrene substrate and the lens are almost indistinguishable led us to change the irradiation configuration, by using an aluminum collimator, with an aperture of 1 mm radius, in order to diminish the contribution to the light signal from scattered radiation.

As was previously shown, in Figure 4.2b, in the good geometry condition there was, on the average, a 37.6 % and 41.2 % increase in the counts in the PMT for 1.76 mm and 0.878 mm thick cell substrates respectively, compared to the case when the lens was irradiated directly with the β-particles from the source. This increase can be attributed to the light being emitted from the polystyrene substrate as a consequence of irradiation by β particles.

Figure 4.4 shows the results for ^{90}Y irradiated HPV-G cells that were plated in different densities on the Petri-dishes in the good geometry condition. As mentioned earlier, these cells were killed using a 70 % ethanol solution prior to the irradiation. Figure 4.4a shows the luminescence observed when the cells were plated in the dishes without any medium. Here the ethanol solution that was used to kill the cells was removed completely. Before irradiation, the cells were kept in a fume hood for a short period of time to allow any residual ethanol to evaporate.

At the lowest levels of source activities, up to 40 μCi, it was observed that there was no evidence of significantly more light being emitted by the cells as compared to the control. In fact, for activity levels up to 20 μCi the light output observed for the control is approximately 34 % higher than the light output observed from petri-dishes with HPV-G cells. This suggests to us that at low activities, the absorption and scattering of light in the cells dominates any increased emission by the cells. For higher activities, the light output increases with activity with all densities of cell plating showing significantly more UV emitted than from the petri-dish alone. This indicates, to us, that the cells plus media are emitting UV as a consequence of their irradiation by beta-particles. The UV emission for a source activity of 180 μCi was observed to be 250 % higher for cells plus dish than dish alone on average. The Monte Carlo calculated flux of β-particles to which the cells would be exposed varies between 9.31×10^{3} to 1.67×10^{5} $\beta.cm^{-2}s^{-1}$ for the source activities mentioned in Figure 4.4 a&b.

We also irradiated cells in the presence of their growth media. For this purpose we looked at two solutions: the RPMI 1640 growth medium which is a coloured solution, and a simple buffered transparent liquid medium. We added 3 ml of solution to the dishes, which created a 3.12 mm thick layer of the solution on top of the cells. Figure 4.4b shows the variation of the measured light yield for a variety of cell densities in the Petri-dishes ranging from 0.1 M to 1.0 M cells. It can be observed that the light output in the case of the cells containing the coloured growth medium is much less than the light emitted from cells with the clear medium. We suggest this clearly indicates absorption in and scattering by

the coloured medium. It can also be noted that in both Figure 4.4a and 4.4b the variation of light output from different cell densities is not significant enough in order to draw a useful conclusion about light output from the cells as opposed to the medium.
Since we were interested in determining the scintillation occurring in both the cells and the growth media, our control was petri-dishes alone. Using Figure 4.2a and Figure 4.3, we calculated the expected light output from the cell substrate material and the lens. This is the curve plotted as "control" in each figure.

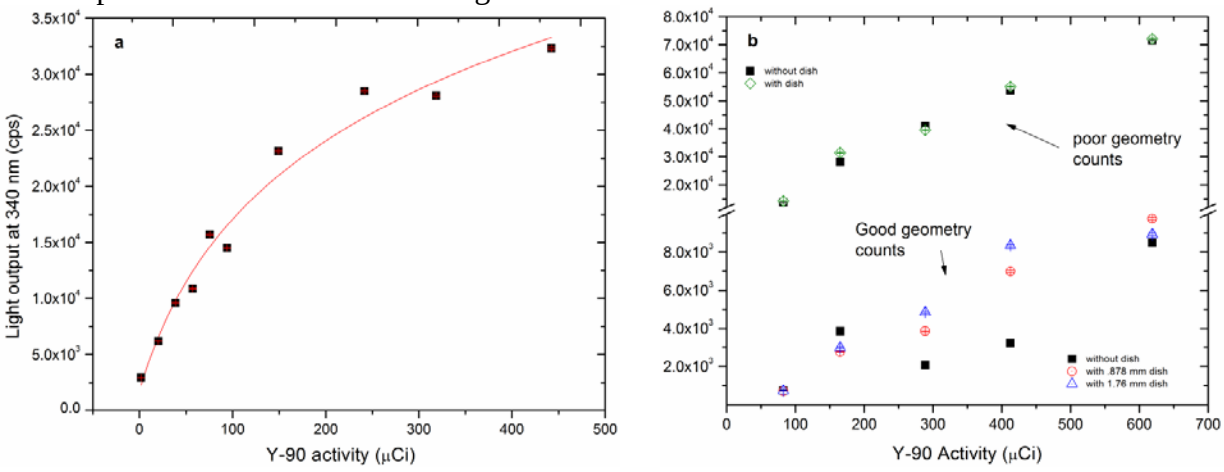

Figure 4.2 Light output against the 90Y activity. (a) Light output when there is a 1.76 mm thick polystyrene substrate present between the source and the lens in the poor geometry condition. The solid line indicates a logarithmic fit according to equation 1. (b) Light output for both good and poor geometry conditions. In this case the observed light is shown for the two different thickness of polystyrene substrate. The black squares indicate the observed light without any polystyrene substrate.

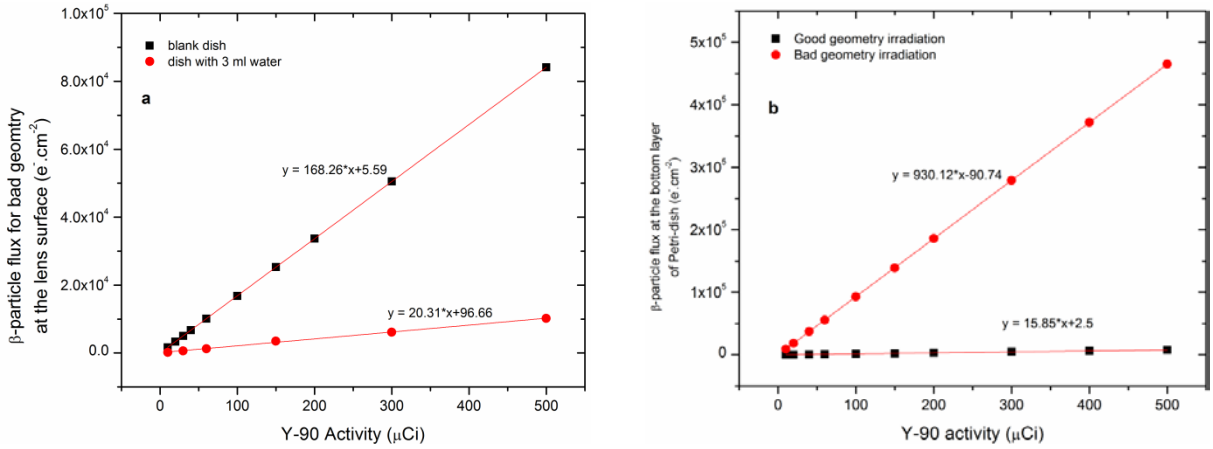

Figure 4.3 Monte-Carlo estimated ß-particle flux for different activities of 90Y. (a) ß-particle flux at the lens for a blank dish and a dish containing 3 ml water in it. (b) the ß-particle flux at the dish surface in the good and poor geometry conditions.

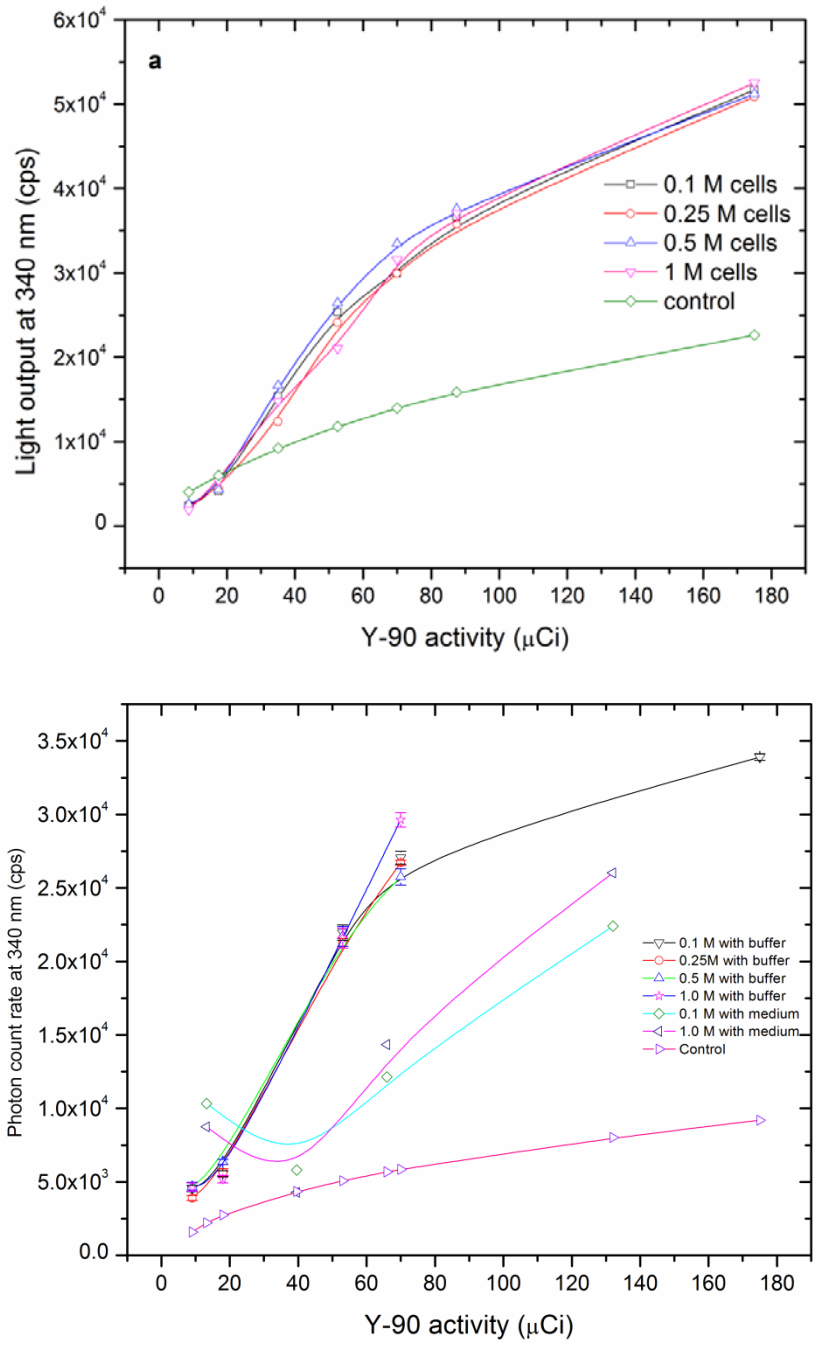

Figure 4.4 Light output from HPV-G cells, plated in different densities on polystyrene dishes, irradiated in the poor geometry condition for various 90Y activities. (a) Only cells (b) cells with clear buffer solution and coloured growth medium. The fitted trends trends are spline fits indicating an overall pattern.

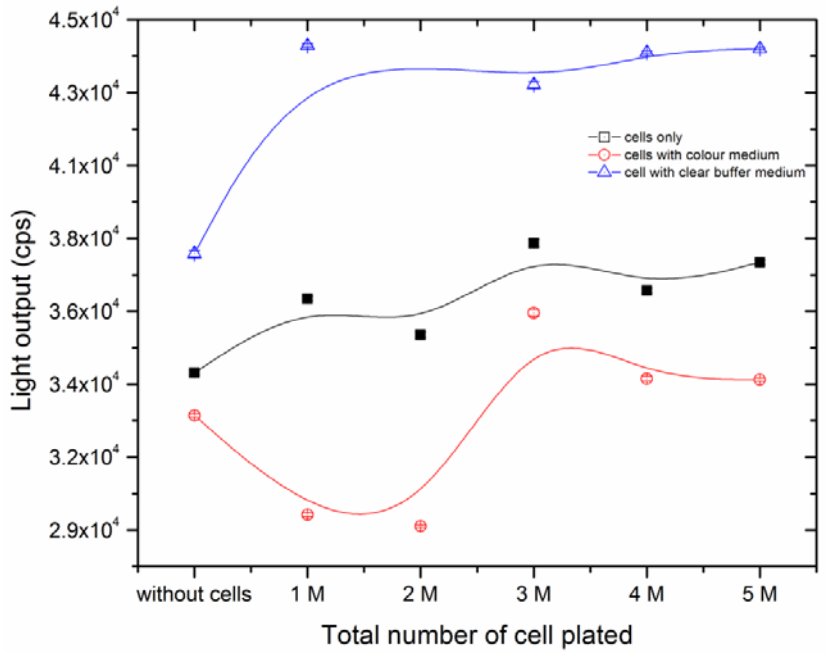

Figure 4.5 Luminescence yield from cell plated in different densities on 35 mm diameter Petri-dishes. 90Y activity used was 398μCi. Fit is merely a spline fit indicating the overall trend.

In order to try and determine the behavior of low LET radiation induced observed light output for varying cellular densities, we performed experiments at a fixed activity and irradiated cells plated in the range of 1×10^6 to 5×10^6 cells in the 35 mm diameter dishes. The flux of β-particles on the cells was estimated to be 3.70×10^5 $\beta.cm^{-2}s^{-1}$ for this experiment. Although the light output observed from the cell containing dishes is significantly higher than from the control dishes, and there are light output differences that depend on the colour of the buffer solution, shown in Figure 4.5, there is no apparent relationship between light output and cell density under these particular conditions. For the cells with the coloured growth medium, the light output observed at cell densities of 1M and 2M was lower than that for the control. We attribute this to absorption and scattering of light by the coloured buffer, including light emitted from the polystyrene dish. Although there is no clear relationship with cell density, other differences make sense. The addition of coloured medium consistently reduces the measured light output, while the addition of clear solution increases light output compared with cells alone, which we attribute to a greater volume of irradiated material.

We considered the fact that scattered radiation may be the reason that no relationship was observed with cell density. We therefore designed a further experiment so that a collimated beam of β particles would irradiate the cells in an area that can be treated as a point source for the photon collimating lens. The cells were seeded in large dishes (100 mm diameter)

in the range from 0.1×10^6 to 5×10^6 total cells in order to obtain a much wider range of cellular densities across the whole substrate. Figure 4.6 shows the observed light output plotted against cell density. The cell density represented on the x-axis is only a rough estimation based upon the total number of cells and the area of the dish. The β-particle flux at the Petri-dish in the presence of aluminum shield was determined to be 7.06×10^3 particles/cm^2 s^{-1} using Geant4 for an activity of 445 μCi.

It can be observed in Figure 4.6a that as the cell density increases in the dish (with no medium added) the observed count rate for 340 nm wavelength photons decreases in a crudely exponential manner. We attribute this to greater absorption and scattering of the photons by the cells, which outweighs the increased emission because of a larger cell density. The luminescence was also studied for wavelengths of 320 nm, however, it was found to not be significantly different from the background count rate. Figure 4.6b shows the relationship between light output and cell density when medium is added to the petri-dish. In this case, the light output does not decrease in the same manner as for cells alone. We suggest that this may be due to the complex interplay between β interaction, UV emission, UV scattering and UV absorption properties of the cell/medium mix as the cell density within medium changes.

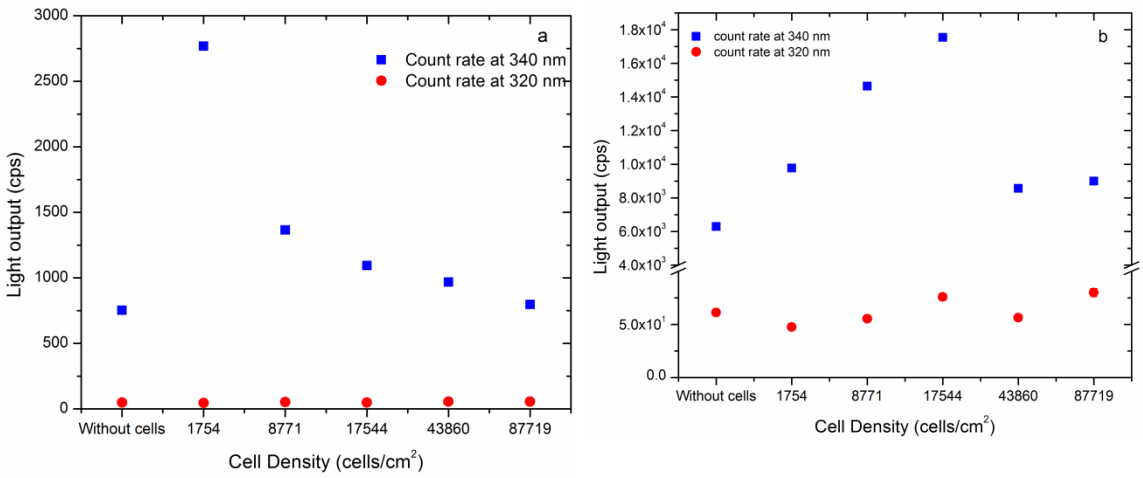

Figure 4.6 UV output from cell irradiation with fixed activity using a collimated beam of 90Y β-particles. (a) cell only and (b) cells with medium. Light output was determined at 340 nm and 320 nm. The background count rate was 45 cps. The 320 nm signal is not significantly different from the background rate.

4.5 Discussion

The experiment presented in Figure 4.2 was originally designed to measure the light output from the interaction of energetic β-particles with the polystyrene cellular substrate of the Petri-dish. Light emission from polymers as a consequence of β particle and other ionizing

radiations is not a new phenomenon and has been studied, generally for the purposes of radiation detection [18] and [19]. It is, of course, the physical basis of many scintillation radiation detector systems. Generally, the scintillation response of most plastic scintillators to the total deposited electron energy is supposed to behave linearly [20]. In our data, presented in Figure 4.2a and Figure 4.2b, the light output appears to be deviating from linearity above 100 μCi in one case, and following a general linear behavior in the other. One reason may be a limitation by having the source in the form of a high specific activity: there could have been source thickness effects. Additionally, since the source was in the form of a liquid, the total volume to represent the same activity might have been different between the two situations, as fresh sources were made for each experiment. A larger volume of the source to represent the same amount of activity would mean that the source would be spread over a larger area on the petri-dish. A lesser spread of the source on the petri-dish would better represent a point source while larger spreads would have created an area source. This could lead to discrepancies between experiments. In later experiments, we tried to keep the specific activity constant so that discrepancies due to the volume of the source could be minimized.

The experiments illustrated in Figures 4.4 and 4.5 indicate that the addition of cells and/or cell medium to the petri-dish results in a statistically significant change in the observed count rate for UVA photons at 340 nm. A relationship between UVA output and cell density was not clear. In this experiment the dishes were exposed to a fluence of 0.4M β-particles/cm^2 and the cell densities varied from approximately 0.1M cells/cm^2 to 0.5M cells/cm^2. A two way analysis of variance performed for the data presented in Figure 4.5 investigating the difference between cells alone and cells with clear cell medium added found a statistically significant difference between the light output of cells and cells plus medium ($p < 0.001$). Adding clear cell medium increased the measurable UVA signal. A two way analysis of variance performed for the data presented in Figure 4.5 investigating the difference between cells alone and cells with coloured cell medium added found a statistically significant difference between the light output of cells and cells plus coloured medium ($p < 0.001$). Adding coloured cell medium decreased the measurable UVA signal. In both cases, there was a suggestive, although not significant ($p=0.1$), effect of cell density on the signal. These results make a certain amount of sense. Adding coloured medium would be expected to increase absorption and scattering and reduce the signal at the detector, while the addition of clear medium adds more material in which to generate UV emission, with less of an effect on absorption and scattering.

After rearrangement of the experimental setup, by introducing an aluminum collimator, increasing the range of cell densities and keeping the fluence to 7000 β-particles/cm^2, we observed an effect of cell density when cells alone were studied. Increasing the number of cells in the dish (while not adding cell medium) reduces the measured light output. The observed count rate reduces by a factor of 2 as the cell density changes from 0.1 M cells to 0.25 M cells per dish. Overall, the effect of increased cell density appears to be a crudely exponential reduction in UVA measured at the PMT. There are only 5 data points, so it is not possible to determine precisely the exact mathematical shape of the relationship. We

suggest that the increase in the number of cells increases the absorption and scattering of photons. We observed the light output at 340 nm but not at 320 nm. The count rate observed at a wavelength of 320 nm was equal to the background rate. We therefore suggest that the emission that arises as a consequence of irradiation is predominantly for wavelengths equal to or higher than 340 nm. When medium was added to the dishes, the relationship between cell density and light output was less clear. Further measurements and refining of the experimental process are clearly required.

We focused on measuring the photon emission at a wavelength of 340 nm, that is, in the UVA range, from HPV-G cells irradiated with low LET β-particles. In our previous studies, we had demonstrated emission of UV photons as a consequence of irradiation by high LET radiation from materials used as cell substrates and materials derived from living cells. We wanted to determine whether cells and cell media also emitted UV as a consequence of irradiation, and as radiation induced bystander effects studies employ both high and low LET radiation, we studied low LET in this instance.

We believe the preliminary data presented here demonstrate emission of UVA from cells, cell media and substrate materials commonly used in radiation biology as a consequence of irradiation with β particles. Of course, the complex molecular structure of biological media means that in addition to emission of UVA there is also absorption and scattering of UVA by cells, media and substrate materials. The resultant external measurement of UV signal at the PMT is therefore a result of several complex interaction processes.

However, the fact that we observed measurable emission of UVA photons as a consequence of β irradiation has potentially important consequences for the understanding of radiation bystander effects: especially the understanding of effects that have previously been believed to be chemically mediated. We measured UVA which, once absorbed in the cells, can lead to a variety of known biological end points. Several studies have shown cell mutations, DNA damage, chromosomal aberrations, and alteration in the cell signaling pathways as a consequence of UV irradiation especially in the long wavelength range [21], [22] and [23]. UV-A produces damage by creating reactive oxygen species and has also been shown to produce the bystander effect [24], [25] and [26]. Many bystander effect studies still emphasize the presence of a biological or chemical signal that diffuses through the medium and causes the observed effects. A strong reason for this belief is the observation of effects in medium transfer bystander experiments. However, we suggest that one of the difficulties in recent interpretation and understanding of the “bystander effect” is that it is, in fact, not a single effect but several effects which result in similar endpoints. The medium transfer experiments do indeed suggest a chemically mediated signal. However, the preliminary data we present here, suggest, we believe, that there is a “physical” bystander effect. UVA that is emitted along the track of ionizing radiation can potentially interact with cells that are not targeted by the original radiation and create effects at a distance from the targeted cells.

4.6 Conclusions

We have presented data for emission of UVA from biological media when it is subjected to low LET radiation. In this case we used β-particles from a source of ^{90}Y. Initial experiments showed that the presence of cells or their medium in a petri-dish significantly increases the observed count rate of photons at a wavelength of 340 nm as compared to an empty control petri-dish. Coloured growth medium added to the cells reduced the count rate, while a transparent buffer in equal volume increased the count rate, as compared to cells alone. This provided evidence that emission, scattering and absorption of light were factors in the experiment. Under collimated irradiation conditions, it was observed that increasing cell density resulted in a decrease in the observed light output. UVA would appear to be emitted by cells, cell medium and cell substrates when irradiated with low LET radiation. However, the overall process is complex. Cells, medium and cell substrates appear to emit light at UVA frequencies under β-particles irradiation but also absorbed and scattered light. We suggest that the emission of UVA as a consequence of ionizations may explain some radiation bystander effects that have previously been attributed to a chemical signal. Further work is clearly necessary to investigate this phenomenon further.

4.7 References

[1] J. Matsubara, V. Turcanu, P. Poindron, and Y. Ina, "Immune effects of low-dose radiation: short-term induction of thymocyte apoptosis and long-term augmentation of T-cell-dependent immune responses.," *Radiation Research*, vol. 153, no. 3, pp. 332–338, 2000.

[2] G. Schettino, M. Folkard, K. M. Prise, B. Vojnovic, a G. Bowey, and B. D. Michael, "Low-dose hypersensitivity in Chinese hamster V79 cells targeted with counted protons using a charged-particle microbeam.," *Radiation research*, vol. 156, no. 5, pp. 526–34, Nov. 2001.

[3] S. Satin G, G. Renders-Pehrson, N. F. Metting, and E. J. Hall, "Adaptive response and the bystander effect induced by radiation in C3H10 T1/2 cells in culture," *Radiation Research*, vol. 156, no. 2, pp. 177–180, 2001.

[4] C. Mothersill and C. Seymour, "Radiation-induced bystander effects: past history and future directions.," *Radiation research*, vol. 155, no. 6, pp. 759–67, Jun. 2001.

[5] S. A. Lorimore, P. J. Coates, and E. G. Wright, "Radiation-induced genomic instability and bystander effects: inter-related nontargeted effects of exposure to ionizing radiation.," *Oncogene*, vol. 22, no. 45, pp. 7058–69, Oct. 2003.

[6] J. Axelsson, S. C. Davis, D. J. Gladstone, and B. W. Pogue, "Cerenkov emission induced by external beam radiation stimulates molecular fluorescence," *Medical Physics*, vol. 38, no. 7, p. 4127, Jun. 2011.

[7] J. W. Rohlf, *Modern Physics from aα to Z0*, 9th ed. Wiley, 1994, p. 664.

[8] S. B. Ahmad, F. E. McNeill, S. H. Byun, W. V. Prestwich, C. Seymour, and C. E. Mothersill, "Ion Beam Induced Luminescence; Relevance to Radiation Induced Bystander Effects," *Nuclear Instruments and Methods in Physics Research Section B: Beam Interactions with Materials and Atoms*, vol. 288, pp. 81–88, Aug. 2012.

[9] J. Pallon, C. Yang, R. J. Utui, M. Elfman, K. G. Malmqvist, P. Kristiansson, and K. A. Sjijland, "Ionoluminescence technique for nuclear microprobes," *Nuclear Instruments and Methods in Physics Research B*, vol. 130, pp. 199–203, 1997.

[10] P. Rossi, C. D. Maggio, G. P. Egeni, A. Galligioni, and G. Gennaro, "Cytological and histological structures identification with the technique IBIL in elemental microanalysis," *Nuclear Instruments and Methods in Physics Research*, vol. 181, pp. 437–442, 2001.

[11] A. Quaranta, A. Vomiero, S. Carturan, G. Maggioni, and G. Della Mea, "Polymer film degradation under ion irradiation studied by ion beam induced luminescence (IBIL) and optical analyses," *Nuclear Instruments and Methods in Physics Research Section B: Beam Interactions with Materials and Atoms*, vol. 191, no. 1–4, pp. 680–684, May 2002.

[12] S. P. D. Bhade, P. J. Reddy, a. Narayanan, K. K. Narayan, D. a. R. Babu, and D. N. Sharma, "Standardization of calibration procedures for quantification of gross alpha and gross beta activities using liquid scintillation counter," *Journal of Radioanalytical and Nuclear Chemistry*, vol. 284, no. 2, pp. 367–375, Mar. 2010.

[13] I. Krajcar Bronić, N. Horvatinčić, J. Barešić, and B. Obelić, "Measurement of 14C activity by liquid scintillation counting.," *Applied radiation and isotopes: including data, instrumentation and methods for use in agriculture, industry and medicine*, vol. 67, no. 5, pp. 800–4, May 2009.

[14] L. A Ryan, R. W Smith, C. B Seymour, and C. E Mothersill, "Dilution of irradiated cell conditioned medium and the bystander effect.," *Radiation Research*, vol. 169, no. 2, pp. 188–196, 2008.

[15] J. E. J Murphy, S. Nugent, C. Seymour, and C. Mothersill, "Mitochondrial DNA point mutations and a novel deletion induced by direct low-LET radiation and by medium from irradiated cells.," *Mutation Research*, vol. 585, no. 1–2, pp. 127–136, 2005.

[16] F. M Lyng, P. Maguire, N. Kilmurray, C. Mothersill, C. Shao, M. Folkard, and K. M Prise, "Apoptosis is initiated in human keratinocytes exposed to signalling factors from microbeam irradiated cells.," *International Journal of Radiation Biology*, vol. 82, no. 6, pp. 393–399, 2006.

[17] W. Viehmann, A. G. Eubanks, G. F. Pieper, and J. H. Bredekamp, "Photomultiplier window materials under electron irradiation: fluorescence and phosphorescence," *Applied Optics*, vol. 14, no. 9, p. 2104, Sep. 1975.

[18] Q. Chen, T. Hajagos, and Q. Pei, "Conjugated polymers for radiation detection," *Annual Reports Section "C" (Physical Chemistry)*, vol. 107, p. 298, 2011.

[19] D. H. Phillips, "Luminescence from Aromatic Polymers, Monomers, and Dimers under High-Energy Electron Excitation," *The Journal of Chemical Physics*, vol. 50, no. 8, p. 3297, Apr. 1969.

[20] G. V. O'Rielly, N. R. Kolb, and R. E. Pywell, "The response of plastic scintillator to protons and deuterons," *Nuclear Instruments and Methods in Physics Research Section A: Accelerators, Spectrometers, Detectors and Associated Equipment*, vol. 368, no. 3, pp. 745–749, Jan. 1996.

[21] G. Emri, E. Wenczl, P. Van Erp, J. Jans, L. Roza, I. Horkay, and A. A Schothorst, "Low doses of UVB or UVA induce chromosomal aberrations in cultured human skin cells.," *The Journal of investigative dermatology*, vol. 115, no. 3, pp. 435–440, 2000.

[22] U. P Kappes, D. Luo, M. Potter, K. Schulmeister, and T. M Rünger, "Short- and long-wave UV light (UVB and UVA) induce similar mutations in human skin cells.," *The Journal of investigative dermatology*, vol. 126, no. 3, pp. 667–675, 2006.

[23] T. J. McMillan, E. Leatherman, A. Ridley, J. Shorrocks, S. E. Tobi, and J. R. Whiteside, "Cellular effects of long wavelength UV light (UVA) in mammalian cells.," *The Journal of pharmacy and pharmacology*, vol. 60, no. 8, pp. 969–76, Aug. 2008.

[24] H. Nishiura, J. Kumagai, G. Kashino, T. Okada, K. Tano, and M. Watanabe, "The Bystander Effect is a Novel Mechanism of UVA-Induced Melanogenesis.," *Photochemistry and photobiology*, vol. 88, no. 2, pp. 389–397, Mar. 2012.

[25] G. Banerjee, N. Gupta, A. Kapoor, and G. Raman, "UV induced bystander signaling leading to apoptosis.," *Cancer letters*, vol. 223, no. 2, pp. 275–84, Jun. 2005.

[26] J. R. Whiteside and T. J. McMillan, "A bystander effect is induced in human cells treated with UVA radiation but not UVB radiation.," *Radiation research*, vol. 171, no. 2, pp. 204–11, Feb. 2009.

Chapter 5

Monte Carlo Simulations for PIXE Measurements

5 Particle Induced X-Ray Emission and Ion Dose Distribution in Biological Micro-beam; Geant4 Monte Carlo Simulations

S.B. Ahmad, J.E. Thompson, F.E. McNeill, S.H. Byun, W.V. Prestwich, C. Seymour and C.E. Mothersill

Short Communication; Accepted for publication in Nuclear Instrumentation and Methods in Physics Research B, September 17, 2012 (permission for reproduction is given in the appendix)

5.1 Chapter Summary

The goal of a microbeam is to deliver a highly localized and small dose to the biological medium. This can be achieved by using a set of collimators that confine the charged particle beam to a very small spatial area of the order of microns in diameter. By using a system that combines an appropriate beam detection method that signals to a beam shut-down mechanism, a predetermined and counted number of energetic particles can be delivered to targetted biological cells. Since the shutter and the collimators block a significant proportion of the beam, there is a probability of the production of low energy x-rays and secondary electrons through interactions with the beam. There is little information in the biological microbeam literature on potential x-ray production. We therefore used Monte Carlo simulations to investigate the potential production of particle-induced x-rays and secondary electrons in the collimation system (which is predominantly made of tungsten) and the subsequent possible effects on the total absorbed dose delivered to the biological medium.

We found, through the simulation, no evidence of the escape of x-rays or secondary electrons from the collimation system for proton energies up to 3 MeV as we found that the thickness of the collimators is sufficient to reabsorb all of the generated low energy x-rays and secondary electrons. However, if the proton energy exceeds 3 MeV our simulations suggest that 10 keV x-rays can escape the collimator and expose the overlying layer of cells and medium. If the proton energy is further increased to 4.5 MeV or beyond, the collimator can become a significant source of 10 keV and 59 keV x-rays. These additional radiation fields could have effects on cells and these results should be verified through experimental measurement. We suggest that researchers using biological microbeams at higher energies need to be aware that cells may be exposed to a mixed LET radiation field and be careful in their interpretation of data.

Two other factors can affect the pattern of dose deposition in the biological medium: the phase space distribution of the beam particles and the production of secondary electrons

(known as δ-rays). We investigated this by projecting simulated particles oriented at small angles with the beam axis. For lower fluence (2.6×10^{4} protons.mm^{-2}), we determined that despite only the target cell being assumed to be hit by the particle beam, some significant level of radiation dose was, in fact, delivered to the adjacent cells. This was most probably due to secondary electrons. The simulation showed that two of the cells adjacent to the target cell received 42 % and 5 % of the dose delivered to the target cell per proton. When the incident fluence on the collimator was increased to 1.3×10^{6} protons.mm^{-2}, it was observed that a significant number of protons deflected from the collimator spread into an area of 4340 μm^2. This is a significant spread when compared to the target area of 25 μm^2. The maximum number of particles that were delivered off-target was 25 % of the particles delivered to the target cell. This equates to a probability of delivering 1 particle anywhere in an area of 4340 μm^2 for every 4 particles delivered to the target cell. This result has significant implications. Results of this work warrant a further investigation because if these results can be re validated, perhaps experimentally or through another simulation code, then they may have significant implications on the interpretation of published data from biological microbeam experiments.

5.2 Introduction

The accurate and precise determination of low radiation dose and the subsequent potential effects is a subject of current discussion amongst the scientific community: both beneficial and harmful effects have been observed in cell cultures for low doses of radiation. The beneficial effects (sometimes called radiation hormesis) usually become evident in the form of increased resistance to radiation damage [1], while the harmful effects are manifested as increased mutation and cell death [2]. The available data for making assessments of radiation risk in humans, on a large scale, is very limited and is principally based on studies of the survivors of the atomic bombs that were detonated above Hiroshima and Nagasaki in 1945.

The principle motivation behind this study presented in this paper is to try and better understand the "radiation induced bystander effect". In radiation induced bystander effect studies, cells that were not the primary target of radiation, have been demonstrated to show effects similar to those observed in specifically targeted cells. Radiation induced bystander effect studies usually take one of the two forms either a) medium is transferred from irradiated cells to non-irradiated cells and subsequent effects in the non-irradiated cells studied or b) specific targeting of cells is achieved by use of a biological micro-beam. Specific cells are targeted and then nearby cells which are presumed to not have received a radiation dose are studied. Microbeams are presumed to deliver extremely low levels of primary particle fluence, or primary deposited dose, only to the points of interest in radiation biology, such as the cytoplasm or cell nucleus [3] and [4], in the cell/s of interest, such as HPVG cells and cultured human stem cells [5], [6], with presumed little dose being delivered to surrounding cells. Irradiation in this manner is designed to target only specific cells by the initial particle, while sparing others. This Monte Carlo study was a preliminary study to determine if these presumptions in biological microbeam experiments are, in fact, true, and to start discussion at an early stage within the community, via a short communication, as to whether the physics processes in the biological microbeam bystander experiments have been understood completely and correctly.

High LET charged particles generate a significant number of δ-rays (electrons) and photons when they interact with various materials and this includes interactions with cells and cellular media. The extent and biological effects of these δ-rays have been studied and well documented [7], [8] although the potential effects are not necessarily always well considered in targeted radiobiology experiments. In addition, the possibility of biological effects that arise as a result of the absorption of photons generated by the primary particle interactions have not been given much attention. Photons can be generated at several points within a microbeam system, for example due to interaction of particles with residual gasses in the beam line, due to interaction of the beam with the cell container material, or due to interaction in the cells. We have performed studies where we irradiated container materials, that could have relevance to radiation biology experiments with protons, and

observed the generation of light at UV frequencies [9]. However, in addition to these longer UV wavelengths, we questioned whether short wavelengths (in the x-ray region) could also be produced. These could have obvious effects in biological experiments.

We hypothesized that the x-ray production is especially dependent upon the mechanism of beam collimation employed in a particular microbeam. Collimation can be performed using slits, apertures and/or magnetic focusing. We have been developing a biological microbeam system at McMaster University that uses slits and apertures that is similar to the Columbia University Microbeam [10]. We chose this method because it is robust. However, the particle beam clearly interacts with the collimation system and we questioned the level of production of secondary electrons and x-ray photons. Some of the earliest developed biological microbeam systems used a combination of glass and some suitable scintillating material to confine the beam to the required size and to detect the primary particles [11], [12]. Photon generation in the collimation system was integral to such microbeams. The scintillation counters have been replaced by gas-filled particle counters that are placed behind the cell layer in the McMaster University microbeam facility. That is, the beam leaves the collimator, passes through the cell and cell medium layer and is then detected by a gas filled counter. The primary beam therefore requires sufficient energy to pass through the cell layer and be detected. The gas filled counter is of a large surface area and only detects whether a particle has passed through the cell layer. It does not provide spatial information regarding the actual particle track nor does it provide any information if the particle stops within the cellular layer. The experimental assumption is that particles travel along the target path which is determined before turning the beam on. We wanted to test the validity of this experimental assumption.

The McMaster microbeam uses slits and apertures made of tungsten and tantalum to collimate the beam down to a few micrometers in diameter. A lot of the beam is “dumped” and collimation of the beam in this manner means that the system delivers currents of the order of several μA for several minutes to the collimation system with only the required small number of protons reaching the cellular layer. Most of the initial proton beam interacts with the collimator, hence the question of whether these energetic charged particles are capable of producing x-rays of low energies which could change the dose deposition characteristics of the microbeam. We were particularly interested in determining the x-ray dose rates to “non-targetted” cells. There is published evidence of such effects. For example, soft x-rays were intentionally generated using particle induce x-ray emission (PIXE) from titanium to create a soft x-ray microbeam [13].

PIXE is a technique used to determine the elemental composition for various materials and is analogous to our biological microbeam although, of course, our intended fluence is much lower. In fact, the McMaster University microbeam system is built from an accelerator that was used for PIXE work at the University of Guelph. PIXE is a well established technique and the cross section data for the production of x-rays from various

materials are available and are incorporated in various Monte-Carlo based simulation codes. We used Geant4 (version 9.5) in order to determine whether x-rays produced in the collimation system are capable of depositing some additional dose to the cells irradiated in the McMaster University microbeam.

5.3 Microbeam irradiation

In the McMaster University microbeam facility, protons pass through three different stages of collimation. Figure 5.1a shows a diagram (drawn to scale) of the actual beam line with the various components used for collimation. The part of beam line shown in Figure 5.1a is the (vertical) section after the analyzing magnet (where particles of a specific energy are selectively bent at a 90^o angle). At the first collimation stage, the beam is collimated in a rectangular shape with the help of adjustable x-y slits. The second stage is an electronically controlled fast shutter. This shutter has a maximum separation of 60 μm. The shutter is synchronized with the proton detection system, sited beyond the cell irradiation platform, so that after the detection of a pre-determined number of protons, the shutter can be closed. At the third stage, the beam is further collimated using a set of tungsten apertures. Figure 5.1b also shows a cross-sectional diagram of the 3^{rd} stage collimator assembly. This assembly consists of three layers; each made of tungsten. The top and bottom layers are 50 μm in thickness while the sandwiched layer is 225 μm in thickness. The top layer is replaceable with different diameter apertures (although usually a 5 μm aperture is employed). This layer is further covered with a very thin layer of silicon-nitride (500 nm) that is used to maintain the vacuum. Particles deposit some of their energy and hence deliver a dose to the cells but have sufficient energy to pass through the cell layer. They reach a gas-filled particle counter directly above the cells where they are counted. This counter is synchronized with the aforementioned electronic shutter that is designed to stop the beam after the counter reaches a predetermined value. Cells are grown over a 5-6 μm polypropylene sheet and then placed over the silicon-nitride for irradiation. The shape of the collimator suggests that if x-rays are produced in the top layer due to proton interactions, then this can increase the uncertainty in dose delivery to the targeted and especially non-targetted cells.

In order to investigate this, we transported particles using Geant4 which makes use of the ECPSSR [14] theory for inner shell (K, L and M) ionizations [15]. For calculation of the electron, x-ray and proton fluence at the cellular layer, we created a matrix of 2500 cells (filled with water) having dimensions of $5\times5\times10$ μm^3 placed adjacent to each other next to a polypropylene sheet. Examples of realistic cells are available in Geant4 (we refer to the microbeam example in Geant4 developed by Sebastien Incerti, Geant4/examples/advanced/microbeam). However, since our intention was not to determine an exact dose profile in a single cell but rather the to establish whether, in principle, there is a mixed radiation field dose distribution over a larger volume due to secondary photon production and the scattering of the incident particles, we used cubic

cells placed next to each other. The distance between the top of the aperture and the bottom of the cells is 2.005 mm. It may be noticed that the configuration shown in Figure 5.1b could lead to a large area (approximately 0.27 mm^2 circular area) of the cells being exposed to the beam due to a large solid angle. However, since the beam is not expected to be oriented at large angle with respect to the vertical direction, the particles are expected to be confined to an area directly above the final aperture.

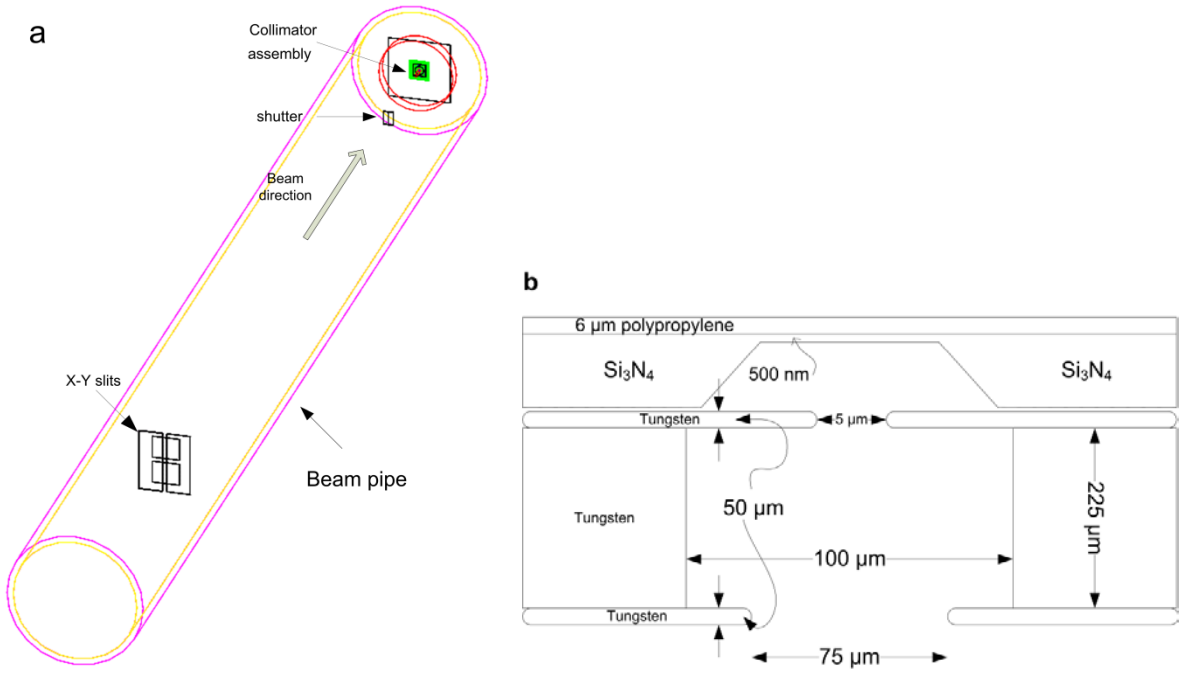

Figure 5.1 (a) Beam line indicating various components of beam collimation, (b) cross-sectional diagram of the final collimating assembly in Microbeam.

5.4 Study of the Effects on the Dose Distribution from Particle Induced X-Ray Emission in Tungsten

The energy of the L (α, β, and γ) characteristic x-rays from tungsten lie between 8.40 keV and 11.43 keV and the K(α and β) characteristic x-rays lie between 59.32 keV and 69.13 keV [16]. Table 5.1 shows the number of simulated x-rays and secondary electrons (and corresponding energy ranges) emitted for protons of energies in the range of 1 MeV and 4 MeV, in tungsten, where the particles are bombarded onto a 50 µm thick tungsten target. We chose the incident statistics that would give a relative error of approximately 1 % or less for the number of generated secondaries. This data (Table 5.1) was generated using the example "TestEm18" available in Geant4.9.5.p01. TestEm18 is used for energy lost by a charged particle in a single layer, due to ionization and bremsstrahlung. The production cuts chosen for x-ray and electron generation were 500 nm which correspond to an energy

threshold of 1.017 keV and 5.523 keV respectively in tungsten. All the other limits were set to the default settings.

Table 5.1 Proton induced x-rays and secondary electrons in Tungsten. Zeros in the table means that the particles below the production threshold were not tracked.

		Incident particle energy			
		1 MeV	2 MeV	3 MeV	4 MeV
x-ray photons per incident particle	Number	$4.03 \pm 0.06 \times 10^{-5}$	$9.83 \pm 0.10 \times 10^{-4}$	$6.36 \pm 0.03 \times 10^{-3}$	$1.85 \pm 0.004 \times 10^{-2}$
	Min Energy (KeV)	1.3966	1.3925	1.367	1.367
	Max Energy (KeV)	12.031	12.031	67.121	69.2
Electron per incident particle	Number	0	0	1.69 ± 0.0004	13.00 ± 0.001
	Min Energy (KeV)	0	0	5.5234	5.5234
	Max Energy (KeV)	0	0	6.5385	8.7228

We used the standard electromagnetic and penelope physics tables (incorporated in Geant4) in order to transport the generated secondary particles. For tungsten irradiated with protons up to energies of 2 MeV, no K shell characteristic x-rays are emitted. Table 5.1 show that for 3 MeV protons there is a possibility for the production of some K characteristic x-rays. However, all of the x-rays generated in the target are reabsorbed as shown in Figure 5.2-A2. As the energy increases above 3 MeV, some 10 keV x-rays can escape the tungsten target and expose the cell layer. If the proton energy is increased further to 4.5 MeV, not only 10 keV x-rays escape from the target but also some K-shell characteristic x-rays (at approximately 60 keV) can escape. It can be inferred from the data presented in Table 5.1 and Figure 5.2 that microbeams (employing tungsten collimation) accelerating protons up to an energy of 3 MeV do not generate an additional x-ray exposure to the cells. As the energy increases beyond 3 MeV, there is a probability of 10 keV x-rays escaping the 50 micron layer of tungsten. However most of these x-rays that are generated near the incident surface are reflected back into the beam line. If the protons are obliquely incident on the collimator edge (see Figure 5.1b) they can produce x-rays that would be reflected along the beam line. Therefore a practical measurement using some PIN diodes or a SiLi (Silicon Lithium drifted) detector could be worthwhile to confirm the presence or absence of x-ray photons at these higher energies. The McMaster University microbeam is not designed to run above 3 MeV, so this cannot be performed experimentally in our laboratory.

The simulation shows that there are 9×10^{-4} % and 12 % chances for the primary charged particles and the δ-rays to be transmitted through a 50 μm thick layer of tungsten for 4 MeV and 4.5 MeV beam energies respectively.

Figure 5.2 is a set of histograms for the proton induced x-ray spectra at three different locations in tungsten for 3 MeV and 4.5 MeV incident proton beam energies. These figures were generated using the same production cuts as mentioned earlier in "TestEm5". The first set of histograms (A1 and B1) shows the x-ray spectrum inside tungsten. The second set of histograms (A2 and B2) shows the transmitted x-ray spectrum and the third set of histograms (A3 and B3) shows the reflected x-ray spectrum. Total number of generated x-rays is much larger in the case of a 4.5 MeV compared to 3 MeV incident particle energy but the spectra look similar. The main difference between the spectra is that the K-shell characteristic x-rays are produced in one case only (i.e. 4.5 MeV). Also in the case of 3 MeV (or lower) energy protons, the generated x-rays are reabsorbed or reflected back into the main beam line, and none of the x-rays are transmitted to the cell layer. However for beam energies of 4.5 MeV or more, there would be a significant proportion of 10 keV and 59 keV x-rays that can be transmitted. As the McMaster University microbeam uses a 3 MV Van de Graff type accelerator, we can conclude that in our system, the generated secondary x-rays or electrons from the beam line or the collimation system do not cause an additional dose to the layer of cells lying above the collimator.

The last set of histograms in Figure 5.2 (A4 and B4) provides a comparison of the energy absorption events in tungsten. For 3 MeV incident protons, the peak energy absorption occurs at 3 MeV indicating all the energy is deposited in the material. However, for 4.5 MeV incident energy protons, there are quite a few energy absorption events where the total energy absorbed in the tungsten is less than 4.5 MeV, and in fact is between 4 and 4.5 MeV. This also indicates that some protons at these energies can be transmitted all the way through the aperture and with the remaining energy.

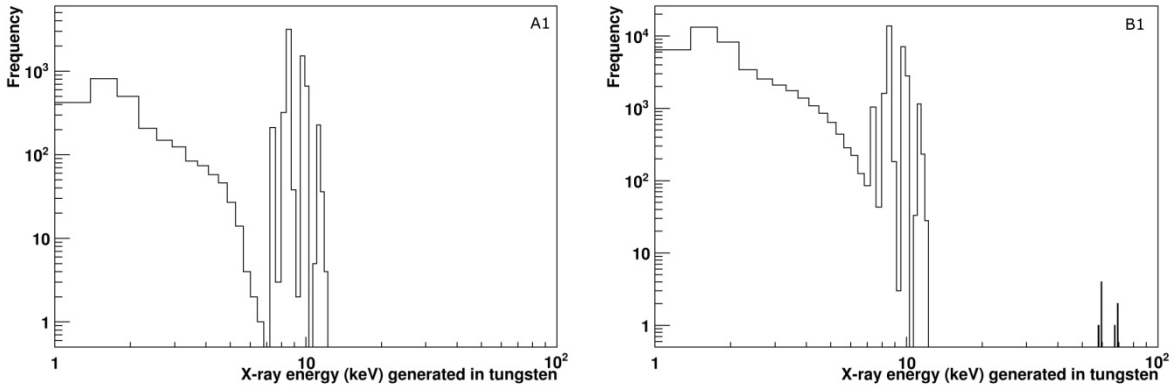

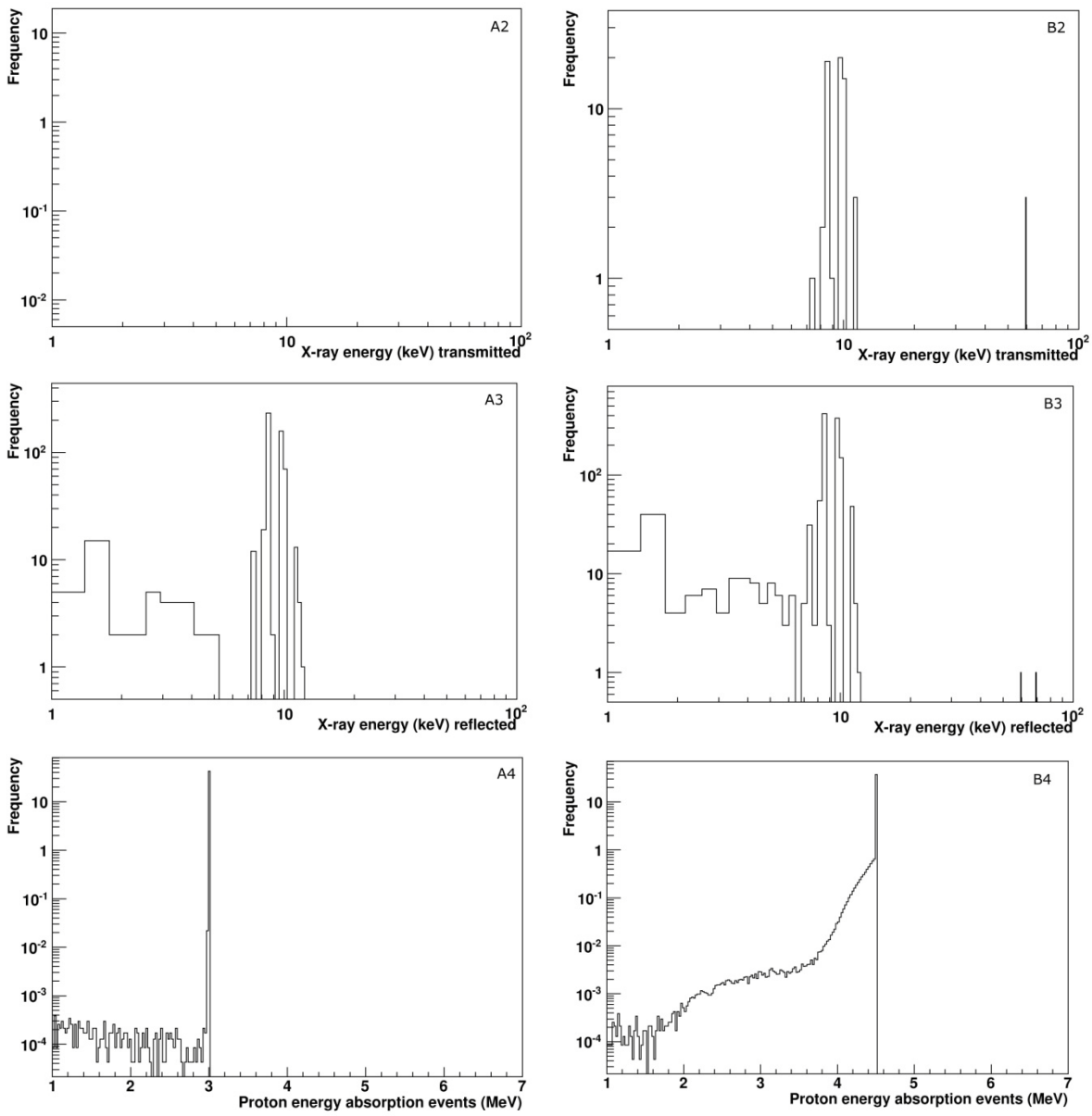

Figure 5.2 Comparison for particle induced x-ray emission for 3 MeV (A[1-4])) and 4.5 MeV (B[1-4])) protons emitted from a 50 µm Tungsten target (plotted in root [8].

5.5 Study of the Effects on the Dose Distribution from Beam Dispersion and Secondary Electrons

Accurate targeting is a major goal in the development of a biological microbeam. The microbeam developers around the world measure their beam targeting accuracy, usually, by using CR-39 track detectors [18–21]. These, of course, show primary high LET particle

tracks well but are not sensitive to low LET secondary radiation. The published data can also suffer from lower overall counting statistics because of the time involved in acquiring the track etch data. There is no generally accepted experimental method for determining the dose distributions that combine high and low LET information in radiobiological studies. Monte Carlo simulations are generally used. Combinations of actual measurements (using MOSFETs) and Monte Carlo measured doses have been applied to x-ray microbeams used for microbeam radiation therapy purposes (MRT) [22–26] where dose rates are high and more readily measurable. For radiobiological studies, the dose delivery and distribution has been studied using Geant4 for at least one microbeam employing magnetic focusing [27]. Published data, for collimated microbeams, is limited and we wished to better understand the potential dose distributions for our particular collimation system as this has major implications for the interpretation of biological results.

In microbeams employing slits and apertures, the phase space distribution of charged particles is important in determining the final dose distribution at the cell layer. In this study we made the assumption that the phase space distribution of the particles remains the same throughout the beam line until the particles reach the final collimating assembly. Using this assumption, we generated the particles in a circular area close to the final aperture assembly. The aperture was irradiated with a fluence of 2.6×10^4 protons.mm^{-2} and 1.3×10^6 protons.mm^{-2} using a 1d accelerator beam option in Geant4 with 5^o dispersion along the beam axis. The 1d accelerator beam is one of the options available in Geant4 through the "General Particle Source (GPS)" that defines the position distribution of simulated particles. The assumption of having the same phase space distribution of particles close to the final collimator as at any other point along the beam line, and the assumption of 5^o dispersion along the beam axis was made, because we were particularly interested in studying the effects of interactions of protons with the collimator edges.

The beam profile in a plane perpendicular to the beam traveling axis and energy profiles are shown in Figure 5.3. The beam energy was considered to have a Gaussian distribution (represented in equation 1) with a Gaussian width, σ, of 0.2 MeV and central beam energy, μ, of 3 MeV. In an actual beam the variation in the particle energy is usually very small (around 1 % or less). However for simulation purposes, we chose a σ value of 0.2 MeV in our case.

$$\mathbf{f(x;\mu,\sigma^2)} = \frac{\mathbf{1}}{\boldsymbol{\sigma\sqrt{2\pi}}}\mathbf{e}^{-\mathbf{1/2}\left(\frac{\mathbf{x-\mu}}{\boldsymbol{\sigma}}\right)^{\mathbf{2}}} \quad \text{..... eq1}$$

For the smaller proton fluence (2.6×10^4 particles.mm^{-2}) on the aperture, the distribution of particles reaching the cellular layer is nicely aligned to the centre of the cellular grid shown in Figure 5.4a. Here the relative error in the number of particles passing through the cells was 0.5 %.

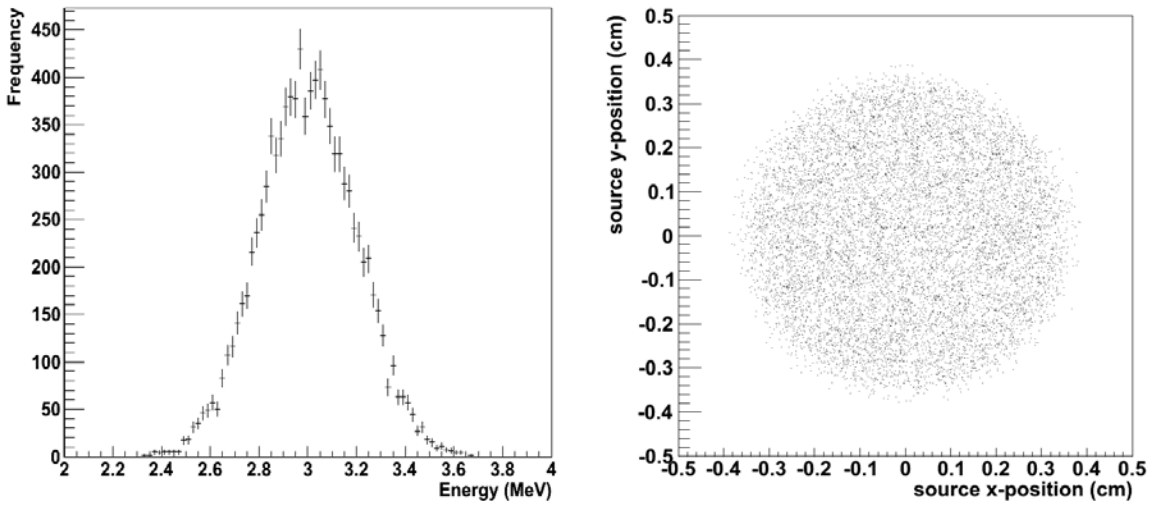

Figure 5.3 Beam profiles. Left; Gaussian energy distribution with σ of 0.2 MeV, Right; source distribution in a plane perpendicular to the beam axis.

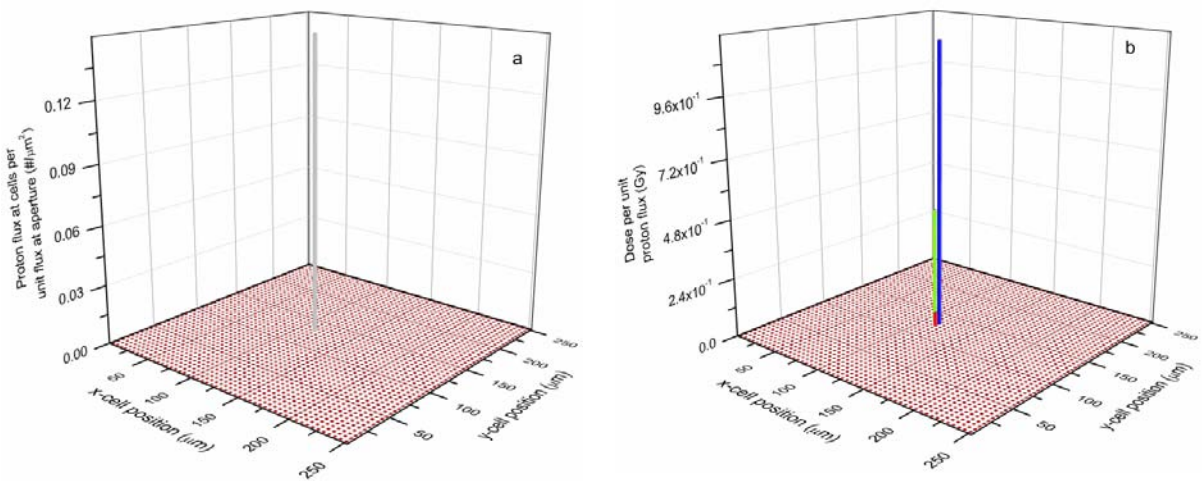

Figure 5.4 Geant4 calculated number of protons passing through a grid of 2500 (5×5×10 μm^3) cells for a proton flux of 2.6×10^4 protons/mm^2 (a) on the aperture and the corresponding dose delivered per cell per proton (b).

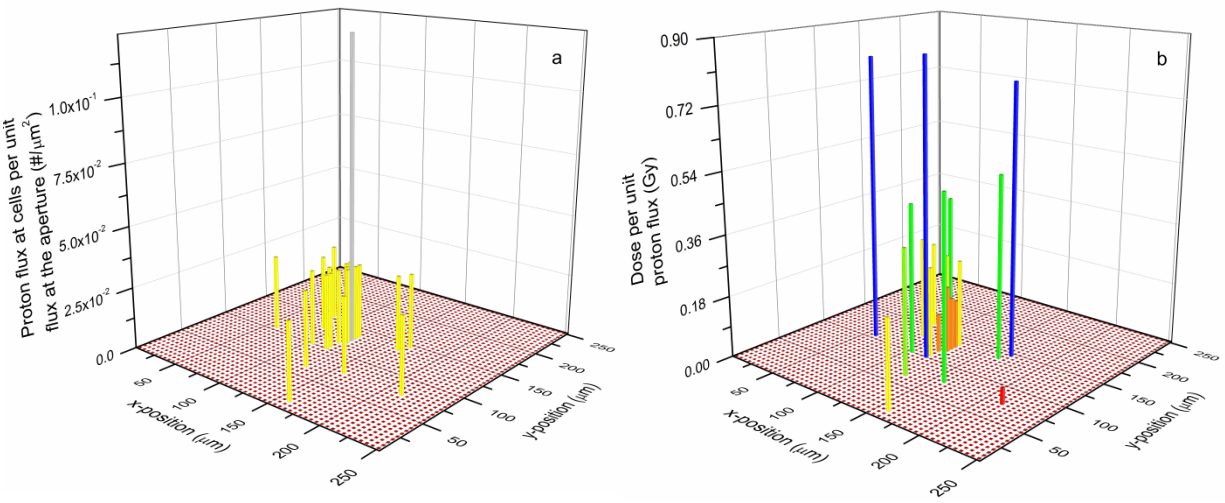

Figure 5.5 Geant4 calculated number of protons passing through a grid of 2500 (5×5×10 μm^3) cells for a proton flux of 1.3×10^6 protons/mm^2 (a) on the aperture and the corresponding dose delivered per cell per proton (b).

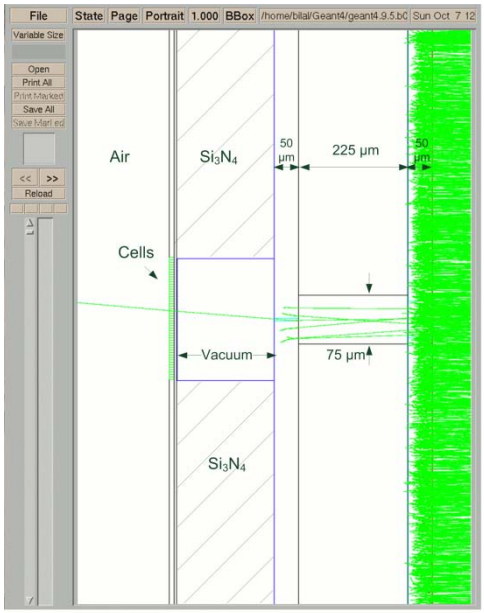

Figure 5.6 Magnified image of the collimator drawn using DAWNFILE. Proton (green trajectories) scattering inside the 5 μm collimator can be visualized in this image.

However the dose delivered to the cells is not strictly confined to the centre of the cellular grid (or the intended target area) as shown in Figure 5.4b. This is not, however, because of the electrons or x-rays generated from the proton interaction at the edges in the collimator. As shown previously for the 3 MeV beam energy, the secondary radiation produced inside

the collimator is reabsorbed. The distribution of dose to some adjacent and technically non-targetted cells could be due to the ionizations created by the primary charged particle tracks inside the cell layer, which lead to δ-rays which deposit some energy to the area surrounding the primary "hit" cell. A second reason could be the fact that the primary particles, generated at a small angle to the beam axis, can pass the edge of the collimator, travelling obliquely, and deposit a dose to cells adjacent to the primary target.

This observation could be important when interpreting radiation induced bystander effect studies where one cell that has been considered not to receive any radiation, has, in fact, actually absorbed some dose due to δ-rays or oblique off-target primary beam particles. The maximum delivered dose per proton in the target cell has been estimated to be 48.28 mGy, calculated in Geant4 using the classical approach of total energy deposited, divided by the total mass of the cell. The dose deposited to the two adjacent cells was determined to be 20.28 mGy and 2.41 mGy. These are not insignificant doses, previous studies have determined a threshold for induction of the bystander effect that is of the order of a few mGy [28]. This result means that a cell that would be considered to be non-targetted in the current interpretation of microbeam biological data has, in fact, received enough direct radiation to induce a biological response. In the absence of knowing about this significant secondary radiation dose, the interpretation would be that the observed response in that cell is due to a chemical signal. It would, however, be due to a direct radiation interaction.

The simulation was also performed by increasing the fluence on the aperture to 1.3×10^6 protons.mm^{-2}. By increasing the total number of particles, it can be seen in Figure 5.5a that the number of hit cells, has been increased and they span over a much wider area (approximately 4340 μm^2). Our simulation shows that this occurs predominantly due to scattering of the particles inside the collimator as shown in Figure 5.6. Here the target area was set to 25 μm^2. There is some experimental evidence for this effect. In previous studies performed for the Columbia University microbeam (where the collimator design is slightly different than ours, see reference [10]) the particles seem to form a "halo" extending out to an overall radius of 8 μm, when the intended target area was approximately 3 μm. This halo was observed to contain 7 % of the beam [10]. In our case, the results of the simulation of our collimator suggest that for a 5% beam dispersion, the halo would extend out to a radius of 66 μm when the intended targeted area has a radius of 5 μm. The two sets of results disagree in terms of the extent of the halo. This is probably firstly a consequence of modeling a 5% level dispersion, when it may in fact be less. A second reason may be the method by which the size of the halo is determined. However, the important point is that both sets of results agree that a halo of primary particle hits does exist beyond the target area. Cells that are not logged as being hit, are hit. The Columbia data suggest approximately 1 in 12, our simulations suggest 1 in 4. The relative error for number of particles passing through the cells was between 0.25 % and 0.5 %

Over this is laid a dose distribution from secondary particles generated by high LET particles in the cell layer. The important new additional information that our Monte Carlo simulation of this halo provides is regarding the dose distribution. The simulation calculates dose deposition from both the high LET primary particles and the low LET secondary particle distribution. Adding this delta ray dose distribution to the primary particle dose distribution shows a greatly extended area of significant radiation dose. We feel that our simulation data (when considered with the published experimental data from the Columbia microbeam) show that non-targetted dose should be taken into account in the interpretation of the biological effects.

By applying the particle filters (using the class G4SDParticleFilter) available in Geant4, we established that even when increasing the current on the aperture, still no x-rays or electrons generated from the collimation system reach the cellular layer. The particles crossing cells several μm away from the central beam axis are all protons. Figure 5.5b shows the dose distribution in the cells calculated in the same manner as in Figure 5.4b.

These simulations show that x-rays or secondary electrons generated due to the interaction of protons in the collimation system do not contribute significantly to the final dose delivered at the cellular level using the McMaster University microbeam which operates at a maximum voltage of 3 MV. However, there is a dose delivered to cells adjacent to the "target" cells either from secondary electrons generated in the cells and medium themselves or from scattered primary beam particles from the aperture.

5.6 Conclusions

Our basic understanding of the mechanisms behind low dose rate effects in cells can only be improved when an accurate and precise understanding of the exact physical doses and dose distributions is achieved. Microbeam accelerators have been suggested as a mechanism by confining the beam to very small sizes using magnets or slits and apertures with the ultimate goal of hitting specific targets in cells. This study, although preliminary and simulation based, does suggest that the idea of being able to study the interaction of radiation in one cell, and one cell only, with no other cells around that cell receiving a radiation dose, is too simplistic. The data shown here suggest that microbeams, which employ slits and apertures may generate low levels of x-rays in the collimation system that could subsequently add to and create a mixed radiation field at the cell layer when operated at energies above 3 MeV. However, it would appear that for the available proton energies in the McMaster University microbeam (less than 3 MeV) the particle induced x-rays are reabsorbed by the collimator materials themselves. Additionally, the shape of the collimator assembly and the phase space distribution of beam particles in a particular microbeam are important parameters in determining the actual irradiated area. Scattering from the edge of the collimator can mean that a significant proportion of particles do not hit the intended target. In systems which use post cell layer large area detection systems the

precise track of the particles cannot, of course, be determined in the actual cell irradiation experiments. Determination of which cells are irradiated is based on probabilities and dose distribution maps. We suggest that further work is required and biological microbeams which use collimator systems should, through combinations of experiment and Monte Carlo simulation, create better dose distribution maps that importantly determine the contributions to dose from summations of the primary beam, the scattered primary beam and the secondary electrons generated in the cells and cell media. It may be determined through simulation and experiment that those cells, in fact, received a significant radiation dose which may explain some of the “bystander “effects.

5.7 References

[1] B. R. Scott, "It's time for a new low-dose-radiation risk assessment paradigm--one that acknowledges hormesis.," *Dose-response : a publication of International Hormesis Society*, vol. 6, no. 4, pp. 333–51, Jan. 2008.

[2] C. Mothersill and C. Seymour, "Radiation-induced bystander effects and adaptive responses—the Yin and Yang of low dose radiobiology?," *Mutation Research/Fundamental and Molecular Mechanisms of Mutagenesis*, vol. 568, no. 1, pp. 121–128, Dec. 2004.

[3] C. Shao, M. Folkard, B. D. Michael, and K. M. Prise, "Targeted cytoplasmic irradiation induces bystander responses.," *Proceedings of the National Academy of Sciences of the United States of America*, vol. 101, no. 37, pp. 13495–500, Sep. 2004.

[4] R. C. Miller, G. Randers-Pehrson, C. R. Geard, E. J. Hall, and D. J. Brenner, "The oncogenic transforming potential of the passage of single particles through mammalian cell nuclei," *Proceedings of the National Academy of Sciences*, vol. 96, no. 1, pp. 19–22, Jan. 1999.

[5] R. C. C. Poon, N. Agnihotri, C. Seymour, and C. Mothersill, "Bystander effects of ionizing radiation can be modulated by signaling amines.," *Environmental research*, vol. 105, no. 2, pp. 200–11, Oct. 2007.

[6] M. V. Sokolov and R. D. Neumann, "Radiation-induced bystander effects in cultured human stem cells.," *PloS one*, vol. 5, no. 12, p. e14195, Jan. 2010.

[7] F. A. Cucinotta, H. Nikjoo, and D. T. Goodhead, "The effects of delta rays on the number of particle-track traversals per cell in laboratory and space exposures.," *Radiation research*, vol. 150, no. 1, pp. 115–9, Jul. 1998.

[8] F. A. Cucinotta, H. Nikjoo, and D. T. Goodhead, "Model for Radial Dependence of Frequency Distributions for Energy Imparted in Nanometer Volumes from HZE Particles," Jul. 2009.

[9] S. B. Ahmad, F. E. McNeill, S. H. Byun, W. V. Prestwich, C. Seymour, and C. E. Mothersill, "Ion Beam Induced Luminescence; Relevance to Radiation Induced Bystander Effects," *Nuclear Instruments and Methods in Physics Research Section B: Beam Interactions with Materials and Atoms*, vol. 288, pp. 81–88, Aug. 2012.

[10] G. Randers-Pehrson, C. R. Geard, G. Johnson, C. D. Elliston, and D. J. Brenner, "The Columbia University single-ion microbeam.," *Radiation research*, vol. 156, no. 2, pp. 210–4, Aug. 2001.

[11] B. V. FOLKARD, "A charged-particle microbeam: I. Development of an experimental system for targeting cells individually with counted particles," *International Journal of Radiation Biology*, vol. 72, no. 4, pp. 375–385, Jan. 1997.

[12] T. Kamiya, W. Yokota, Y. Kobayashi, M. Cholewa, M. S. Krochmal, G. Laken, I. D. Larsen, L. Fiddes, G. Parkhill, and K. Dowsey, "Development of an automated single cell irradiation system combined with a high-energy heavy ion microbeam system," *Nuclear Instruments and Methods in Physics Research Section B: Beam Interactions with Materials and Atoms*, vol. 181, no. 1–4, pp. 27–31, Jul. 2001.

[13] A. D. Harken, G. Randers-Pehrson, G. W. Johnson, and D. J. Brenner, "The Columbia University proton-induced soft x-ray microbeam.," *Nuclear instruments & methods in physics research. Section B, Beam interactions with materials and atoms*, vol. 269, no. 18, pp. 1992–1996, Sep. 2011.

[14] W. Brandt and G. Lapicki, "Energy-loss effect in inner-shell Coulomb ionization by heavy charged particles," *Physical Review A*, vol. 23, no. 4, pp. 1717–1729, Apr. 1981.

[15] A. Mantero, H. Ben Abdelouahed, C. Champion, Z. El Bitar, Z. Francis, P. Guèye, S. Incerti, V. Ivanchenko, and M. Maire, "PIXE simulation in Geant4," *X-Ray Spectrometry*, vol. 40, no. 3, pp. 135–140, May 2011.

[16] R. Birch and M. Marshall, "Computation of bremsstrahlung X-ray spectra and comparison with spectra measured with a Ge(Li) detector," *Physics in Medicine and Biology*, vol. 24, no. 3, pp. 505–517, May 1979.

[17] "ROOT | A Data Analysis Framework." [Online]. Available: http://root.cern.ch/drupal/. [Accessed: 10-May-2012].

[18] M. Oikawa, T. Satoh, T. Sakai, N. Miyawaki, H. Kashiwagi, S. Kurashima, S. Okumura, M. Fukuda, W. Yokota, and T. Kamiya, "Focusing high-energy heavy ion microbeam system at the JAEA AVF cyclotron," *Nuclear Instruments and Methods in Physics Research Section B: Beam Interactions with Materials and Atoms*, vol. 260, no. 1, pp. 85–90, Jul. 2007.

[19] K.-D. Greif, H. J. Brede, D. Frankenberg, and U. Giesen, "The PTB single ion microbeam for irradiation of living cells," *Nuclear Instruments and Methods in Physics Research Section B: Beam Interactions with Materials and Atoms*, vol. 217, no. 3, pp. 505–512, May 2004.

[20] S. Peng, M. Folkard, S. Gilchrist, R. J. Locke, Z. Yu, and B. D. Michael, "Measurements of the targeting accuracy of the Gray Laboratory charged-particle microbeam," *Nuclear Instruments and Methods in Physics Research Section B: Beam Interactions with Materials and Atoms*, vol. 179, no. 1, pp. 145–150, Jun. 2001.

[21] M. Folkard, B. Vojnovic, K. M. Prise, and B. D. Michael, "The application of charged-particle microbeams in radiobiology," *Nuclear Instruments and Methods in Physics Research Section B: Beam Interactions with Materials and Atoms*, vol. 188, no. 1–4, pp. 49–54, Apr. 2002.

[22] M. De Felici, R. Felici, M. S. del Rio, C. Ferrero, T. Bacarian, and F. A. Dilmanian, "Dose distribution from x-ray microbeam arrays applied to radiation therapy: An EGS4 Monte Carlo study," *Medical Physics*, vol. 32, no. 8, p. 2455, Jul. 2005.

[23] J. Stepanek, H. Blattmann, J. A. Laissue, N. Lyubimova, M. Di Michiel, and D. N. Slatkin, "Physics study of microbeam radiation therapy with PSI-version of Monte Carlo code GEANT as a new computational tool," *Medical Physics*, vol. 27, no. 7, p. 1664, Jul. 2000.

[24] E. a. Siegbahn, J. Stepanek, E. Bräuer-Krisch, and a. Bravin, "Determination of dosimetrical quantities used in microbeam radiation therapy (MRT) with Monte Carlo simulations," *Medical Physics*, vol. 33, no. 9, p. 3248, 2006.

[25] M. D. Felici, E. A. Siegbahn, J. Spiga, A. L. Hanson, R. Felici, C. Ferrero, A. Tartari, M. Gambaccini, J. Keyriläinen, E. Bräuer-Krisch, P. Randaccio, and A. Bravin, "Monte Carlo code comparison of dose delivery prediction for microbeam radiation therapy," *Journal of Physics: Conference Series*, vol. 102, no. 1, p. 012005, Feb. 2008.

[26] G. I. Kaplan, A. B. Rosenfeld, B. J. Allen, J. T. Booth, M. G. Carolan, and A. Holmes-Siedle, "Improved spatial resolution by MOSFET dosimetry of an x-ray microbeam," *Medical Physics*, vol. 27, no. 1, p. 239, Jan. 2000.

[27] S. Incerti, H. Seznec, M. Simon, P. Barberet, C. Habchi, and P. Moretto, "Monte Carlo dosimetry for targeted irradiation of individual cells using a microbeam facility.," *Radiation protection dosimetry*, vol. 133, no. 1, pp. 2–11, Jan. 2009.

[28] Z. Liu, C. E. Mothersill, F. E. McNeill, F. M. Lyng, S. H. Byun, C. B. Seymour, and W. V. Prestwich, "A dose threshold for a medium transfer bystander effect for a human skin cell line.," *Radiation research*, vol. 166, pp. 19–23, Jul. 2006.

Chapter 6

Conclusions and Future Recommendations

6 Conclusions and Future Recommendations

Ionizing radiation, while travelling in media, produces a cascade of secondary radiation. The secondary radiation types that have been given most attention, until now, in terms of their biological significance, are the secondary electrons, specifically called δ-rays, and high frequency electromagnetic waves in the x-ray and gamma-ray range. However, lower frequency electromagnetic secondary radiation (in the optical and UV wavelength range) can also be emitted as a result of the ionizations and excitations resulting from charged particle interactions. The presence of, or disturbances in the, low frequency electromagnetic waves i.e. UV or light could have a role in mediating biological responses at the cellular level. If the electromagnetic wavelength of the emitted radiation is close to the ultraviolet region, then an emitted UV photon could, in theory, be absorbed in a non-irradiated (by the primary radiation beam) cell and subsequently produce effects similar to those that have been observed in non-targetted cells in radiation induced bystander effect studies.

This electromagnetic radiation comes from the de-excitation of the excited molecules or atoms[1,2]. Another process that can generate light when charged particles pass through a dielectric medium is the "Cerenkov process". Energetic particles loose energy through Cerenkov process when their phase velocity becomes greater than the speed of light in a particular medium. Generally this phenomenon can be observed for electrons moving in a dielectric medium. If the refractive index of tissue is considered to be 1.4 then the minimum energy required by the electrons in order to generate Cerenkov light is 0.219 MeV. Energy lost through Cerenkov process is, however, much less than that lost through ionizations. This phenomenon is well established and the number of Cerenkov photons produced, in a particular wavelength range, per unit path length can be calculated using the Frank-Tamm equation[3].

However, the actual mechanism for potential production of UV in bystander effects studies is not relevant to the discussion of potential effects. The question is firstly whether UV is emitted at all as a consequence of irradiation and secondly whether there is enough UV to explain observed biological effects. My thesis has tackled the first question: is UV

---

[1] Zengliang, Y. (2006). Introduction to ion beam biotechnology, (Chapter 3, 31–31). NY, USA: Springer online.com.

[2] Walter, R. L., Willis, R. D., Gutknecht, W. F., & Joyce, J. M. (1974). Analysis of biological, clinical, and environmental samples using proton-induced X-ray emission. Analytical chemistry, 46(7), 843–55.

[3] I. E. Tamm and I. M. Frank, "Coherent radiation of the fast electron in medium.," Dokl. Akad. Nauk SSSR, vol. 14, Jan. 1937.

emitted? I will in this chapter highlight the future work that needs to be performed to answer the second question: is the level of emitted UV able to explain some radiation bystander effects?

Construction of a Single Photon Counting System

The overall aim of this thesis was, as just stated, to investigate the emission of UV photons, as a consequence of ionizing radiation, in materials that are used in radiation biology experiments, including the cells and their growth media. Our hypothesis was that some radiation induced bystander effects could be explained by a physical signal mechanism, rather than as thought, until now, by a chemically mediated bystander signal mechanism. If UV emission could be demonstrated, it could permit alternative hypotheses of "effects at a distance" to be explored.

In order to accomplish this goal, I designed and built an experimental system in which materials could be irradiated using a proton beam from a linear accelerator. The system development work was described in Chapter 2 and published in Nuclear Instruments and Methods B. I built a single photon counting system to detect UV as a consequence of irradiation with charged particles. In the subsequent experiments using the system, my goal was to measure the absolute quantity of UV emitted due to the ion interaction with specific materials. The system was shown to be effective; UV could be detected when materials were irradiated. There were, however, limitations to the system that meant the goal of quantitative measurements of UV emission were not completely achieved.

Measurement of the emission of UV as a consequence of charged particle irradiation from container materials used in radiation biology experiments

One of the commonly used materials in radiation biology experiments is polystyrene. Prior to radiation exposures, the cells are usually plated in some suitable polystyrene container and are then exposed to radiation. Intuitively, it is obvious that a radiation beam has to go through the container before irradiating the cells, and so the container would be exposed before the cells receive any radiation. Initial experiments during the system development focused on polystyrene and this was discussed in the Nuclear Instruments and Methods B paper that forms Chapter 2. A major conclusion of that paper is that ion beam irradiation can indeed induce significant emission of electromagnetic radiation emission in the UV range in polystyrene.

The success of this polystyrene study provided the rationale for the investigation of other materials that are also used in radiation biology. To this end, I investigated the UV luminescence from Polypropylene, Mylar, Teflon, and Cellophane, which are all materials commonly used as container and wrapping materials in radiation biology experiments. A major conclusion of Chapter 3, which is a paper submitted to Physics in Medicine and

Biology is that all of these materials were found to give off a measureable and significant UV signal when irradiated with charged particle beams.

For all of these materials, the system detected of the order of 10^8 UV photons per Sr second at a wavelength of 320±5 nm and 10^5 photons per Sr second at a wavelength of 280±5 nm when the materials were subjected to dose rates of the order of a few nGy per second per proton. I suggest that this is a significant enough level of UV emission per unit dose that the potential biological effect should be investigated and the question of whether this level of UV can explain part or all of the effects observed in bystander effect studies should be further explored. As mentioned earlier most of the single photon counting devices are designed to measure weak luminescence signals, therefore their maximum tolerable count rate is not more than 10^8-10^9 counts per second. We believe that in some cases of our measurements the emitted photon count rate could be much more than what was observed because the observed count rate reached the maximum capacity of our photon counter. In future if this system can be deployed at the microbeam accelerator or the beam current in KN accelerator can be reduced, somehow, then the absolute measurement can be performed in a much better way.

Measurement of the emission of UV as a consequence of charged particle irradiation from biologically derived materials

A further conclusion of Chapter 3 was that the NIST standard materials, oyster tissue and citrus leaves, were also found to emit significant light at UV frequencies when irradiated with protons in the single photon counting measurement system. These materials were used as a surrogate for livings cells or cell media. The potential emission of UV by the cells and their media as a consequence of irradiation by charged particles is, of course, the most interesting question. However, the system that was built to measure UV emission as a consequence of proton irradiation required the materials to be measured under vacuum so it was not possible to study cells or medium. Instead, powdered materials derived from living systems were studied as a first step and were indeed found to emit UV as a consequence of proton irradiation.

It is evident from these data resulting from the study of a wide variety of materials that they all produce significant emission of UV photons upon irradiation with charged particles. Therefore, in radiation biology experiments where the cells are considered to have received targetted radiation, this suggests that targeting of cells may not be possible. The neighbouring cells may be exposed, in fact, to UV photons emitted by the container materials, as the charged particle beam passed through the container wall. Cells are not “untargetted” at all, but may be irradiated by a secondary radiation type. This clearly needs to be investigated further to unfold effects that are “direct radiation”, “secondary radiation, including UV” and “chemically mediated bystander”.

In-vivo studies can be performed for very short term exposure of UV radiation for the measurement of gene expression that could be involved in effects observed in bystander cells. Effects of low level UV exposure are available in the literature for plant studies[4]. In plants low level UV exposures can trigger several genes that regulate DNA repair, detoxification of reactive oxygen species etc. These studies can be extended for human cells.

Measurement of the emission of UV by cells and cell media as a consequence of β-particle irradiation

An important conclusion of Chapter 4 of this thesis, which has been submitted as a manuscript to Dose Response, is that UV photons have been shown to be emitted by the cell and the cell growth medium itself as a consequence of ionizing radiation. The work also demonstrated that the UV is emitted as a consequence of *low LET* irradiation and allows us to infer that UV will be emitted by cells and cell media as a consequence of irradiation by any type of ionizing radiation. Since the primary radiation type creates particle tracks and a similar pattern of ionizations and excitations in cells and growth media as in the container material, it is not surprising that UV is emitted. Therefore, bystander cells (i.e. cells that were not subject to the primary particle track) could also receive UV photons emitted from cells that were targets of the primary radiation.

The study for the production of charged particle induced luminescence could be expanded further by using heavier charged particles to determine whether there is a dependence of the emission of UV upon the LET of the incident particle[5,6]. Low level activity alpha particle sources are easily available. However since their ranges are very short, a special type of cell substrate will be required to which cells can adhere and through which the incident particles have sufficient energy to pass. This type of cell substrate can be made using very thin (4-6 microns thick) mylar and polypropylene sheets that are commercially

---

[4] Brosch, M., Schuler, M. a., Kalbina, I., Connor, L., & Strid, Ke. (2002). Gene regulation by low level UV-B radiation: identification by DNA array analysisElectronic supplementary information (ESI) available: DNA microarray analysis and conserved direct and inverted elements in PAL, CHI, CHS and PR-5 promoters. *Photochemical & Photobiological Sciences*, *1*(9), 656–664. doi:10.1039/b202659g

[5] Fink D (Ed)., Fundamentals of ion irradiated polymers, Springer-Verlag Berling Heidelberg, 2004, pp 361-364.

[6] Torrisi L, Desiderio A, Foti G, High energy proton induced luminescence on F-doped polyvinyltoluene, Nuclear Instruments and Methods in Physics research B, 166-167, 2000, 664-668.

available. However the petri-dishes or flasks with this thin substrates are not commercially available and so would have to be custom made. Similar petri-dishes are used in the microbeams as cell substrates. By utilizing the existing setup for cell exposure UV photon measurements can also be performed in microbeams.

It was observed that the presence of a colourless medium increased the observed light output while the use of a coloured medium reduced it. The composition of the coloured and colourless medium was perhaps slightly different but the difference in observed light output could, I suggest, be due to a stronger absorption and scattering of light and UV by the coloured medium. However, this is obviously an effect that warrants further investigation: a series of simple experiments could be performed to determine whether it is absorption and scattering due to the colour in the media that is reducing the UV signal in the detector. Calibrated drops of different colours could be added to a colourless growth medium and the corresponding UV or light output could be measured.

An additional question arises regarding the question of the production of light and UV in the cells and cell growth media. It is usual practice in bystander effect experiments to not expose the growth medium to light because certain compounds (such as riboflavin) can form toxic complexes with certain amino acids and metals. However, if this medium is being exposed to the light and UV generated as a result of the charged particle traversals, could this also produce toxic complexes? And could the production of toxic complexes (outside of the targeted cells) explain some “bystander effects”? This question could be partially addressed by performing suitable biological assays on the cells to determining the presence of toxic complexes that are known to be induced by exposure to light.

In this thesis, I describe experiments where the cells were irradiated using a collimated beam of electrons: it was found that the measured luminescence decreased with the increasing cellular density. In the paper that forms the basis for Chapter 4, we suggested that this may be evidence of re-absorption or scattering of UV photons within the surroundings: the absorption and scattering may increase because of an increased density of cell membranes and structures within the cell that can interact with light.

Potential effects of cell membranes and structure within the cell could be further investigated by studying cell lines other than HPV-G cells. There have been some studies where human tissues from the breast and other parts of the body have been investigated for ion induced luminescence, although the objective in those studies was different from my work. These studies could be re-performed with the objective of investigating the contribution of emitted light in producing effects seen in the radiation induced bystander effect studies. Until now most ion-beam induced luminescence studies performed on cells and cell tissues have been performed on freeze dried cells in order to keep them under vacuum. In my experiments, the cells were not freeze dried however they were dead (due to McMaster University’s biosafety regulations). I suggest that future luminescence

experiments at McMaster University should be performed on live cells to see the role of, if any, metabolic activity in the cells. Published studies suggest that the metabolic activity in cells can most certainly be associated with the emission or absorption of photons at specific wavelengths. This topic has been a subject of great interest to researchers working in the field of bio-photons. If the cellular physiological and morphological changes observed in the case of mutagenic radiation (bio-photons) research are considered to have a connection with radiation induced bystander effects, then this could open a whole new paradigm of research where the focus for the emission of secondary photons at UV frequencies, as a result of charged particle traversal through the medium, would be shifted to other relevant wavelengths, perhaps even down to infrared region.

We made the choice of measuring ultraviolet frequencies in our ion beam induced luminescence (IBIL) experiments because of its known potent biological effect on human cells and other living organisms. For humans, UV is a concern because it is emitted by the sun and everyone who is exposed to sunlight is exposed to UV as well. UV has been reported to induce genomic instability after several generations in exposed cells. It has also been reported to produce a bystander response in unexposed cells. The major portion (95 %) of UV reaching the earth's surface lies in the range of UVA (320 nm to 400 nm) and is generally absorbed by the skin or sub-dermal connective tissues. Because of this perspective, the radiation biology studies performed for UV damage usually require cellular exposures that mimic the exposures from sun. This is typically performed using UV lamps that have outputs ranging from a few Watts per m^2 to several 100 Watts per m^2. 1 watt of exposure corresponds to $5.05 \times \lambda(nm) \times 10^{15}$ photons per second. Cells are usually exposed to this level of UV exposure for several minutes.

It is unlikely that UV light emitted as a consequence of charge particle traversal through the medium will be at this high level of exposure. These levels of UV exposure (being of the order of levels of exposure from sunlight) can induce erethema. It is not, however, these acute deterministic effects at high exposure that we suggest are of potential interest, but low dose effects. We suggest there is a direct analogy to ionizing radiation effects here. Erethema is seen at extremely high ionizing skin doses of the order of a Gray. The threshold for the bystander effect is of the order of a few mGy, at levels several thousand times lower.

In my experiments I determined that for proton irradiated container materials the measured light output could be as much as a few $\mu W/Sr.m^2$ at 340 nm and 320 nm wavelengths. Cells would be exposed to this light from the container material, and then they could also be exposed to light emitted from within themselves. There are very limited studies that address the issue of exposing cells internally at UV frequencies. Photodynamic therapy (PDT) is one example where cells can be exposed to an internal source of light for short periods of time. However the photon wavelengths used in PDT are usually higher than the UV photon wavelengths.

Further work is required to study the potential effects of low doses of UV to determine whether the levels of exposure observed in this work can lead to effects. There are some examples of potential effects in the literature to cells[7,8]. For example, it has been known for quite some time that the short term exposure to ultraviolet light causes a delayed fluorescence in the cells which can be subsequently "trapped" in normal cells and may be later used a part of metabolic activity.

In addition, it should be noted that these studies are of measurements of light outside of the cells i.e. it is the level of UV that can escape the cells and cell medium. These externally measured photon count rates of light emission as a consequence of charged particle irradiation are not, of course, the UV levels to which cells are exposed. Cells have high absorption coefficients (around 1000 cm^{-1}) for wavelengths in the UV range, it can be expected that a lot of light emitted by the cells and media would be absorbed in the immediate vicinity of its creation, and so will not be observed by an external detector. This warrants further investigation, perhaps through combinations of models and experiments in order to determine the levels of internal UV exposures in cells.

Another linked area of study that should be established in the future is to determine the span of UV absorption around the region of its creation i.e. how far are UV photons transported before they are absorbed, and potentially creating an effect I suggest that a photon transport based Monte-Carlo code could be employed for this purpose. The Geant4 Monte-Carlo toolkit can simulate the transport of optical photons in different media for which the absorption, scattering and attenuation properties are known. Data from the models could be compared to microbeam "bystander effect" experiments. In several studies, researchers have determined the physical range of the bystander signal which has been observed as far as 1 mm away from the targetted and currently presumed chemical signal emitting cells. Of course, in order for this to be the mechanism of interaction, any chemical signal must have excellent diffusion characteristics or have the ability to multiply after encountering other cells in its path. Some researchers have developed Monte-Carlo codes based upon the aforementioned assumption (i.e. chemical bystander signals can multiply) and compared the results to the actual data. However if the bystander signal is a physical signal with a certain probability of being absorbed (and producing an effect) per unit length, the effect at a distance, and the fall off in bystander signal with distance may

---

[7] Howie, S., Norval, M., & Maingay, J. (1986). Exposure to Low-Dose Ultraviolet Radiation Suppresses Delayed-Type Hypersensitivity to Herpes Simplex Virus in Mice. *Journal of Investigative Dermatology*, *86*(2), 125–128. doi:10.1111/1523-1747.ep12284128.

[8] Sucré, E., Vidussi, F., Mostajir, B., Charmantier, G., & Lorin-Nebel, C. (2012). Impact of ultraviolet-B radiation on planktonic fish larvae: alteration of the osmoregulatory function. *Aquatic toxicology (Amsterdam, Netherlands)*, *109*, 194–201. doi:10.1016/j.aquatox.2011.09.020.

make more intuitive sense. There are some data that suggest that this hypothesis of a UV signal is not far-fetched. For example, in microbeam studies performed using three dimensional tissue structures, it has been observed that the penetration depth (i.e. the depth to which the signal intensity falls to e^{-1}) for the bystander signal is approximately 600 µm. (We calculated this penetration depth from the published figures.) It is known that the penetration depths of UVB and UVA are of the same order, and range up to 150 µm and 1 mm, respectively, in normal skin tissue. The penetration depends, of course, very heavily on pigment levels in tissue. Studies of penetration depths in dark-skin people and light skin people show different mean path lengths for UV because of the differences in melatonin levels. However, we can say that the path lengths for UV and the path lengths for the bystander effect are of the same order. Interestingly, in some bystander effect studies it has been shown that the induction of melanin in cells reduces the bystander signal significantly, which may suggest that it is a mechanism linked to photon absorption which reduces the bystander signal.

The fifth chapter of this thesis goes beyond the investigation of the potential emission of ultraviolet light as a consequence of charged particle irradiation, and considers another potential secondary radiation produced in microbeam experiments which could affect the data. I studied the potential of particle induced x-ray emission in the McMaster University biological microbeam system which has been built to deliver precise and low level doses in radiation biology experiments. In this particular system, the beam is collimated using slits and apertures that are subject to high ion beam currents. We wished to determine whether the interaction of the ion beam with these slit and aperture materials could produce low levels of x-rays that could result in significant radiation doses at the cellular level. Obviously, if there is an x-ray field superimposed over the charged particle interactions with cells, this could affect the interpretation of the biological microbeam data. I used the Monte Carlo method to investigate the production of particle induced x-rays and secondary electrons in the collimation system and its possible effects on the final dose delivery to the biological medium. We found no evidence of the escape of x-rays or secondary electrons from the collimation system for proton energies of up to 3 MeV. The thickness of the collimators was sufficient to reabsorb all the generated low energy x-rays and secondary electrons. The McMaster University microbeam system can run up to proton energies of 3MeV. Therefore, we conclude that in this particular system, there is no expected added field from x-ray production in the collimator apertures and slits. However in biological microbeam systems where the proton energy exceeds 3 MeV, a significant proportion of 10 keV and 59 keV x-rays could be emitted by a slit and aperture type collimators. I conclude that radiation biology investigators employing high proton energy microbeam facilities need to consider the possibility of a low energy x-ray field being superimposed on their microbeam measurements.

In the modeling of the McMaster University microbeam, I also performed work on the phase space distribution of the charged particles in various orientations with the beam axis

and concluded that there is a significant probability of hitting "non-targetted" cells in microbeams that employ a collimator to confine the beam. Previous microbeam studies, that employ slits and apertures for collimation, show approximately 7 % of the beam actually hits an area that is approximately 10 times larger than the intended targeted area. 1-2 % of the microbeam can hit an even larger area due to collimator scatter and Columbic repulsion. However these published findings are solely based upon a predictive model. If the beam is considered to have a slightly wider dispersion around the centre then this can potentially change the expected outcome. In my work, I studied a dispersion of 5^{o} around the beam's central axis and determined that there is a 1 in 4 chance that the beam would hit in an area that is approximately 175 times larger than the "target area". This may be a large beam dispersion to consider, but is another factor that microbeam investigators need to keep in mind when performing radiation induced bystander effect studies using microbeam methods. The targeting in microbeam systems can, however, be improved by means of other techniques such as magnetic focusing but this is more technically challenging. In addition, magnetic focusing would need to be studied in case this led to other methods of producing secondary radiation types. I suggest that more caution needs to be used in describing microbeam methods as being a method by which a cell can be hit by a single particle an no other cells affected by radiation. This combination of issues should and could be addressed in any future microbeam based radiation induced bystander effect studies. I suggest that perhaps a Monte-Carlo method can predict the contribution of the effects due to chemically mediated, physically mediated (due to secondary radiation), and off-target hitting by the primary beam.

There are several different microbeam systems used by the radiation biologist to deliver low level doses to cells. Production of photons having high energies (x-rays) is possible in these systems but we found no evidence in studies using the McMaster University microbeam design that x-ray production could interfere with the accuracy of the dose delivery. However, in my thesis I conclude that the production of UV and visible photons is measurable and potentially significant and this observed effect should be incorporated in the calculation of the overall damage to the cell. More rigorous efforts should be spent in determining the precise number of UV photons emitted per primary radiation quanta of interest and whether these UV photon levels can be shown to have effects in non-targetted cells.

Appendix

Nuclear Instruments and Methods in Physics Research: Section B permission for reproduction of published work in Thesis

Excerpt from the section of "Rights and Responsibilities/Intellectual property" posted on NIMB website. http://www.elsevier.com/wps/find/authorsview.authors/rights

What rights do I retain as a journal author*?

☐ the right to make copies (print or electronic) of the journal article for your own personal use, including for your own classroom teaching use;

☐ the right to make copies and distribute copies of the journal article (including via e-mail) to research colleagues, for personal use by such colleagues for scholarly purposes*;

☐ the right to post a pre-print version of the journal article on Internet websites including electronic pre-print servers, and to retain indefinitely such version on such servers or sites for scholarly purposes* (with some exceptions such as The Lancet and Cell Press. See also our information on electronic preprints for a more detailed discussion on these points)*;

☐ the right to post a revised personal version of the text of the final journal article (to reflect changes made in the peer review process) on your personal or institutional website or server for scholarly purposes*, incorporating the complete citation and with a link to the Digital Object Identifier (DOI) of the article (but not in subject-oriented or centralized repositories or institutional repositories with mandates for systematic postings unless there is a specific agreement with the publisher. Click here for further information);

☐ the right to present the journal article at a meeting or conference and to distribute copies of such paper or article to the delegates attending the meeting;

☐ for your employer, if the journal article is a 'work for hire', made within the scope of the author's employment, the right to use all or part of the information in (any version of) the journal article for other intra-company use (e.g. training);

☐ patent and trademark rights and rights to any process or procedure described in the journal article;

☐ **the right to include the journal article, in full or in part, in a thesis or dissertation;**

☐ the right to use the journal article or any part thereof in a printed compilation of your works, such as collected writings or lecture notes (subsequent to publication of the article in the journal); and

☐ the right to prepare other derivative works, to extend the journal article into book-length form, or to otherwise re-use portions or excerpts in other works, with full acknowledgement of its original publication in the journal.